Project # 55179
Renewed as 73896

INTERIM REPORT
U.S. Department of Energy

Acoustic Probe for Solid-Gas-Liquid Suspension

Principle Investigator: Dr. L.L. Tavlarides
Co-Principle Investigator: Dr. Ashok Sangani
Institution: Syracuse University

Collaborators: Dr. P. Spelt[+]
Dr. M.A. Norato[+]
Dr. M. Greenwood[*]
Mr. M. Hedges[+]
Institutions: Syracuse University[+]
Pacific Northwest National Laboratory*

Grant Number: DE-FG07-96-ER14729
Grant Project Officers: Dr. Oscar P. Manley
(Review and Evaluation of Research)
Dr. Gordon Roesler Massey
(Review and Evaluation of Application of Research)
Project Duration: First Funding Period 9-15-96 to 9-14-2000
Second Funding Period 9-15-2000 to 9-14-2003

Table of Contents

3. Executive Summary

The main objective of the project during the first period of funding is to develop an acoustic probe for monitoring particle size and volume fraction in slurries in the absence and presence of gas bubbles. The goals are to commission and verify the probe components and system operation, develop theory for the forward and inverse problems for acoustic wave propagation through a three phase medium, and experimentally verify the theoretical analysis. The acoustic probe will permit measurement of solid content in gas-liquid-solid waste slurries in tanks and pipelines across the Department of Energy complex. Particularly, in the second funding period, a prototype probe will be fabricated, commissioned and tested to demonstrate the capability to accurately measure slurries of one to five weight percent solids.

Our research work has established a solid theoretical foundation for predicting attenuation and phase speed of acoustic waves propagating through solid-liquid suspensions, both in the presence as well as absence of gas bubbles. The theory is based on ensemble averaging of the equations of motion in the solid and liquid phases to obtain expressions for the "effective properties" of the slurry mixture in terms of coefficients which appear in the equations of motion for the solid particle. The attenuation theory accounts for losses due to viscous dissipation, nonadiabatic thermal effects, and incoherent scattering, and as a result can cover a wide range of frequencies and particle sizes. The theory also applies to polydispersed suspensions of spherical particles. The theory agrees with results obtained by previous investigations who examined limiting cases of thermal attenuation at small volume fraction (Allegra and Hawley, 1972) and viscous attenuation at large frequencies (Sangani, Zhang and Prosperetti, 1991). The comprehensive theory developed allows us to interrogate a relatively large range of particle sizes and physical properties. The attenuations predicted from theory are in generally good agreement with experimental data obtained by Pulse/FFT data acquisition methods for solid-liquid slurries of soda-lime glass particles of 14.9 microns and 65 microns mean radius and polystyene particles of 79 microns mean radius at concentrations ranging from 5 to 50 percent solids by volume in water. The primary attenuation mechanisms for the former system are due to viscous and scattering losses, whereas, for the latter system, thermal and scattering losses dominate. Good comparisons are also obtained for 0.11 micron radius polystyrene particles in water from 5 to 50 percent solids by volume (Allegra and Hawley, 1992) where attenuation is dominated by thermal affects.

Another goal of the project was to devise a technique to remove the noise introduced by the presence of a small amount of gas bubbles in the suspension to infer the properties of the solid-liquid suspension. Experiments and analyses were made for the solid-gas-liquid slurries of soda lime glass particles of 14.9 micron mean radius at 5 and 10 percent by volume in water with gas bubbles from 25 to 150 micron radius at low volume fractions. The primary conclusion is that the noise is significant at low frequencies near the bubble resonance frequencies and the noise is minimal at high frequencies. We show it is possible to estimate the effects of bubbles and eliminate the slight noise produced by bubbles at higher frequencies to yield the volume fraction of the particles.

An inverse theory was also developed to determine the concentration and solids particle size distribution in a solid-liquid slurry given the attenuation as a function of frequency using regularization techniques that have been successful for bubbly liquids. We have found that the success of solving the inverse problem is limited since it depends strongly on the physical properties of the particles and the frequency range used in the inverse calculations. We have determined bounds necessary for determining the particle size distribution.

The first six months of the new funding period focused on demonstrating the capability to accurately measure volume fractions of dilute suspensions in the range of 0.004 to 0.050 percent. The Pulse/FFT method accurately measures attenuation for soda lime glass beads (14.9 micron radius), clays in water, and a Hanford surrogate salt simulant in this range. A linear relationship is obtained for attenuation versus volume fraction, and the theory accurately predicts the monodispersed soda-lime glass bead data. The linear relationship should readily permit application of the acoustic monitor to dilute slurries.

The results of this project has relevance to the DOE mission of mobilizing, transporting and processing solid-liquid slurries by providing a reliable and safe monitor of percent solids in these slurries. Significant impact is expected for application as an accurate, safe and reliable monitor which is non-invasive is required to quantify across site transfer of dilute and concentrated slurries from storage tanks to processing facilities for high level waste treatment. Transfer of this technology to the DOE complex is the primary objective of the second funding period of this project whereby a proto-type acoustic monitor will be designed, commissioned and demonstrated to accurately measure low weight percent slurries in a flow loop and on a test transfer line.

4. Research Objectives

The primary objective of the research project during the first funding period was to develop an acoustic probe to measure volume percent solids in solid-liquid slurries in the presence of small amounts of gas bubbles. This problem was addressed because of the great need for a non-invasive, accurate and reliable method for solids monitoring in liquid slurries in the presence of radiolytically generated gases throughout the DOE complex. These measurements are necessary during mobilization of salts and sediments in tanks, transport of these slurries in transfer lines to processing facilities across a site, and, in some instances, during high level waste processing. Although acoustic probes have been commonly used for monitoring flows in single-phase fluids (McLeod, 1967), their application to monitor two-phase mixtures has not yet fully realized its potential. A number of investigators in recent years have therefore been involved in developing probes for measuring the volume fractions in liquid solid suspensions (Atkinson and Kytomaa, 1993; Greenwood et al., 1993; Martin et al., 1995) and in liquid-liquid suspensions (Bonnet and Tavlarides, 1987; Tavlarides and Bonnet, 1988, Yi and Tavlarides, 1990; Tsouris and Tavlarides, 1993, Tsouris et al., 1995). In particular, Atkinson and Kytomaa (1993) showed that the acoustic technique can be used to determine both the velocity and the volume fraction of solids while Martin et al. (1995) and Spelt et al. (1999) showed that the acoustic probe can also be used to obtain information on the size distribution of the particles. In a recent testing of in-line slurry monitors with radioactive slurries suspended with Pulsair Mixers (Hylton & Bayne, 1999), an acoustic probe did not compare well with other instruments most

probably due to presence of entrained gases and improper acoustic frequency range of interrogation.

The work of the investigators cited has established the potential of the acoustic probe for characterizing/monitoring two-phase flows in relatively ideal, well-characterized suspensions. Two major factors which we judge has prevented its wide-spread use in the processing industry, particularly for dilute suspensions, is careful selection of the frequency range for interrogation and quantification and removal of the noise introduced by bubbles from the acoustic signal obtained from the suspension.

Our research during the first funding period to develop an acoustic probe for solid-gas-liquid suspensions has resulted in a theory, supported by our experiments, to describe small-amplitude dilute suspensions (Norato, 1999, Spelt et al., 1999, Spelt et al., 2001). The theory agrees well with experimental data of sound attenuation up to 45 vol % suspensions of 0.11 and 77 micron radius polystyrene particles in water and 0.4 to 40 vol %, suspensions of 32 micron soda-lime glass particles in water. Also, analyses of our attenuation experiments for solid-gas-liquid experiments suggest the theory can be applied to correct for signal interference due to the presence of bubbles over a selected frequency range to permit determination of the solid-liquid volume fraction. Further, we show experimentally that a reliable linear dependency of weight percent solids with attenuation is obtained for low weight fractions at high frequencies of interrogation where bubble interference is minimal.

There was a collaborative effort during the first funding period with the Pacific Northwest National Laboratories in that Dr. Margaret Greenwood was a co-investigator on the project. Dr. Greenwood provided a high level of experimental knowledge and techniques on ultrasound propagation, measurement and data processing. During the second funding period the slurry test loop at Oak Ridge National Laboratories under the direction of Mr. Tom Hylton will be employed to demonstrate the measurement capabilities of the proto-type acoustic monitor.

5. Methods and Results

Our research during the last three and one-half years has established a solid theoretical foundation for predicting attenuation and phase speed of acoustic waves propagating through solid-liquid suspensions, both in the presence as well as absence of gas bubbles (Spelt et al., 1998; Spelt et al., 2001). The attenuation theory accounts for losses due to viscous dissipation, nonadiabatic thermal effects, and incoherent scattering, and as a result can cover a wide range of frequencies and particle sizes. The theory also applies to polydisperse suspensions of spherical particles. The theory agrees with the results obtained by previous investigators who examined limiting cases. For example, our theory agrees with that of Allegra and Hawley (1972) who considered only the case of thermal attenuation at small volume fractions and with Sangani, Zhang and Proseperetti (1991) who considered only the case of viscous attenuation at large frequencies. The comprehensive theory developed allows us to interrogate a relatively large range of particle sizes or particle physical properties. The theory was also tested against the experimental data obtained by previous investigators (e.g. (Allegra and Hawley, 1972)) and in our laboratory.

Demonstration of our theory is accomplished experimentally with the set-up shown in Figure 1. An ultrasonic pulse generator (Panametrics 5052 PR) generates an electric pulse and sends it to the emitting transducer. The actuated emitting transducer transmits an acoustic pulse through the sample actuating the receiving transducer, where the signal is transmitted to and read by an oscilloscope (Lecroy 9310A). An FFT analysis of the amplitude is performed on the spike pulse, outputting voltage as a function of frequencies of the pulse. This procedure is performed on the suspending liquid, and the solid-liquid or solid-gas bubble-liquid slurry. The voltages are used to calculate attenuation.

Comparison between the theory and the experiments is shown in Figures 2-6. Figure 2 shows attenuation as a function of frequency for glass particles with about 15 micron radius at 5 and 10 percent volume fractions. For these particles the viscous and scattering losses are the primary attenuation mechanisms for the range of frequency considered in the figure. Figure 3 shows the comparison for about 77 micron radius polystyrene particles in water at 5 percent volume fractions. For this system the thermal attenuation is important at smaller frequencies and scattering at higher frequencies. The two theoretical curves correspond to assuming that (i) the suspension is monodisperse and (ii) the particle size distribution is Gaussian with a standard deviation of 1 micron. The peaks seen in the figure correspond to resonances in shape oscillations. Figure 4 shows attenuation as a function of volume fraction for 63 micron glass particles in water at various frequencies. The viscous and scattering losses are important in these relatively dense suspensions. Good agreement here suggests that the theory is reasonably accurate in predicting the volume fraction dependence even at high volume fractions. Figure 5 shows comparison with the data for 0.11 micron polystyrene particles in water obtained by Allegra and Hawley (1972). For this system the attenuation is dominated by the thermal effects.

In Spelt et al. (1999) we investigated in detail the inverse problem so determining the particle size distribution of the particles given the attenuation as a function of frequency. We devised and compared various analytical techniques for solving the inverse problem and determined the conditions, e.g. the particle size and frequency range, necessary for determining the particle size distribution.

As mentioned earlier, one of the aims of our project was to devise a technique whereby the noise introduced by the presence of small amount of gas bubbles in the suspension can be removed to infer the properties of solid-liquid suspension. We have done detailed analysis of the noise introduced by bubbles. The primary conclusion is that the noise is significant at frequencies that are not much greater than the resonance frequencies of bubbles. Beyond the resonance frequency of the bubbles, the attenuation due to the presence of bubbles decrease with the increasing frequency while the attenuation due to solids increase with the increasing frequency. Thus the noise is minimal at sufficiently high frequencies. It is possible then to use the data at low frequencies to estimate the effects of bubbles and eliminate the slight noise produced by the bubbles at higher frequencies to yield volume fraction of the particles. We have illustrated this through our experiments on solid-liquid suspensions sparged with bubbles. The

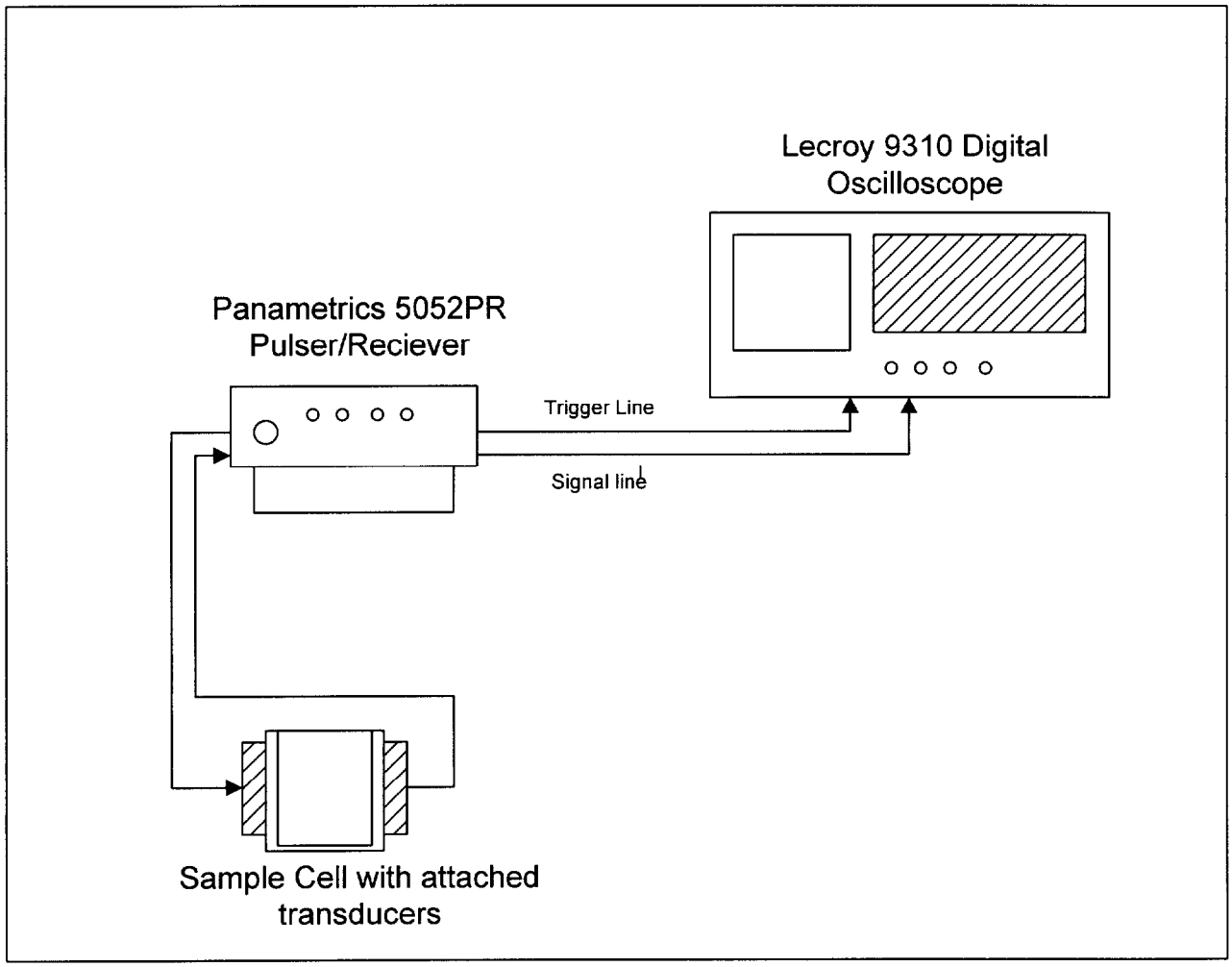

Figure 1. Schematic diagram of Pulse/FFT setup used to measure attenuation. A spike pulse is generated by the pulser/receiver and is transmitted to the transmitting transducer which is in contact with the sample. After traveling through the sample and being acquired by the receiving transducer the pulse is routed through the pulser/receiver to the oscilloscope.

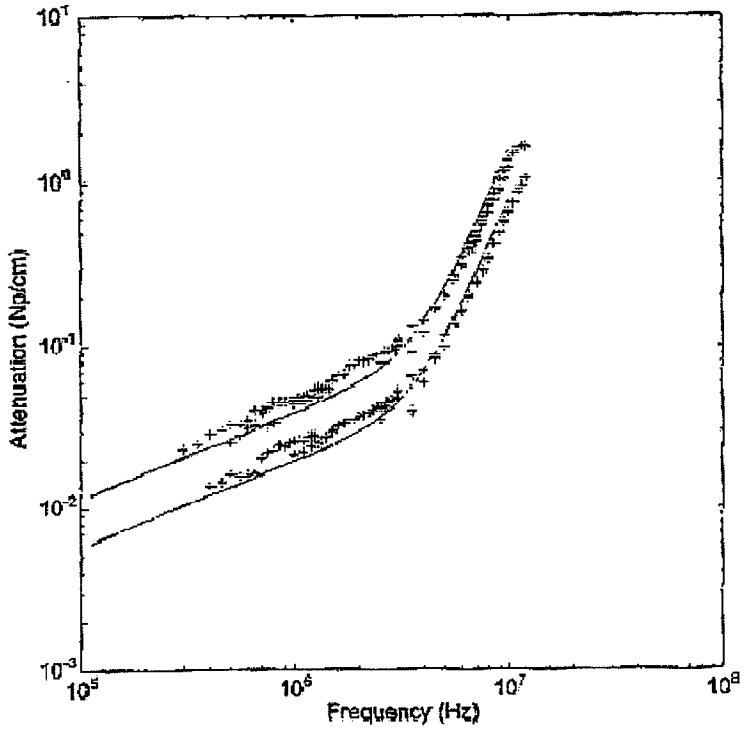

Figure 2. Comparison between experimental results and forward problem theory predictions for the attenuation versus frequency curves for soda-lime glass slurries at 5% and 10% solids by volume. The experimental solids size distribution has a mean radius of 14.9 microns with standard deviation of 3.56 microns. The forward theory predictions are based on a log-normal distribution with a mean radius of 14 microns and standard deviation of 7 microns.

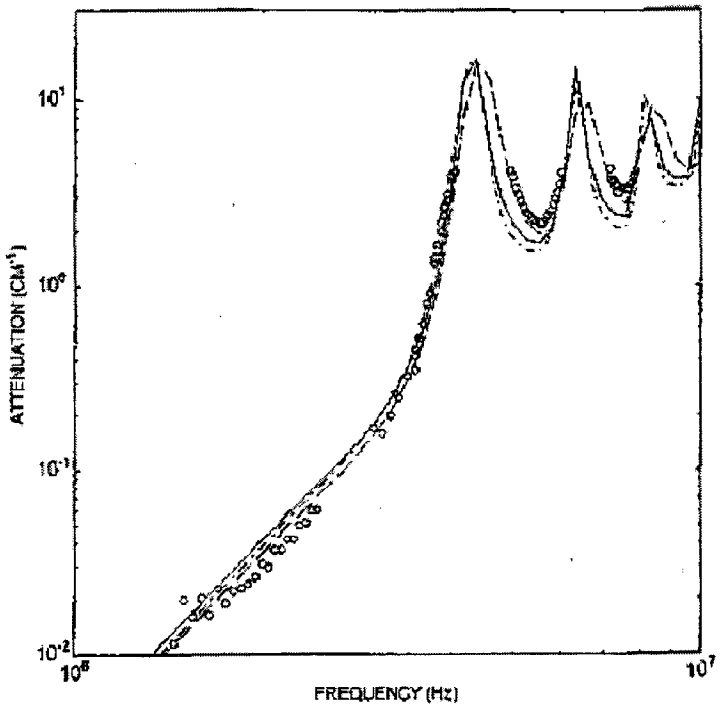

Figure 3. Experimental and theoretical results for the attenuation in a mixture of polystyrene particles (mean radius 79 ± 3 micron and 1.8 micron standard deviation) in water at 0.05 volume fraction. Circles are experiments, solid and broken lines are the theory for monodispersed particles of 79 microns and 77 microns radius, respectively.

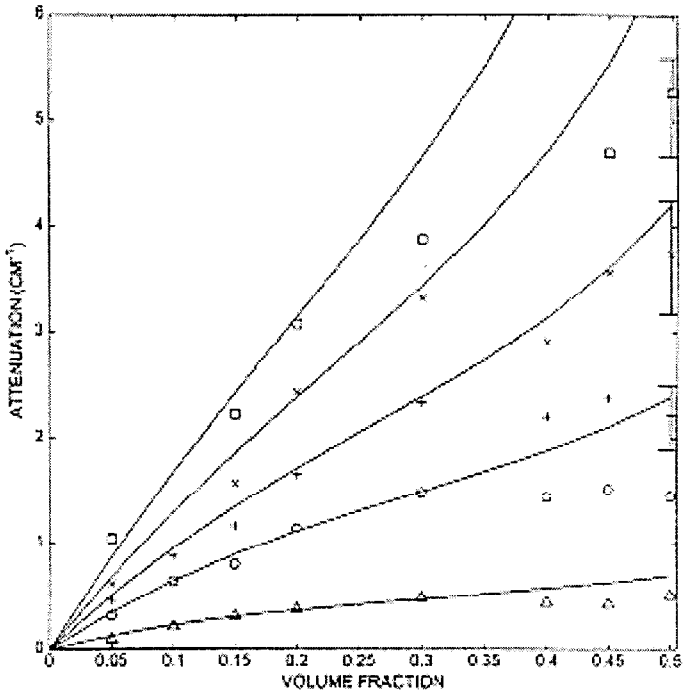

Figure 4. Experimental and theoretical results for the attenuation as a function of volume fraction for different frequencies, using glass particles (63 ± 8.5 microns radius) and glycerol. Markers: experiments, and solid lines: theory for monodispersed particles. Frequencies: 2.5 MHz (Δ); 3.5 MHz (o); 4 MHz (+); 4.5 MHz (x); 5 MHz (□).

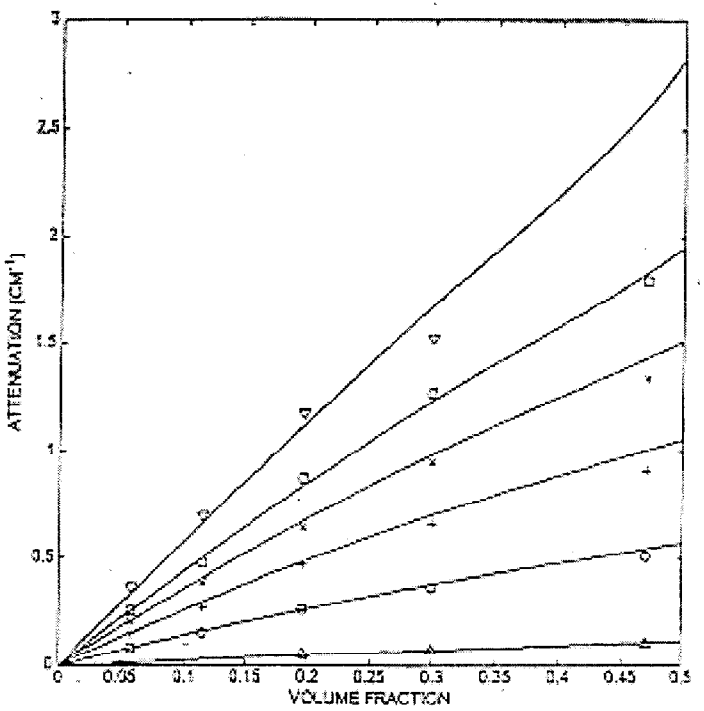

Figure 5. Attenuation as a function of solids volume fraction for the data of Allegra and Hawley (1972). The symbols represent experimental data at 3 MHz (Δ); 9 MHz (o); 15 MHz (+); 21 MHz (x); 39 MHz (∇). The curves represent the results of the effective medium approach used in this study.

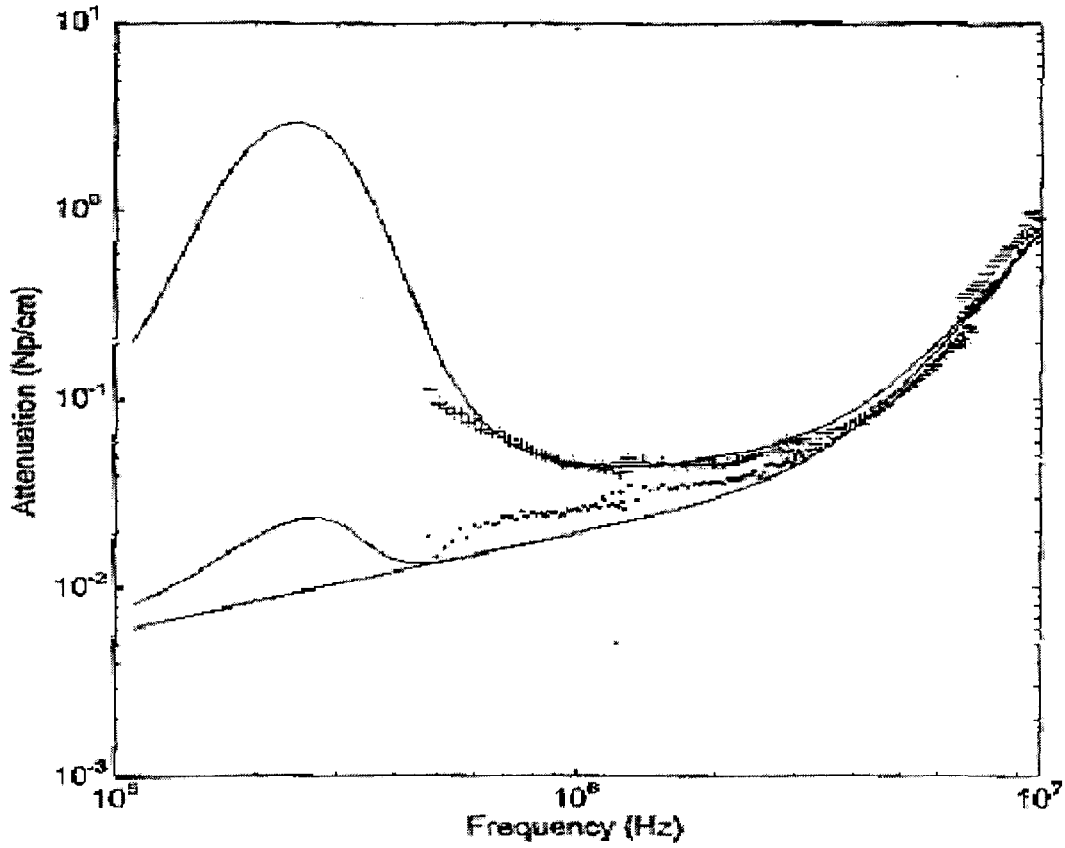

Figure 6. Results of predicting the attenuation due to the presence of bubbles in a solid-gas-liquid slurry and simply subtracting that attenuation from the total attenuation. The symbols represent experimental data for the solid-liquid and solid-gas-liquid slurries and the difference after subtracting the bubble attenuation.

preliminary results have been presented in the PhD dissertation of the student supported by the research (Norato, 1999); a more complete work will be submitted for publication in the near future. Figure 6 shows a comparison between theory and experiments for a gas-solid-liquid system. Note that the attenuation as a function of frequency goes through a minimum as the attenuation due to bubbles diminish while that due to solids increase with increasing frequency.

The above mentioned work deals with solids weight fraction above 5 percent. Our current activities extend the method to dilute suspensions in the weight percent range of 1-5 percent. We have conducted experiments for these low weight percents. The results are shown in Figures 7-9. We note from Figure 7 that the experimental data for soda-lime glass beads are in a reasonably good agreement with the theory based on monodispersed suspensions with no adjustable parameters. Figures 8 and 9 show that attenuation is significant for the entire range of volume fractions. Figure 9 shows results for a crystallized salt solution prepared according to surrogate protocol procedures for average Hanford supernate containing suspended salt particles (Glocar et al., 2000). These results show that with suitable calibration of the particle size, it would be possible to determine the volume fraction of particles from such attenuation frequency data. In principle only one calibration point would be needed, as a linear relationship appears to hold.

6. Relevance, Impact and Technology Transfer

The following answers the nine questions posed for this section.

a. This scientific work has direct application to monitor, in real time, solid-liquid slurry suspensions in the presence of gas bubbles at volume fractions of solids from 0.005 to 0.50. Monitors can potentially be installed both on transfer lines, in a non-invasive manner, or in-tanks through riser entry ports.

b. This new technology has the potential to improve cleanup approaches and significantly reduce future costs, schedules and risks and meet DOE compliance requirements in the following ways:

b.1) By assuring uniform suspensions of solids through a tank during mobilization, sluicing, or emptying of tank salts and sediments. Time and costs to execute these operations will be minimized.

b.2) Transfer of low weight percent slurries in transfer lines from DOE operated tank farms to a contractor staging tanks for processing can be done in an accurate manner. This assurance will permit compliance of schedule requirements and appropriate guarantee of required and expected material transfers.

b.3) The monitor can be employed to determine onset of transfer line plugging to prevent such occurrences and alert personnel for quick and appropriate response

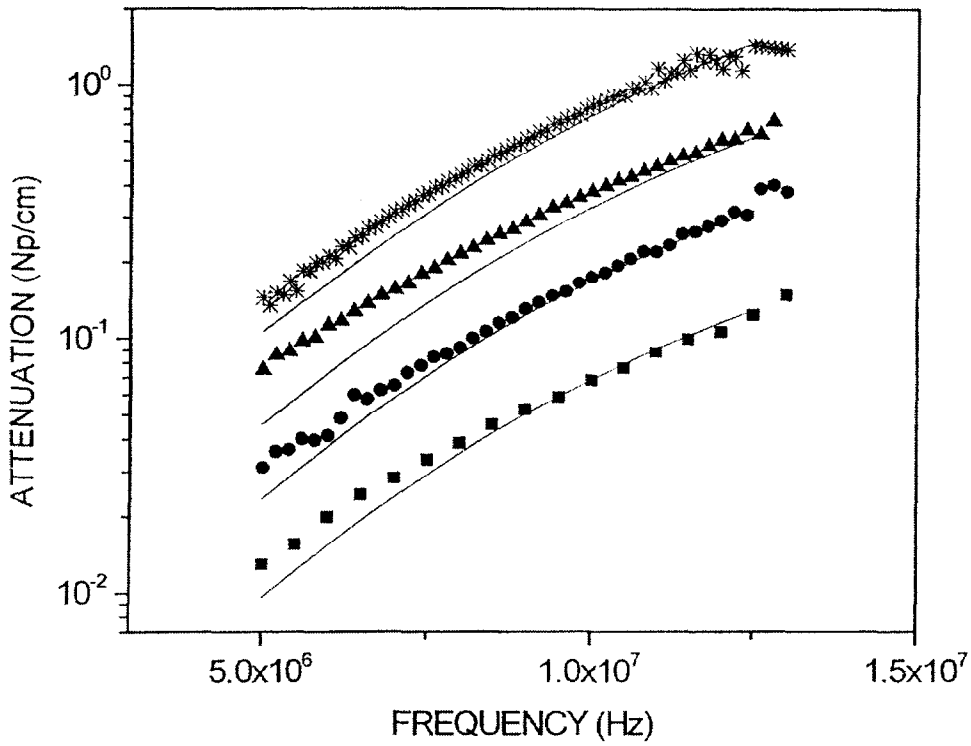

Figure 7. Attenuation versus frequency for slurries of 15 micron glass particles in water at various weight percent solids. The comparisons of theory (solid lines) with experiments (symbols) are given in ascending order for 1.0, 2.5, 5.0 and 12.0 weight percent solids.

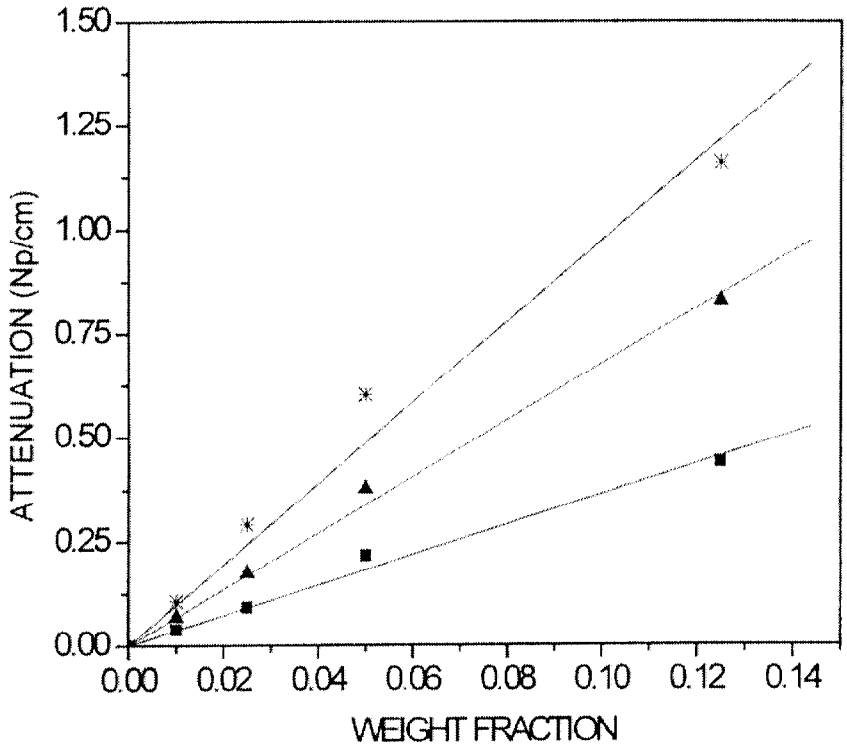

Figure 8. Attenuation versus weight fraction for slurries of 16 micron glass particles in water at three frequencies. Data shown with symbols are compared with a linear fit shown as solid lines. The curves in ascending order are for frequencies of 8, 10, and 12 MHz.

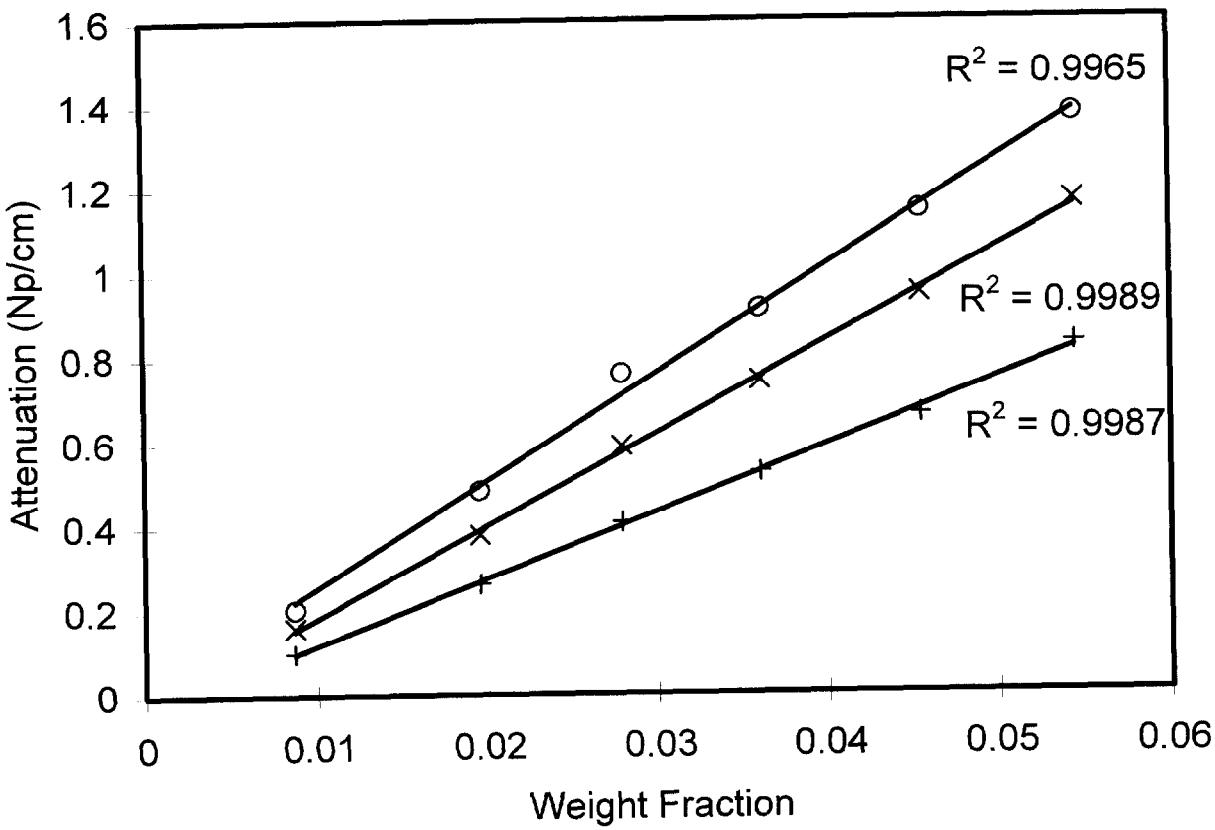

Figure 9 Attenuation versus weight fraction for the crystallized salt solution at three frequencies. The frequencies studied are (o) 12 MHz (x), 10 MHz, and (+) 8 MHz.

b.4) The monitor can be used to assure homogeneous suspensions of a mixture of solids in processing vessels during HLW and LAW treatment, for example, to guarantee glass former slurries uniformity for feeding melters.

c. The continuation of the project during the second funding period will result in a proto-type monitor which will be demonstrated at the ORNL flow loop. Also, efforts will be made to test it at the Hanford site. This effort should be completed by 9-30-03. Rapid deployment could follow subsequently pending success and availability of funds.

d. The project impact at Syracuse University resulted in continuation of this scientific effort leading to the proto-type development. The University infrastructure to conduct this research has improved through equipment acquisition and laboratory development. We have graduated one PhD, one MS and trained during the first funding period. We have had a collaboration with Dr. Margaret Greenwood from PNNL during the first funding period and a two-way transfer of knowledge was accomplished. We have an agreement with ORNL to test the prototype monitor on the ORNL two phase flow loop during the second funding period, and this should provide a quality test facility and personnel for this aspect of the project. See section c above for answers to the remaining questions.

e. Larger scale proto-type monitor development and testing are warranted, required and in progress with the second funding period of this project. The knowledge attained during the first period of funding is the basis for the proto-type monitor development and expected success in demonstration and future deployment.

f. Our collaboration with PNNL scientist Dr. Margaret Greenwood resulted in training Dr. Michael Norato (during his Ph.D. thesis work on the project) and transfer of knowledge. Our subsequent improvements of the monitor using the Pulse/FFT provides another technique PNNL can employ for their acoustic ultrasound investigations. Our particle size measurement and estimation techniques from attenuation measurements also should be of benefit to PNNL activities in this application.

g. We have increased out understanding in this area by improving our knowledge to monitor (experimental developments) and interpret attenuation signals (theoretical developments) heretofore not as accurately possible. These results provide the basis for continued development of the acoustic monitor.

h. The hurdles to overcome are the topics of the current funding period. These include:

h.1) Development of software and data acquisition system to determine volume fraction of particles.

h.2) Construct, test and commission in-line/at-tank acoustic monitor.

h.3) Conduct flow loop tests of monitor at ORNL and refine as needed.

h.4) Test refined monitor at Hanford.

i. Ms. Judith Ann Bamberger (509-375-3898-FON; Judith.bamberger@pnl.gov) offered to collaborate on the project. Should we have success on h.3 above she offered to assist in implementation/testing at a Hanford test loop. Dr. Rajiv Srivastava, Florida International University, also offered to collaborate in ways yet to be determined.

7. Project Productivity

The project accomplished most of the targeted goals. We requested and received a one-year no cost extension on the project due to typical delays in progress. We were not able to develop a theory to invert the acoustic signal to permit unambiguous prediction of the solid particle size distribution, along with the volume fraction. We show regions of physical properties and signal interrogation ranges where this may be possible. The results we have obtained were, however, quite valuable and are the basis for the continuation as described above.

8. Personnel supported:

8.1. P.I. Prof. Lawrence L. Tavlarides, Syracuse University
Co-P.I.: Professor Ashok Sangani, Syracuse, University
Co-Investigator: Dr. Margaret Greenwood
Post-Doctoral: Dr. Peter Spelt, currently at Imperial College, London, UK
Ph.D. Student: Dr. Michael A. Norato, currently at Westinghouse SRTC
M.S. Student: Mr. Mark Hedges, currently at Kionex, Inc.
Research Associate: Mr. Alexander Shcherbakov, on leave N.T.U. Kiev, Ukraine

9. Publications

9.1 Noratok, M.A., "Acoustic Probe for the Characterization of Solid-Gas-Liquid Slurries," Ph.D. Thesis, Syracuse University, May 1999.

9.2 Hedges, M., "Ultrasound Characterization of Low Volume Fraction Solid-Liquid Slurries," M.S. Thesis, Syracuse University, January 2001.

9.3 Spelt, P.D.M., Norato, M.A., Sangani, A.S., and Tavlarides, L.L., "Determination of Particle Size Distributions from Acoustic Wave Propagation," Physics of Fluids, Vol. 11 ns, 1065-1080 (1999).

9.4 Spelt, P.D.M., Norato, M.A., Sangani, A.S., Greenwood, M.S., and Tavlarides, L.L., "Attenuation of Sound in Concentrated Suspensions: Theory and Experiments," Jl. of Fluid Mechanics, 420, 1-36 (2001).

9.5 In preparation from Norato's Thesis.

9.6 In preparation from Hedges' Thesis.

10. Interactions

10.1 M. Norato, P. Spelt, A. Sangani, M. Greenwood, L.L Tavlarides, "An Acoustic Probe for the Characterization of Three-Phase Slurries," 1997 Annual AIChE Meeting, Los Angeles, CA, November 20, 1997, paper 148f.

10.2 L.L. Tavlarides, "Acoustic Probe for Solid-Gas-Liquid Suspensions," Argonne National Laboratory, Argonne, IL, Ultrasonics/Acoustics Workshop, October 25, 1997.

10.3 M.A. Norato, A.S. Sangani, L.L. Tavlarides, M. Greenwood, "Acoustic Wave Propagation in Solid-Liquid Suspension," 16th Biennial North American Mixing Conference, MIXING XVI, Williamsburg, VA, June 16, 1997.

10.4 M.S. Greenwood, M.A. Norato, A.S. Sangani, P.D.M. Spelt, L.L. Tavlarides, "Ultrasound Attenuation Measurements in Solid-Gas-Liquid Slurries and the Solution of the Inverse Problem," Annual AIChE Meeting, Miami Beach, paper 187f, November 17, 1998.

10.5 M.S. Norato, A.S. Sangani, P.D.M. Spelt, L.L. Tavlarides, "Acoustics of Slurries Containing Small Amounts of Bubbles: Measurement and Theory for Forward and Inverse Problems," Annual AIChE Meeting, Miami Beach, paper 126b, November 18, 1998.

10.6 M. Norato, P. Spelt, M. Greenwood, A. Sangani, L.L. Tavlarides, "Acoustic Probe for Solid/Gas Liquid Suspension, 18th Biennial North American Mixing Conference, Banff, Canada. August 15-20, 1999.

10.7 M.S. Greenwood, M.A. Norato, A.S. Sangani, P.D.M. Spelt, L.L. Tavlarides, "Attenuation of Sound in Concentrated Suspension: Theory and Experiments," AIChE Meeting, Dallas, TX, Oct. 31-Nov. 5, 1999.

10.8 L.L. Tavlarides, "Acoustic Probe for Solid.Gas/Liquid Suspensions," DOE Characterization and Monitor Workshop, Atlanta, Georgia, Dec. 14-15, 1999.

10.9 L.L. Tavlarides, (with P. Spelt, M.A. Norato, M. Greenwood, A. Sangani), "Acoustic Probe for Characterization of Solid-Gas-Liquid Slurries," US DOE EMSP National Workshop, April 24-27, 2000, Atlanta, GA.

10.10 L.L. Tavlarides, A. Sangani, P. Spelt, M. Hedges, M.A. Norato and M. Greenwood, "Acoustic Probe for Characterization of Solid-Gas-Liquid Slurries," Tank Focus Area Midyear Review, Salt Lake City, UT, March 11-15, 2001.

11. Transitions

The work is being transitioned through the second funding period.

12. Patents

None

13. Future Work

Continuation of funding in progress.

14. Literature Cited

Atkinson, C.M. and Kytomaa, H.K., "Acoustic Properties of Solid-Liquid Mixtures and the Limits of Ultrasound Diagnostics-I. Experiments. J. Fluids Eng. **115**, 665 (1993).

Bonnet, J.C. and Tavlarides, L.L., "Ultasonic Technique for Dispersed Phase Hold-Up Measurements," I&EC. Res. **26**, 811 (1987).

Golcar, G.R., Colton, N.G., Durab, J.G., and Smith, H.D., "Hanford Tank Waste Simulants Specifications and Their Applicability for the Retrieval, Pretreatment, and Vitrification Processes," PNWD-2455/BNFL-RPT-012 Rev. 0, 2000.

Greenwood, M.S., Mai, J.L., and Good, M.S., "Attenuation Measurements of Ultrasound in a Kaolin-Water Slurry: A Linear Dependence Upon Frequency, J. Acoust. Soc. Am. **94**, 908 (1993).

Hylton, T.D. and Bayne, C.K., "Testing of In-Line Slurry Monitors and Pulsair Mixers with Radioactive Slurries," ORNL/TM-1999/111, July, 1999.

Martin, J., Rakotomalala, N., and Salin, D., Phys. Rev. Lett. **74**, 1457 (1995).

McLeod, F., "Directional Doppler Flowmeter," Intl. Conf. Med. Bio. Eng., Stockholm, 213 (1967).

Norato, M.A., "Acoustic Probe for the Characterization of Solid-Gas-Liquid Slurries," Ph.D. Thesis, Syracuse University, May 1999.

Spelt, P.D.M., Norato, M.A., Sangani, A.S., and Tavlarides, L.L., "Determination of Particle Size Distributions from Acoustic Wave Propagation," Physics of Fluids, Vol. 11 ns, 1065-1080 (1999).

Spelt, P.D.M., Norato, M.A., Sangani, A.S., Greenwood, M.S., and Tavlarides, L.L., "Attenuation of Sound in Concentrated Suspensions: Theory and Experiments," Jl. of Fluid Mechanics, **420**, 1-36 (2001).

Tavlarides, L.L. and Bonnet, J.C., "An Ultrasonic Technique for Dispersed Phase Holdup Measurements," US Patent No. 4,726,221 (1988).

Tsouris, C. and Tavlarides, L.L., "Volume Fraction Measurement of Water in Oil by an Ultrasonic Technique," I&EC Res. **32**, 998 (1993).

Tsouris, C., Norato, M.A., and Tavlarides, L.L., "A Pulse-Echo Ultrasonic Probe for Local Volume Fraction Measurements in Liquid-Liquid Dispersions," I&Res. **34**, 3154 (1995).

Yi, J.H. and Tavlarides, L.L., "Model for Hold-Up Measurements in Liquid-Liquid Dispersions Using an Ultrasonic Technique," I&EC Res. **29**, 475 (1990).

15. Feedback

None

16. Appendices

A1 – Publication 9.1
A2 – Publication 9.2
A3 – Publication 9.3
A4 – Publication 9.4

J. Fluid Mech. (2001), vol. 430, pp. 51–86. Printed in the United Kingdom

© 2001 Cambridge University Press

Attenuation of sound in concentrated suspensions: theory and experiments

By PETER D. M. SPELT[1]†, MICHAEL A. NORATO[1], ASHOK S. SANGANI[1]‡, MARGARET S. GREENWOOD[2] AND LAWRENCE L. TAVLARIDES[1]

[1]Department of Chemical Engineering and Materials Science, Syracuse University, Syracuse, NY 13244, USA

[2]Pacific Northwest National Laboratory, Battelle Memorial Institute, Richland, WA 99352, USA

(Received 26 February 1999 and in revised form 6 September 2000)

Ensemble-averaged equations are derived for small-amplitude acoustic wave propagation through non-dilute suspensions. The equations are closed by introducing effective properties of the suspension such as the compressibility, density, viscoelasticity, heat capacity, and conductivity. These effective properties are estimated as a function of frequency, particle volume fraction, and physical properties of the individual phases using a self-consistent, effective-medium approximation. The theory is shown to be in excellent agreement with various rigorous analytical results accounting for multiparticle interactions. The theory is also shown to agree well with the experimental data on concentrated suspensions of small polystyrene particles in water obtained by Allegra & Hawley and for glass particles in water obtained in the present study.

1. Introduction

We consider the problem of predicting the attenuation of sound waves propagating through suspensions. When the particle volume fraction in the suspension is very small the particle interactions may be neglected and the attenuation can be determined as a function of the sound wave frequency by examining the interaction of a single particle with the incident wave as has been done by a number of investigators in the past. For example, Carstensen & Foldy (1947) examined the problem of dilute bubbly liquids while Epstein & Carhart (1953) and Allegra & Hawley (1972) examined, respectively, the case of dilute emulsions and dilute slurries. Since the attenuation behaviour is strongly dependent on the particle radius, the attenuation–frequency data for dilute suspensions may be used for determining the particle size distribution as shown by Duraiswami, Prabhukumar & Chahine (1998), who considered the case of bubbly liquids. The corresponding problem for dilute suspensions has been examined by Spelt *et al.* (1999).

The particle interactions can have a significant effect on the acoustic behaviour of non-dilute suspensions and at present rigorous calculations accounting for these interactions are lacking. Direct attack on the problem, i.e. solving the linearized

† Present address: Centre for Composite Materials, Imperial College, Prince Consort Road, London SW7 2BY, UK.

‡ Author to whom correspondence should be addressed: e-mail asangani@syr.edu

energy, momentum, and continuity equations for multiparticle systems, appears to be a daunting task even with the development of efficient computers. Thus, it is necessary to develop a suitable approximate theory and to assess its validity by comparison with the experimental data obtained with different kinds of suspensions.

We use the method of ensemble averaging to derive linearized continuity, momentum, and energy equations for the suspensions. These equations are closed by introducing effective properties of the suspensions, namely the effective conductivity, viscosity (or viscoelasticity), compressibility, and density. To estimate these properties as a function of frequency and physical properties and volume fractions of the individual phases, we must determine the relation between the conditionally averaged temperature and velocity fields inside a test particle and the temperature and velocity fields of the suspension. A self-consistent, effective-medium approximation is used for this purpose.

The predictions of the theory are compared with several known rigorous analytical calculations accounting for multiparticle interactions in dense suspensions in the limiting case of relatively small frequencies for which the acoustic wavelength is large compared with the particle radius. At very low frequencies, for which the thermal and viscous (Stokes) lengths become large compared with the particle radius, we expect the velocity and temperature fields to satisfy, respectively, the Stokes and Laplace equations. The effective properties such as the viscosity, conductivity, and permeability, for monodisperse suspensions in this limit are well-established (e.g. Ladd 1990; Mo & Sangani 1994). It is shown that the effective-medium approximation is in excellent agreement with these results. For moderate frequencies, at which the Stokes layer is very small compared with the particle radius and the wavelength is large compared with the radius, the velocity field satisfies the Laplace equation outside the Stokes layers. Added mass and Basset force coefficients, which contribute to the effective density of the suspension, have been determined by Sangani, Zhang & Prosperetti (1991) for this limiting case. Once again, the effective-medium predictions are shown to be in excellent agreement with these rigorous calculations.

We also compare the predictions of the theory with the experimental data on attenuation. Probably the best data in the literature are due to Allegra & Hawley (1972) who measured attenuation in a polystyrene–water system at frequencies for which the thermal effects contribute most significantly to the attenuation. Our theory is shown to be in excellent agreement with their data. To test the theory for the cases in which the attenuation due to viscous and scattering effects is significant, we have measured attenuation in glass–water and glass–water/glycerol systems at small to intermediate frequencies. For smaller particles, for which the viscous attenuation dominates, the theory and experiments are in very good agreement with each other. For larger particles, for which the scattering dominates, the agreement is very good only up to about 30% volume fractions.

The organization of the rest of the paper is as follows. In § 2 we derive rigorous average equations for linear acoustics and introduce effective properties of the suspensions. In § 3 we compare the predictions of the effective-medium theory with various analytical results and show how the effective properties vary with the frequency and particle volume fraction. Section 4 describes the experimental set-up used for obtaining attenuation data. Section 5 gives a comparison between the theory and various experimental data. In § 6 we present some results on the phase speed of sound waves, and discuss the possibility of using phase speed measurements for measuring particle volume fractions. Finally, § 7 summarizes important findings of the study.

2. Theory

2.1. *Linearized equations*

Let us consider a small-amplitude plane acoustic wave with frequency ω propagating through a uniform, monodisperse suspension of solid particles of radius a. We write the density as $\rho + \rho' e^{-i\omega t}$, the temperature as $T + T' e^{-i\omega t}$, and the velocity as $\boldsymbol{u} e^{-i\omega t}$. A note regarding the notation: both the equilibrium and small fluctuation values are important for the density and temperature and we therefore use primes to denote the amplitudes of the fluctuations in these quantities. Only the amplitudes of the velocity and the other field variables (stress, heat flux, etc.) will be needed, and we denote the amplitudes of these quantities without a prime so that the resulting equations look less cluttered. When the amplitudes ρ', T' and $\boldsymbol{u}$ are small, the terms involving the products of these quantities can be neglected from the continuity, momentum, and energy equations to obtain the following linearized equations:

$$-i\omega\rho' + \rho\nabla\cdot\boldsymbol{u} = 0, \tag{1}$$

$$-i\omega\rho u_i = \frac{\partial\sigma_{ij}}{\partial x_j}, \tag{2}$$

$$-i\omega\rho C_v T' = -\frac{\partial q_j}{\partial x_j} - \rho C_v \beta^{-1}(\gamma - 1)\nabla\cdot\boldsymbol{u}. \tag{3}$$

In writing the last equation, we have made use of the linearized equation of state to eliminate the pressure from the usual energy equation. The stress tensor amplitude σ_{ij} for a Newtonian fluid is given by

$$\sigma_{ij} = \left[\left\{-\frac{c^2\rho}{i\omega\gamma} + \mu_v\right\}\nabla\cdot\boldsymbol{u} - \left\{\frac{\rho(\gamma-1)C_v}{\beta T}\right\}T'\right]\delta_{ij} + d_{ij} \tag{4}$$

where d_{ij} is the deviatoric stress amplitude

$$d_{ij} = \mu\left[\frac{\partial u_i}{\partial x_j} + \frac{\partial u_j}{\partial x_i} - \tfrac{2}{3}\delta_{ij}\nabla\cdot\boldsymbol{u}\right]. \tag{5}$$

C_v is the constant volume specific heat, $\gamma = C_p/C_v$ is the ratio of specific heats, μ and μ_v are, respectively, the shear and bulk coefficients of viscosity, c is the adiabatic sound speed through the fluid, and β is the coefficient of thermal expansion. Note that the first and the third terms inside the square brackets on the right-hand side of (4) are related to the thermodynamic pressure amplitude:

$$p' = \left(\frac{\partial p}{\partial\rho}\right)_T \rho' + \left(\frac{\partial p}{\partial T}\right)_\rho T' = \frac{c^2}{\gamma}\rho' + \frac{\rho(\gamma-1)C_v}{\beta T}T'. \tag{6}$$

Finally, $q_j = -\kappa\partial T'/\partial x_j$ in (3) is the heat flux amplitude, κ being the thermal conductivity.

Inside the solid particles equations similar to (1)–(3) apply with the stress tensor given by (Landau & Lifschitz 1986)

$$\sigma_{ij} = \left[\left\{\frac{\tilde{\lambda} + \frac{2}{3}\tilde{\mu}}{-i\omega}\right\}\nabla\cdot\boldsymbol{u} - \left\{\frac{\rho(\gamma-1)C_v}{\beta T}\right\}T'\right]\delta_{ij} + \tilde{d}_{ij}, \tag{7}$$

where $\tilde{\lambda}$ and $\tilde{\mu}$ are the Lamé constants for the particles which are assumed to be perfectly elastic. Note that for solids it is customary to write the stress in terms of displacement instead of velocity. For small-amplitude oscillatory motions the

amplitudes of the two are, of course, related by a factor of $1/(-\mathrm{i}\omega)$, and this fact has been used in writing the first term on the right-hand side of the above equation. Note also that the factor $\tilde{\lambda}+(2/3)\tilde{\mu}$ is the bulk modulus of the solid. Thus, the isotropic part of the stress tensor represented by the terms inside the square brackets in the above equation arises from the density and temperature changes in the solid. The deviatoric stress tensor $\tilde{d}_{ij}$ is defined in the manner similar to (5), with the fluid viscosity replaced by the 'particle viscosity', $\mu_p = \tilde{\mu}/(-\mathrm{i}\omega)$. Note that the Lamé constant $\tilde{\mu}$ is sometimes referred to as the shear modulus.

The above linearized equations must be solved subject to the boundary conditions of continuity of velocity, temperature, heat flux, and traction ($\sigma_{ij}n_j$, n_j being the unit outward normal at the particle surface) at the interface between the particles and the fluid. In concentrated suspensions particle interactions are significant and the rigorous evaluation of sound speed and attenuation through the suspension would require the very difficult task of solving the above set of equations in a domain containing many particles.

The problem as outlined here involves a number of variables. It may be possible to simplify it in some limiting cases of small or large frequencies or when the physical properties (e.g. density and compressibility) of the two phases are widely different as in the case of acoustic propagation in bubbly liquids (Prosperetti 1984). However, it is desirable to measure the attenuation over a wide range of frequencies in order to characterize the suspension, and for most solid–liquid suspensions the ratio of physical properties does not differ significantly from unity. Thus, it is necessary to solve the full problem as described above.

2.2. *Ensemble-averaged linearized equations for suspensions*

In this subsection we ensemble-average the equations for the amplitudes of density, velocity, and temperature in the fluid and solid phases, and obtain thereby the linearized continuity, momentum, and energy equations for the suspension. It will be shown that the resulting equations have a form similar to the equations for a single phase provided that the suspension is assigned suitable properties, which we refer to as the effective properties of the suspensions. An important outcome of the averaging process will be that it will yield rigorous expressions for various effective properties of the suspension. Unlike the case of single-phase fluids, the effective properties will be seen to be functions of the wave frequency, and the equations we derive are therefore restricted to small-amplitude sinusoidal acoustic waves.

Let us denote by $g(\boldsymbol{x})$ the particle indicator function defined to be unity when the point $\boldsymbol{x}$ is inside any of the particles and zero when $\boldsymbol{x}$ is in the fluid. The properties and field variables of the liquid and particles will be denoted by subscripts l and p, respectively. The ensemble-averaged variables will be denoted by angular brackets.

Multiplying the continuity equation for the liquid by the liquid indicator function $1-g$ and for the particle by g, adding the two, and averaging the resulting equation we obtain the continuity equation for the suspension:

$$-\mathrm{i}\omega\langle\rho'\rangle + \rho_l\langle(1-g)\nabla\cdot\boldsymbol{u}_l\rangle + \rho_p\langle g\nabla\cdot\boldsymbol{u}_p\rangle = 0. \tag{8}$$

The last two terms on the left-hand side of the above equation must now be expressed in terms of the divergence of the average velocity, i.e. $\nabla\cdot\langle\boldsymbol{u}\rangle$, so that the resulting equation resembles the continuity equation of a single-phase medium (cf. (1)). We begin with the identity

$$\rho_l\langle(1-g)\nabla\cdot\boldsymbol{u}_l\rangle + \rho_p\langle g\nabla\cdot\boldsymbol{u}_p\rangle = \rho_l\nabla\cdot\langle\boldsymbol{u}\rangle + (\rho_p-\rho_l)\langle g\nabla\cdot\boldsymbol{u}_p\rangle + \rho_l\langle(\boldsymbol{u}_l-\boldsymbol{u}_p)\cdot\nabla g\rangle. \tag{9}$$

The gradient of the indicator function is zero at all points except at the particle–fluid interface where it is proportional to the Dirac delta function owing to the step jump in g across the particle–fluid interface. More specifically,

$$\nabla g = -\boldsymbol{n}\delta(\boldsymbol{x} - \boldsymbol{x}_s), \tag{10}$$

where $\boldsymbol{x} = \boldsymbol{x}_s$ represents the surface of the particles, δ is the Dirac delta function, and $\boldsymbol{n}$ is the unit normal vector, pointing into the fluid, at the particle surface.

Because the velocity is continuous across the solid–fluid interfaces, the last term in (9) vanishes; the second term on the right-hand side contains an as yet unknown quantity, $\langle g\nabla \cdot \boldsymbol{u}_p \rangle$, which is related to the average amplitude of the dilatation rate inside the particles. We shall restrict our analysis to the suspensions which are isotropic on a macroscale. For such suspensions the above quantity will be expected to be proportional to the amplitude of other scalar quantities such as $\nabla \cdot \langle \boldsymbol{u} \rangle$, the average amplitude for the mixture dilatation rate. We therefore introduce the closure relation

$$\langle g(\boldsymbol{x})(\nabla \cdot \boldsymbol{u}_p)(\boldsymbol{x}) \rangle = \phi \lambda_\rho \nabla \cdot \langle \boldsymbol{u} \rangle(\boldsymbol{x}), \tag{11}$$

where ϕ is the volume fraction of the solids. The passage of a wave will induce non-zero amplitudes of other scalar quantities such as $\langle T' \rangle$ and $\langle \sigma_{kk} \rangle$ also, and one may write a more general expression in which the average particle dilatation rate is expressed as a linear combination of all these scalar variables. In that case one must determine separately how variation in temperature, pressure and density affect separately the dilatation inside the particles. However, since all these scalar variables will be related to each other through algebraic relations that depend on the frequency and effective wavenumbers for the special case of sinusoidal acoustic waves, it is unnecessary to decompose the particle dilatation into various terms. Likewise, the dilatation rate for particles may also depend on the higher-order scalar derivatives such as $\nabla^2 \nabla \cdot \langle \boldsymbol{u} \rangle$. Since the average equations for the suspension are expected to obey wave equations, the Laplacian of the average dilatation rate can always be written in terms of the dilatation rate and the effective wavenumbers. Thus, it will suffice to use (11) for the dilatation rate inside the particles keeping in mind that λ_ρ must be evaluated such that it accounts for not only the first derivative of the suspension velocity, but also its higher-order derivatives and temperature and pressure. The calculation for λ_ρ to be presented in the next section does account for all these effects.

We note that in the present study we are interested in deriving a dispersion relation for the passage of small-amplitude acoustic waves through a suspension, and not a set of average equations valid for all suspension flows. The latter can indeed be a daunting task as equations such as (11) will not apply to the general case for which, as mentioned above, the effects of temperature, pressure, etc. must all be written separately, and the closure relation will possibly also include the higher-order derivatives. The procedure, however, is general enough in the sense that it can be used to determine the dispersion relation for other small-amplitude acoustic problems. For example, it can also be used for determining the dispersion relation for fluid-saturated porous media, which are sometimes modelled as fixed beds. Note that for the fixed bed case although the average particle velocity $\langle \boldsymbol{u}_p \rangle \equiv \langle g\boldsymbol{u}_p \rangle / \phi$ is zero, the left-hand side of (11), and hence λ_ρ, are non-zero. The radial oscillations of the fixed particles will contribute to λ_ρ in such a situation. Note that $\nabla \cdot \langle \boldsymbol{u} \rangle$ is non-zero in all acoustic problems.

Substituting for $\langle g\nabla \cdot \boldsymbol{u}_p \rangle$ from (11) into (9) yields the continuity equation for the

suspension given by

$$-\mathrm{i}\omega\langle\rho'\rangle + \rho_{c,e}\nabla\cdot\langle\boldsymbol{u}\rangle = 0, \tag{12}$$

with the effective equilibrium density of the suspension to be used in the suspension continuity equation, i.e. $\rho_{c,e}$, given by

$$\rho_{c,e} = \rho_l + (\rho_p - \rho_l)\phi\lambda_\rho. \tag{13}$$

Physically, λ_ρ represents the ratio of average dilatation amplitude in the particle phase to that in the fluid–particle mixture or the suspension. This coefficient will depend, in addition to wave frequency, on the compressibilities of both phases, volume fraction, spatial distribution of the particles, and other variables appearing in the governing equations listed in the previous subsection. Thus, we see that, in general, the effective equilibrium density of the suspension to be used in the suspension continuity equation cannot be given by some arbitrary mixture rule, e.g. the volume-averaged density or the mass-averaged density. An approximate scheme for estimating λ_ρ will be described in § 2.4.

We now proceed to derive the momentum equation for the suspension starting from (2) and its counterpart for the particles. Using the same procedure as in the continuity equation we obtain

$$-\mathrm{i}\omega\rho_{m,e}\langle u_i\rangle = \left\langle \mathrm{g}\frac{\partial\sigma_{ij,p}}{\partial x_j}\right\rangle + \left\langle (1-\mathrm{g})\frac{\partial\sigma_{ij,l}}{\partial x_j}\right\rangle. \tag{14}$$

The effective (equilibrium) density of the suspension to be used in the momentum equation, $\rho_{m,e}$, is given by

$$\rho_{m,e} = \rho_l + (\rho_p - \rho_l)\phi\lambda_v \tag{15}$$

with the coefficient λ_v defined by

$$\phi\lambda_v\langle\boldsymbol{u}\rangle(\boldsymbol{x}) = \langle g(\boldsymbol{x})\boldsymbol{u}_p(\boldsymbol{x})\rangle. \tag{16}$$

Physically, λ_v represents the ratio of average velocity amplitude inside the particles to that in the suspension. Once again this coefficient, and other such coefficients to be introduced in this subsection, will, in general, depend on complex multiparticle interactions, and the details of its evaluation will be described later.

The right-hand side of (14) can be simplified using the identity

$$\begin{aligned}\frac{\partial\langle\sigma_{ij}\rangle}{\partial x_j} &\equiv \frac{\partial}{\partial x_j}\langle \mathrm{g}\sigma_{ij,p} + (1-\mathrm{g})\sigma_{ij,l}\rangle \\ &= \left\langle \mathrm{g}\frac{\partial\sigma_{ij,p}}{\partial x_j}\right\rangle + \left\langle (1-\mathrm{g})\frac{\partial\sigma_{ij,l}}{\partial x_j}\right\rangle + \left\langle (\sigma_{ij,p}-\sigma_{ij,l})\frac{\partial \mathrm{g}}{\partial x_j}\right\rangle.\end{aligned} \tag{17}$$

The last term in the above equation, being related to the jump in the traction across the interface, vanishes owing to the boundary condition $\sigma_{ij,p}n_j = \sigma_{ij,l}n_j$ at the particle–fluid interface. Thus, we see that the right-hand side of (14) simply equals the divergence of the average stress in the suspension, i.e. the momentum equation for the suspension is given by

$$-\mathrm{i}\omega\rho_{m,e}\langle u_i\rangle = \frac{\partial\langle\sigma_{ij}\rangle}{\partial x_j}. \tag{18}$$

We must supplement the above momentum equation with an expression for the average stress. The linearity of the equations implies that the stress amplitude will be linear in the gradient of average velocity amplitude and $\langle T'\rangle$.

Let us first consider the isotropic part of the average stress or, equivalently, the stress trace. Multiplying the isotropic part in (4) by $1-g$ and that in (7) by g and averaging, we obtain

$$\tfrac{1}{3}\langle\sigma_{kk}\rangle = \left\{\frac{\langle c^2\rho\gamma^{-1}\rangle_e}{-\mathrm{i}\omega} + \mu_{v,e}\right\}\nabla\cdot\langle\boldsymbol{u}\rangle - T^{-1}\left\langle\rho(\gamma-1)C_v\beta^{-1}\right\rangle_{m,e}\langle T'\rangle \tag{19}$$

with

$$\langle c^2\rho\gamma^{-1}\rangle_e = c_l^2\rho_l/\gamma_l + \phi\lambda_\rho\left[\left\{\tilde{\lambda}+2\tilde{\mu}/3\right\} - c_l^2\rho_l/\gamma_l\right], \tag{20}$$

$$\mu_{v,e} = \mu_v(1-\phi\lambda_\rho), \tag{21}$$

and

$$\left\langle\rho(\gamma-1)C_v\beta^{-1}\right\rangle_{m,e} = \rho_l(\gamma_l-1)C_{v,l}\beta_l^{-1} + \phi\lambda_T\left(\rho_p(\gamma_p-1)C_{v,p}\beta_p^{-1} - \rho_l(\gamma_l-1)C_{v,l}\beta_l^{-1}\right). \tag{22}$$

The coefficient λ_ρ was defined earlier (cf. (11)). λ_T, on the other hand, is a new coefficient which is defined as the ratio of average temperature amplitude inside the particles to that in the mixture, i.e.

$$\phi\lambda_T\langle T'\rangle(\boldsymbol{x}) = \langle g(\boldsymbol{x})T_p'(\boldsymbol{x})\rangle. \tag{23}$$

Both the effective $c^2\rho/\gamma$ and the bulk viscosity of the suspension depend on the coefficient λ_ρ. This is not surprising since both depend on the average dilatation amplitude inside the particles. The result that the effective bulk viscosity $\mu_{v,e}$ of the suspension depends only on the bulk viscosity of the fluid may appear strange at first sight, but it is really a consequence of the way the isotropic part of the stress is defined for the liquid and solids (cf. (4) and (7)). The stress arising from the thermal expansion or, equivalently, temperature fluctuations depends on $\rho(\gamma-1)C_v/\beta T$ of the two phases and the relative temperature fluctuations in the two phases.

Since the deviatoric stress amplitudes in the individual phases depend only on the velocity gradient amplitude, we expect the average deviatoric stress to be linear in the gradient of average velocity amplitude. It also must be traceless. If we further assume that the suspension is macroscopically isotropic, then the average deviatoric stress is characterized by a single effective (shear) viscosity, μ_e. Thus, we write

$$\langle d_{ij}\rangle = \mu_e\left(\frac{\partial\langle u_i\rangle}{\partial x_j} + \frac{\partial\langle u_j\rangle}{\partial x_i} - \tfrac{2}{3}\delta_{ij}\nabla\cdot\langle\boldsymbol{u}\rangle\right). \tag{24}$$

To obtain an expression for the effective viscosity we need to evaluate only one component of the average deviatoric stress. We shall take, without loss of generality, the mean velocity amplitude to be given by

$$\langle\boldsymbol{u}\rangle(\boldsymbol{x}) = -\nabla\mathrm{e}^{\mathrm{i}\boldsymbol{k}_{ce}\cdot\boldsymbol{x}} = -\mathrm{i}\boldsymbol{k}_{ce}\mathrm{e}^{\mathrm{i}\boldsymbol{k}_{ce}\cdot\boldsymbol{x}}, \tag{25}$$

where $\boldsymbol{k}_{ce}$ is the effective wavenumber vector for the compressional wave through the suspension. We shall choose this vector to be aligned along the x_1-axis. The 11-component of the deviatoric stress is given by

$$\langle d_{11}\rangle = 2\left\langle\mu\frac{\partial u_1}{\partial x_1}\right\rangle - \frac{2}{3}\left\langle\mu\frac{\partial u_k}{\partial x_k}\right\rangle. \tag{26}$$

The last term on the right-hand side of the above equation, being related to the dilatation amplitudes, can be readily related to the coefficient λ_ρ introduced earlier.

The first term on the right-hand side can be expressed in terms of a coefficient λ_d defined by

$$\phi\lambda_d \frac{\partial\langle u_1\rangle}{\partial x_1} = \left\langle g(\boldsymbol{x}) \frac{\partial u_1^p}{\partial x_1}(\boldsymbol{x}) \right\rangle. \tag{27}$$

With this definition it is straightforward now to relate $\langle d_{11}\rangle$ to the gradient in velocity amplitude:

$$\langle d_{11}\rangle = 2\left[\mu_l + \phi\lambda_d\left(\mu_p - \mu_l\right)\right] \frac{\partial\langle u_1\rangle}{\partial x_1} - \tfrac{2}{3}\left[\mu_l + \phi\lambda_\rho\left(\mu_p - \mu_l\right)\right] \frac{\partial\langle u_k\rangle}{\partial x_k}. \tag{28}$$

Substituting for $\langle \boldsymbol{u}\rangle$ from (25) in (28) and in (24) with $i = j = 1$ and comparing the resulting expressions yields the following expression for the effective viscosity:

$$\mu_e = \mu_l + \tfrac{1}{2}\phi(\mu_p - \mu_l)\left(3\lambda_d - \lambda_\rho\right). \tag{29}$$

Finally, the energy equation for the suspension, obtained by averaging $1 - g$ times the energy equation for the liquid plus g times that for the solid, is given by

$$-\mathrm{i}\omega\langle\rho C_v\rangle_e\langle T'\rangle = -\frac{\partial\langle q_j\rangle}{\partial x_j} - \left\langle\rho C_v\beta^{-1}(\gamma - 1)\right\rangle_{e,e} \nabla\cdot\langle\boldsymbol{u}\rangle. \tag{30}$$

Here an argument similar to (17) has been used to simplify the energy-flux term (thereby using the boundary condition at the particle surface that the heat flux is continuous). In (30) the effective heat capacity of the suspension is given by

$$\langle\rho C_v\rangle_e = \rho_l C_{v,l} + \phi\lambda_T\left(\rho_p C_{v,p} - \rho_l C_{v,l}\right) \tag{31}$$

with λ_T defined by (23). The effective property $\langle\rho C_v(\gamma - 1)\beta^{-1}\rangle_{e,e}$ appearing in the last term on the right-hand side of (30) is related to λ_ρ, and the expression for evaluating it is obtained by replacing λ_T in (22) by λ_ρ.

The average heat flux amplitude is written as

$$\langle q_j\rangle = -\kappa_e \frac{\partial\langle T'\rangle}{\partial x_j} \tag{32}$$

with the effective conductivity

$$\kappa_e = \kappa_l + \phi\lambda_\kappa\left(\kappa_p - \kappa_l\right), \tag{33}$$

where the coefficient λ_κ is the ratio of the average temperature gradient amplitude inside the particles to that in the suspension, i.e.

$$\phi\lambda_\kappa \frac{\partial\langle T'\rangle}{\partial x_i} = \left\langle g(\boldsymbol{x}) \frac{\partial T_p'}{\partial x_i}(\boldsymbol{x}) \right\rangle. \tag{34}$$

In summary, the continuity, momentum, and energy equations for the suspension are given by (8), (18) and (30), the average stress tensor by (19) and (24), and the average heat flux by (32). These equations resemble the equations for the single phase given in § 2.1 with suitably defined effective properties of the suspension. It must be noted that these equations are rigorous for small-amplitude sinusoidal waves through any suspension. The effective properties of the suspension will be functions of frequency and physical properties of the two phases as well as the microstructure of the suspension. Note also that properties such as $\rho_{c,e}$, the effective density to be used in the suspension continuity equation, will not depend only on the density and compressibility of the two phases but also on their thermal properties since its determination will require solving all the microscale equations simultaneously.

2.3. *Wave equations for the suspension*

To find an expression for the attenuation of sound waves in a suspension it is necessary to derive wave equations from the linearized acoustic equations for the suspension as was done by Epstein & Carhart (1953) for pure liquid. We shall follow that derivation closely here. As shown by these investigators the acoustics equations permit three waves: a thermal wave, a shear or rotational wave, and a compressional wave. The last one is the most significant as far as the attenuation of a plane acoustic wave is concerned. The other waves are important in determining the disturbance produced by a test particle in the suspension as we shall see in the next subsection.

We decompose the average velocity amplitude in scalar and vector potentials, given by

$$\langle \boldsymbol{u} \rangle = -\nabla \Phi + \nabla \times \boldsymbol{A}. \tag{35}$$

Since the curl of a gradient of any scalar function is zero, $\boldsymbol{A}$ can be specified to within a gradient of an arbitrary scalar function. To remove this arbitrariness an additional restriction is imposed that $\boldsymbol{A}$ be divergence free, i.e. $\nabla \cdot \boldsymbol{A} = 0$. It may be noted that the vorticity amplitude equals $-\nabla^2 \boldsymbol{A}$.

Introducing the decomposition in the momentum equation for the suspension (18), and rearranging, we obtain

$$\nabla \left[\mathrm{i}\omega \rho_{m,e} \Phi + \left\{ \frac{\langle c^2 \rho \gamma^{-1} \rangle_e}{-\mathrm{i}\omega} + \mu_{v,e} + \tfrac{4}{3}\mu_e \right\} \nabla^2 \Phi + \frac{1}{T} \langle \rho(\gamma - 1) C_v \beta^{-1} \rangle_e \langle T' \rangle \right]$$
$$= \nabla \times \left[\mathrm{i}\omega \rho_{m,e} \boldsymbol{A} - \mu_e \nabla \times (\nabla \times \boldsymbol{A}) \right]. \tag{36}$$

Here, we have used the vector identity $\nabla^2 \boldsymbol{a} = \nabla(\nabla \cdot \boldsymbol{a}) - \nabla \times (\nabla \times \boldsymbol{a})$. The energy equation (30) becomes

$$-\mathrm{i}\omega \langle \rho C_v \rangle_e \langle T' \rangle = \kappa_e \nabla^2 \langle T' \rangle + \langle \rho C_v \beta^{-1} (\gamma - 1) \rangle_{e,e} \nabla^2 \Phi. \tag{37}$$

Both sides of (36) must vanish separately because a rotational vector field cannot balance an irrotational field. Hence the right-hand side being zero gives, after using the above-mentioned vector identity and $\nabla \cdot \boldsymbol{A} = 0$,

$$\nabla^2 \boldsymbol{A} + k_{se}^2 \boldsymbol{A} = \boldsymbol{0} \tag{38}$$

with $k_{se}^2 \equiv \mathrm{i}\omega \rho_{m,e} / \mu_e$; k_{se} is the effective wavenumber for shear waves through the suspension.

The left-hand side of (36) being zero gives an expression for $\langle T' \rangle$ in terms of the velocity potential:

$$\langle T' \rangle = T \left[-\mathrm{i}\omega \rho_{m,e} \Phi - \left\{ \frac{\mathrm{i}}{\omega} \langle c^2 \rho \gamma^{-1} \rangle_e + (\mu_{v,e} + \tfrac{4}{3}\mu_e) \right\} \nabla^2 \Phi \right] \Big/ \langle \rho(\gamma - 1) C_v \beta^{-1} \rangle_{m,e}. \tag{39}$$

Eliminating $\langle T' \rangle$ from the energy equation for the suspension (37) by substituting for $\langle T' \rangle$ from the above yields

$$\Phi + (E - F + G) \nabla^2 \Phi - EF \nabla^4 \Phi = 0, \tag{40}$$

with

$$E = \frac{\langle c^2 \rho \gamma^{-1} \rangle_e}{\rho_{m,e} \omega^2} - \frac{\mathrm{i}}{\rho_{m,e} \omega} (\mu_{v,e} + \tfrac{4}{3}\mu_e), \tag{41}$$

$$F = \frac{\mathrm{i}\kappa_e}{\omega \langle \rho C_v \rangle_e}, \tag{42}$$

$$G = \frac{\langle \rho C_v \beta^{-1}(\gamma - 1) \rangle_{e,e} \langle \rho(\gamma - 1) C_v \beta^{-1} \rangle_{m,e}}{T \rho_{m,e} \omega^2 \langle \rho C_v \rangle_e}. \tag{43}$$

Equation (40) can be written in the form

$$\left(k_{ce}^{-2}\nabla^2 + 1\right)\left(k_{te}^{-2}\nabla^2 + 1\right)\Phi = 0, \tag{44}$$

so that $\Phi = \Phi_c + \Phi_t$ with

$$\left(\nabla^2 + k_{ce}^2\right)\Phi_c = 0, \tag{45}$$

$$\left(\nabla^2 + k_{te}^2\right)\Phi_t = 0. \tag{46}$$

The effective wavenumbers for the compressional and thermal waves are given by, respectively,

$$k_{ce}^{-2} = \tfrac{1}{2}(E - F + G) + \tfrac{1}{2}\left\{(E - F + G)^2 + 4EF\right\}^{1/2}, \tag{47}$$

$$k_{te}^{-2} = \tfrac{1}{2}(E - F + G) - \tfrac{1}{2}\left\{(E - F + G)^2 + 4EF\right\}^{1/2}. \tag{48}$$

As mentioned earlier the compressional wavenumber is the most important one as far as the acoustic wave propagation of the plane wave is concerned. The imaginary part of k_{ce} gives the attenuation while ω divided by the real part of k_{ce} gives the phase speed.

For future reference we note that the expression (39) for $\langle T' \rangle$ now can be written as

$$\langle T' \rangle = b_{ce}\Phi_c + b_{te}\Phi_t \tag{49}$$

with

$$b_{ce} = T\left[-\mathrm{i}\omega\rho_{m,e} + \left\{\frac{i}{\omega}\langle c^2\rho\gamma^{-1}\rangle_e + \left(\mu_{v,e} + \tfrac{4}{3}\mu_e\right)\right\}k_{ce}^2\right] \Big/ \langle \rho(\gamma - 1)C_v\beta^{-1}\rangle_{m,e}. \tag{50}$$

The expression for b_{te} is similar with k_{ce} in the above replaced by k_{te}.

2.4. *An effective-medium model*

To determine the attenuation and phase speed we must now estimate various effective properties of the suspensions. This requires determining five coefficients: λ_ρ, λ_v, λ_T, λ_d, and λ_κ. Let us begin with the evaluation of λ_ρ which represents the ratio of average dilatation amplitude inside the particles to that in the suspension. This is defined by (11), which is equivalent to

$$\phi\lambda_\rho \nabla \cdot \langle \boldsymbol{u} \rangle(\boldsymbol{x}) = \int_{|\boldsymbol{x} - \boldsymbol{x}_1| \leqslant a} \langle \nabla \cdot \boldsymbol{u}_p \rangle(\boldsymbol{x}|\boldsymbol{x}_1) P(\boldsymbol{x}_1) \mathrm{d}V(\boldsymbol{x}_1). \tag{51}$$

Here, we have introduced a conditionally averaged field. Thus, $\langle \boldsymbol{u} \rangle(\boldsymbol{x}|\boldsymbol{x}_1)$ is the ensemble-averaged velocity amplitude at point $\boldsymbol{x}$ given a particle centred at $\boldsymbol{x}_1$. $P(\boldsymbol{x}_1)$ is the probability density for finding a particle with its centre in the vicinity of $\boldsymbol{x}_1$. For uniform, monodisperse suspensions $P(\boldsymbol{x}_1) = n = 3\phi/(4\pi a^3)$, n being the number density of the particles and ϕ the particle volume fraction.

We shall use an effective-medium approximation for determining the conditionally averaged fields, and hence, the integrals such as the one appearing on the right-hand side of (51). All effective-medium approximations must satisfy the criterion that far from the test particle, i.e. for $|\boldsymbol{x} - \boldsymbol{x}_1| \to \infty$, the conditionally averaged fields such as $\langle \boldsymbol{u} \rangle(\boldsymbol{x}|\boldsymbol{x}_1)$ must approach the corresponding unconditionally averaged fields such as $\langle \boldsymbol{u} \rangle(\boldsymbol{x})$. On the other hand, for $|\boldsymbol{x} - \boldsymbol{x}_1| \leqslant a$, i.e. for a point inside the test particle, the conditionally averaged fields must satisfy the equations governing the particle

phase. The simplest kind of effective medium approximation then assumes that the conditionally averaged equation satisfies the suspending fluid equations for $a \leqslant r \leqslant R$ and the unconditionally averaged equations for the suspension for $r \geqslant R$. Here, $r \equiv |\boldsymbol{x} - \boldsymbol{x}_1|$ is the distance from the centre of the particle. Different effective-medium approximations differ in their choice of R. Some investigators choose $R = a$ which eliminates the fluid region altogether. This makes the subsequent analysis very simple but, unfortunately, the estimates obtained with $R = a$ are typically inferior, and in some cases unphysical. For example, it may yield negative effective properties at high volume fractions. Other investigators choose $R = a\phi^{-1/3}$ with the incorrect reasoning that the volumes occupied by the particle and fluid for $r \leqslant R$ must be proportional to the volume fractions of the two phases. In the present study we shall choose R to be given by

$$\frac{R}{a} = \left(\frac{1 - S(\mathbf{0})}{\phi}\right)^{1/3}, \tag{52}$$

with $S(\mathbf{0})$ the zero-wavenumber limit of the suspension structure factor defined by

$$S(\mathbf{0}) = \int \left[P(\boldsymbol{r}|\mathbf{0}) - P(\mathbf{0})\right] \mathrm{d}\boldsymbol{r}, \tag{53}$$

where $P(\boldsymbol{r}|\mathbf{0})$ is the probability density for finding a particle with its centre near $\boldsymbol{r}$ given that there is a particle with its centre at origin. Note that $P(\boldsymbol{r}|\mathbf{0}) = \delta(\boldsymbol{r})$ for $r < 2a$. The above choice of R is such that

$$\int_{r \geqslant 2a} [P(\boldsymbol{r}|\mathbf{0}) - P(\mathbf{0})] \mathrm{d}\boldsymbol{r} = \int_{R \leqslant r \leqslant 2a} P(\mathbf{0}) \mathrm{d}\boldsymbol{r}. \tag{54}$$

In other words, the excess particle density outside the exclusion region in a suspension is distributed over a distance r ranging from R to $2a$ in the effective medium.

The structure factor of the suspension can be determined experimentally by a light-scattering technique but in the absence of such information one may choose $S(\mathbf{0})$ to correspond to that of a hard-sphere molecular system for which the well-known Carnahan–Starling approximation yields quite accurate estimates of the structure factor as a function of the volume fraction:

$$S(\mathbf{0}) = \frac{(1 - \phi)^4}{1 + 4\phi + 4\phi^2 - 4\phi^3 + \phi^4}. \tag{55}$$

The effective-medium radius R based on $S(\mathbf{0})$ was first introduced by Dodd *et al.* (1995) who compared the results of rigorous multiparticle interactions for determining the short-time self- and gradient-diffusivity of proteins in bilipid membranes with those obtained by the effective-medium approximation and found a very good agreement between the two. In the problems concerned with determining the collective mobility or the sedimentation velocity, where each particle is acted upon with a constant force, it was shown in Mo & Sangani (1994) that the conditionally averaged velocity has the correct leading-order behaviour at large r only when R is chosen according to (52).

For small volume fractions, $S(\mathbf{0})$ given by (55) behaves as $1 - 8\phi + O(\phi^2)$, and $R \to 2a$. Thus, in 'well-stirred' dilute random suspensions the effective medium begins at $r = 2a$ according to (52) and the fluid region $a < r < 2a$ corresponds to the excluded-volume region. Note that the more usual choice $R = a\phi^{-1/3}$ would, on the other hand, suggest that the effective medium begins at a very large distance from the test particle in a dilute suspension, which is unphysical except for the situations such

as dilute periodic or 'well-separated' random suspensions defined by Jeffrey (1973) (For such arrays $S(\mathbf{0})$ is small when ϕ is small and (52) also gives $R/a = O(\phi^{-1/3})$.) Thus it is not surprising that R based on (52) will give better estimates of the effective properites at small to moderate volume fractions compared to those obtained with $R = a\phi^{-1/3}$. Indeed, Sangani & Mo (1997) have shown that the coefficients of $O(\phi^2)$ corrections to the effective conductivity and elasticity obtained using (52) are much closer to the rigorous results for these coefficients obtained by detailed pair interaction calculations than those obtained with $R = a\phi^{-1/3}$.

Before we close this brief review of effective-medium approximations, we should perhaps note here one more class of effective-medium approximations made in the literature. These involve immersing a pair of particles in the effective medium. Examples are the calculations by Kim & Russel (1985) who estimated the permeability of a fixed bed of particles and Ju & Chen (1994)'s calculations for the effective viscosity and elasticity of suspensions with a hard-sphere spatial distribution. These calculations generally require far greater effort – comparable to direct multiparticle calculations – and do not necessarily yield superior estimates compared with the simple approximations based on a single particle. On the other hand, the single-particle approximations will be inadequate for the suspension problems in which the changes in microstructure due to imposed flow and their effects in turn on the suspension properties must be addressed.

Returning now to the problem of estimating the coefficients λ_p etc. using the effective-medium model consisting of a particle–fluid assembly of radius R immersed in a medium with the effective properties of the suspension, we write the velocity inside the test particle in terms of scalar and vector potentials as in the previous subsection. For the plane wave travelling along the x_1-axis with $\langle \boldsymbol{u} \rangle(\boldsymbol{x}) = -\mathrm{i}\boldsymbol{k}_{ce} \exp(\mathrm{i}\boldsymbol{k}_{ce} \cdot \boldsymbol{x})$ we have, for $|\boldsymbol{x} - \boldsymbol{x}_1| \leqslant a$,

$$\Phi_{cp}(\boldsymbol{x}|\boldsymbol{x}_1) = \exp(\mathrm{i}\boldsymbol{k}_{ce} \cdot \boldsymbol{x}_1) \sum_{n=0}^{\infty} \mathrm{i}^n (2n+1) A_{pn} P_n(\mu) j_n(k_{cp} r), \tag{56}$$

$$\Phi_{tp}(\boldsymbol{x}|\boldsymbol{x}_1) = \exp(\mathrm{i}\boldsymbol{k}_{ce} \cdot \boldsymbol{x}_1) \sum_{n=0}^{\infty} \mathrm{i}^n (2n+1) B_{pn} P_n(\mu) j_n(k_{tp} r), \tag{57}$$

$$A_p(\boldsymbol{x}|\boldsymbol{x}_1) = \exp(\mathrm{i}\boldsymbol{k}_{ce} \cdot \boldsymbol{x}_1) \sum_{n=0}^{\infty} \mathrm{i}^n (2n+1) C_{pn} P_n^1(\mu) j_n(k_{sp} r), \tag{58}$$

where $r = |\boldsymbol{x} - \boldsymbol{x}_1|$, $\mu = \cos\theta$, θ being the angle between $\boldsymbol{x} - \boldsymbol{x}_1$ and $\boldsymbol{k}_{ce}$, j_n is the spherical Bessel function of both the first kind (regular at $r = 0$), P_n is the Legendre polynomial of degree n, and P_n^1 is the associated Legendre polynomial of degree n and order 1. A_p is the only non-zero (azimuthal) component of $\boldsymbol{A}$.

Similar expressions can be written for $a < r < R$ for which the relevant wavenumbers in the expressions for Φ_{cl}, Φ_{tl}, A_l are, respectively, k_{cl}, k_{tl}, and k_{sl}. The spherical harmonics of both the first kind and second kind (corresponding to waves emanating from $r = 0$) must be included in the expression. This leads to a set of six unknowns for each mode n describing the motion in the liquid shell. Finally, for $r > R$, the potentials consist of the plane wave corresponding to the unconditional motion plus outgoing waves with wavenumbers k_{ce}, k_{te}, and k_{se}. Thus, a total of 12 unknowns are needed in describing the motion for each mode n. These are determined from the boundary conditions of continuity of velocity, traction, temperature, and heat flux amplitudes at $r = a$ and $r = R$. Note that the conditional density and temperature amplitudes can

be determined from the expressions for Φ_c, Φ_t, and A using the expressions given in the previous subsection. We keep a total of N modes (typical calculation used $N = 5$) and solve the resulting $12N$ equations numerically.

We return now to the calculation of λ_ρ. We use $\nabla \cdot \boldsymbol{u}_p = -\nabla^2 \Phi_p = k_{cp}^2 \Phi_{cp} + k_{tp}^2 \Phi_{tp}$ to convert the integral in (51) to integrals over Φ_p. Let us introduce a coefficient η_c given by

$$\phi \eta_c \Phi_c(\boldsymbol{x}) \equiv \int_{|\boldsymbol{x}-\boldsymbol{x}_1| \leqslant a} \Phi_{cp}(\boldsymbol{x}|\boldsymbol{x}_1) P(\boldsymbol{x}_1) \mathrm{d}V(\boldsymbol{x}_1). \tag{59}$$

Similarly, a coefficient η_t is introduced with $\Phi_{cp}(\boldsymbol{x}|\boldsymbol{x}_1)$ in the above replaced by $\Phi_{tp}(\boldsymbol{x}|\boldsymbol{x}_1)$. The coefficient λ_ρ is related to these two coefficients by

$$z_{ce}^2 \lambda_\rho = z_{cp}^2 \eta_c + z_{tp}^2 \eta_p. \tag{60}$$

The integration in (59) must be carried out over all $\boldsymbol{x}_1$ such that $|\boldsymbol{x} - \boldsymbol{x}_1| \leqslant a$. To convert this to an integration over $\boldsymbol{r}$ we use the identity

$$\begin{aligned} \exp[\mathrm{i}\boldsymbol{k}_{ce} \cdot \boldsymbol{x}_1] &= \exp[\mathrm{i}\boldsymbol{k}_{ce} \cdot \boldsymbol{x}] \exp[-\mathrm{i}rk_{ce}\mu] \\ &= \exp[\mathrm{i}\boldsymbol{k}_{ce} \cdot \boldsymbol{x}] \sum_{m=0}^{\infty} \mathrm{i}^m (-1)^m (2m+1) j_m(k_{ce} r) P_m(\mu). \end{aligned} \tag{61}$$

Now using $P(\boldsymbol{x}_1) = n$, substituting for Φ_{cp} from (56) into (59), making use of the above identity, and carrying out the integration, we obtain

$$\eta_c = \frac{3}{z_{ce}^2 - z_{cp}^2} \sum_{n=0}^{\infty} (2n+1) A_{pn} \left[z_{cp} j_{n-1}(z_{cp}) j_n(z_{ce}) - z_{ce} j_n(z_{cp}) j_{n-1}(z_{ce}) \right], \tag{62}$$

where $z_{cp} = k_{cp} a$ and $z_{ce} = k_{ce} a$. In the above expression j_{-1} should be taken to be $\cos(z)/z$. In deriving the above expression use has been made of the identity (Gradshteyn & Ryzhik 1994 – note that there is a sign error in their 5.54(1))

$$\begin{aligned} \int r^2 j_n(\alpha r) j_n(\beta r) \mathrm{d}r &= \frac{\pi}{2(\alpha\beta)^{1/2}} \int r J_{n+1/2}(\alpha r) J_{n+1/2}(\beta r) \mathrm{d}r \\ &= \frac{\beta r^2 j_n(\alpha r) j_{n-1}(\beta r) - \alpha r^2 j_{n-1}(\alpha r) j_n(\beta r)}{\alpha^2 - \beta^2} \end{aligned} \tag{63}$$

(recall that $j_n(z) = (\pi/2z)^{1/2} J_{n+1/2}(z)$).

The expression for η_t is similar to (61) with A_{pn} in that expression replaced by B_{pn} and z_{cp} by z_{tp}. Now λ_ρ can be evaluated by substituting for η_c and η_t in (60).

The coefficient λ_T, which represents the ratio of average temperature amplitude inside the test particle to that in the suspension, is also related to η_c and η_t. Inside the particle the temperature amplitude is a linear combination of the potentials as given by $\langle T_p' \rangle(\boldsymbol{x}|\boldsymbol{x}_1) = b_{cp} \Phi_{cp} + b_{tp} \Phi_{tp}$, where b_{cp} and b_{tp} are given by expressions similar to that for b_{ce} given earlier (cf. (50)). Now, since the unconditionally averaged thermal potential, $\Phi_t(\boldsymbol{x})$, is zero, the average temperature amplitude is given by $\langle T' \rangle(\boldsymbol{x}) = b_{ce} \Phi_c$, and therefore

$$\lambda_T = (b_{cp}/b_{ce})\, \eta_c + (b_{tp}/b_{ce})\, \eta_t. \tag{64}$$

The other λ coefficients can be evaluated in a similar manner and are interconnected. To determine λ_v, we need to calculate the average of the x_1-component of the velocity amplitude inside the test particle at $\boldsymbol{x}_1$. Decomposing this velocity into

three parts corresponding to contributions from the three potentials, we write

$$\lambda_v = \lambda_v^{\Phi_c} + \lambda_v^{\Phi_t} + \lambda_v^{A}, \tag{65}$$

where λ_v^{Φ} and λ_v^{A} are the irrotational and rotational field contributions, respectively. It can be shown that

$$\lambda_v^{\Phi_c} = \eta_c + \frac{3}{z_{ce}} \sum_{n=0}^{\infty} A_{pn} j_n(z_{cp}) \left[n j_{n-1}(z_{ce}) - (n+1) j_{n+1}(z_{cp}) \right]. \tag{66}$$

The expression for $\lambda_v^{\Phi_t}$ is similar with η_c, z_{cp}, and A_{pn} in the above expression replaced by, respectively, η_t, z_{tp}, and B_{pn}. In deriving (66) use has been made of (61) and

$$\exp\left[-\mathrm{i}\boldsymbol{k}_{ce} \cdot \boldsymbol{r}\right] \nabla_r \Phi(\boldsymbol{r}) = \nabla_r \left\{ \exp\left[-\mathrm{i}\boldsymbol{k}_{ce} \cdot \boldsymbol{r}\right] \Phi(\boldsymbol{r}) \right\} + \mathrm{i}\boldsymbol{k}_{ce} \exp\left[-\mathrm{i}\boldsymbol{k}_{ce} \cdot \boldsymbol{r}\right] \Phi(\boldsymbol{r}), \tag{67}$$

with $\boldsymbol{r} = \boldsymbol{x} - \boldsymbol{x}_1$. The divergence theorem is used to evaluate the integral of the first term on the right-hand side of (67); the second term on the right-hand side is related to η_c in (66).

To evaluate the rotational contribution to λ_v we use the identity

$$\exp\left[-\mathrm{i}\boldsymbol{k}_{ce} \cdot \boldsymbol{r}\right] \nabla_r \times \boldsymbol{A}(\boldsymbol{r}) = \nabla_r \times \left\{ \exp\left[-\mathrm{i}\boldsymbol{k}_{ce} \cdot \mathbf{r}\right] \boldsymbol{A}(\boldsymbol{r}) \right\} + \exp\left[-\mathrm{i}\boldsymbol{k}_{ce} \cdot \boldsymbol{r}\right] \mathrm{i}\boldsymbol{k}_{ce} \times \boldsymbol{A}(\boldsymbol{r}). \tag{68}$$

The last term on the right-hand side of the above expression does not contribute to the x_1-component of the velocity, and the contribution from the first term can be readily evaluated to give

$$\lambda_v^{A} = \frac{3}{z_{ce}} \sum_{n=1}^{\infty} n(n+1) C_{pn} j_n(z_{sp}) \left[j_{n+1}(z_{ce}) + j_{n-1}(z_{ce}) \right]. \tag{69}$$

The result for λ_v can be used to determine other λ coefficients as well. Thus, it can be shown that

$$\lambda_\kappa = \left(b_{cp}/b_{ce}\right) \lambda_v^{\Phi_c} + \left(b_{tp}/b_{ce}\right) \lambda_v^{\Phi_t}. \tag{70}$$

Finally, λ_d, defined by (27), is written as

$$\lambda_d = \lambda_v + \lambda_d^{\Phi_c} + \lambda_d^{\Phi_t} + \lambda_d^{A}, \tag{71}$$

where we again made use of (67), with Φ replaced by $\boldsymbol{u}$. The result for $\lambda_d^{\Phi_c}$ is

$$\begin{aligned} \lambda_d^{\Phi_c} = \frac{3}{z_{ce}^2} \sum_{n=0}^{\infty} A_{pn} \Bigg[& \left\{ z_{cp} j_n'(z_{cp}) + (n+1) j_n(z_{cp}) \right\} \left\{ \left(\frac{(n+1)^2}{2n+3} + \frac{n^2}{2n-1} \right) j_n(z_{ce}) \right. \\ & \left. - \frac{(n+1)(n+2)}{2n+3} j_{n+2}(z_{ce}) - \frac{n(n-1)}{2n-1} j_{n-2}(z_{ce}) \right\} \\ & + \frac{(n+1)(2n+1)}{2n+3} j_n(z_{cp}) \left\{ (n+2) j_{n+2}(z_{ce}) - (n+1) j_n(z_{ce}) \right\} \Bigg]. \end{aligned} \tag{72}$$

An expression for $\lambda_d^{\Phi_t}$ is obtained from $\lambda_d^{\Phi_c}$ by replacing A_{pn} by B_{pn} and z_{cp} by z_{tp}. The contribution from $\boldsymbol{A}$ is given by

$$\lambda_d^{A} = \frac{3}{z_{ce}^2} \sum_{n=1}^{\infty} (n+1) C_{pn} \left[-\frac{n(n+2)}{2n+3} X_{n,n+2} - \frac{n(2n+1)}{(2n+3)(2n-1)} X_{n,n} + \frac{n(n-1)}{2n-1} X_{n,n-2} \right] \tag{73}$$

	Polystyrene	Glass	Water	Glycerol/water
Density ($g\,cm^{-3}$)	1.055	2.3	1.0	1.08
Thermal conductivity ($J\,K^{-1}\,m\,s$)	1.15×10^{-1}	9.6×10^{-1}	5.87×10^{-1}	4.5×10^{-1}
Specific heat ($J\,g^{-1}K$)	1.19	0.836	4.19	4.19
Thermal expansion coefficient (K^{-1})	2.04×10^{-4}	3.2×10^{-6}	2.04×10^{-4}	3.22×10^{-4}
Sound speed ($cm\,s^{-1}$)	2.3×10^{5}	5.2×10^{5}	1.48×10^{5}	1.6×10^{5}
Shear viscosity ($g\,cm^{-1}\,s^{2}$)	—	—	1.01×10^{-2}	$3 \times 2 \times 10^{-2}$
Bulk viscosity ($g\,cm^{-1}\,s^{2}$)	—	—	3×10^{-2}	9.6×10^{-2}
Shear rigidity ($g\,cm^{-1}\,s^{2}$)	1.27×10^{10}	2.8×10^{11}	—	—

TABLE 1. The values of the physical properties used in the present study.

with the short-hand notation

$$X_{n,m} \equiv -\tfrac{3}{2} j_n(z_{sp}) j_m(z_{ce}) - \tfrac{1}{2}\left[z_{sp} j_n'(z_{sp}) j_m(z_{ce}) + z_{ce} j_n(z_{sp}) j_m'(z_{ce})\right]. \tag{74}$$

The scheme for estimating various effective properties and attenuation is as follows: (i) Assume initially that the effective properties of the suspension are the same as that of pure liquid. (ii) Determine the coefficients A_{pn}, B_{pn}, etc. by solving the twelve equations resulting from the application of boundary conditions at $r = a$ and $r = R$ for each mode n up to $n = 5$. (iii) Estimate λ_ρ, λ_κ, λ_v, etc. using the expressions given in this section. (iv) Estimate the effective properties of the suspension. (v) Repeat steps (ii)–(iv) until all the effective properties have converged to within a specified limit. The attenuation of the wave is given by the imaginary part of k_{ce}.

3. Comparison with known analytical results

We shall assess the effective-medium approximation in two steps. In the first, we consider various limiting situations where we expect some of the effective properties to be dominated by multiparticle interactions in Stokes or Laplace fields for which rigorous results have been obtained in recent years through direct numerical solution of the multiparticle system with hard-sphere spatial configurations. The second step will be to compare the theory with the experimental data available in the literature and some new data generated in our laboratory. This will be done in § 5.

As we have seen the acoustic problem has many variables. This makes it meaningless to present results in terms of one or two non-dimensional numbers. We shall instead choose a particular solid–liquid system and then vary either the radius of the particle or the frequency. The relevant physical properties for glass–water and polystyrene–water systems to be considered in the present study are given in table 1. In some calculations we shall vary the thermal conductivity or density of the particles without varying other physical properties to explore the effect of these properties. In some limiting cases it may be possible to solve a simplified set of equations instead of the $12N$ set of equations required by our scheme. However, since our primary purpose is to assess the effective-medium approximation and the computer program written for this purpose we use the same program in all the comparisons shown here.

The effective viscosity of the suspension will be in general complex with the imaginary part multiplied by frequency being the elasticity of the suspension. Results of rigorous multiparticle computations are available in the literature for the case when inertia is negligible (Stokes flow) and a uniform strain rate is applied to suspensions of rigid particles in an incompressible, Newtonian fluid. The spatial distribution

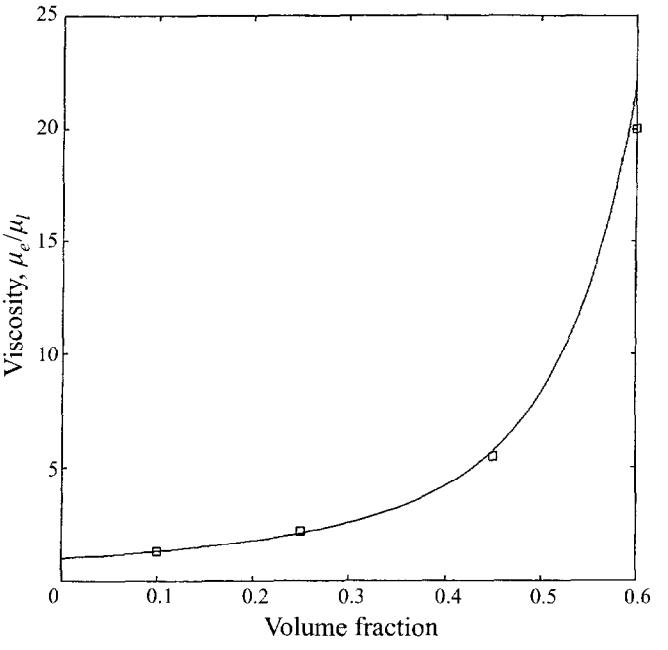

FIGURE 1. Ratio of effective viscosity to liquid viscosity as a function of volume fraction. Limiting values for wavelengths large compared to particle size and viscous boundary layers much larger than the particles. Solid line is theory; squares are numerical simulation results from Sangani & Mo (1997).

of the particles corresponded to the hard-sphere molecular systems for which $S(\mathbf{0})$ given by (55) applies. Ladd (1990) obtained the results with volume fractions (ϕ) in the range 0–0.45. Mo & Sangani (1994) and Sangani & Mo (1997) repeated and confirmed his results and also obtained an additional result for $\phi = 0.6$. Their results are shown in figure 1. To see how well the effective-medium model developed in the present study approximates these values we must pick frequencies for which the quasi-steady Stokes flow approximation will be expected. The ratio of unsteady to viscous terms in the momentum equation for the liquid is $\rho_l \omega a^2/\mu_l$. For $a = 10^{-5}$ cm and $f = \omega/2\pi = 10^6$ Hz this number equals 6×10^{-3} (we have taken water as the suspending liquid but multiplied the viscosity by 10). The wave nature of the governing equations depends on the ratio $k_{cl}a$ which equals 2π times the ratio of particle radius to the wavelength in pure liquid. When this number is small the liquid may be treated as essentially incompressible. For a and f listed above, $k_{cl}a$ for water equals 4.2×10^{-4}. Finally, our calculations account for small deformations of the particles. For particles to be treated as rigid, their shear modulus $\tilde{\mu}$ divided by the frequency must be much larger than the viscosity of the water. At $\omega = 10^6/2\pi$ s^{-1}, the ratio $\tilde{\mu}/(\omega\mu_l)$ equals 2×10^7 and therefore the glass particles may be treated as rigid.

The solid curve in figure 1 represents the estimates of the effective viscosity obtained by the effective medium model for the aforementioned conditions. The ratio $\mathrm{Re}(\mu_e)/\mu_l$ varies from unity to about 20 as ϕ is varied from 0 to 0.6. At high volume fractions significant viscous dissipation occurs in the narrow gap regions between the pairs of particles in close proximity and this dominates the effective viscosity behaviour at high ϕ. This phenomenon cannot be expected to be modelled accurately by the

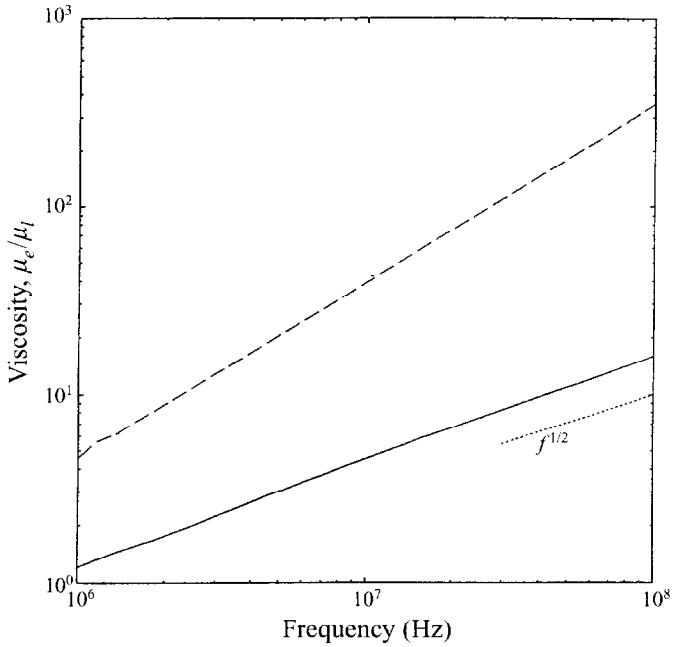

FIGURE 2. Real part minus its limiting value at large wavelengths (—) and minus imaginary part (– – –) of the ratio of effective viscosity to liquid viscosity as a function of frequency. Particle volume fraction is 0.3. The viscous boundary layers at the lowest frequencies are small compared to the particle size (at 1 MHz, $(\mu_l/(\rho_l\omega^2a^2))^{1/2} = 0.01$).

single-particle approximation used here and therefore the excellent agreement found here for $\phi = 0.45$ and 0.6 may be regarded as fortuitous. It should also be noted that the particles in highly concentrated suspensions may begin to be supported by the other particles through the formation of a continuous network such that the suspension behaves like a fluid-filled porous medium. The present analysis should not be applied to such suspensions.

Figure 2 shows that the real and imaginary parts of the effective viscosity increase with frequency in the range where the unsteady term begins to become comparable to the viscous term in the liquid momentum equation. The results for the real part of the effective viscosity may be rationalized as follows. At relatively large frequencies we expect the viscous effects to be confined to small Stokes layers of thickness $\delta = O((\mu_l/\rho_l\omega)^{1/2})$ surrounding each particle. The effective viscosity is the rate of energy dissipation per unit volume of the suspension divided by the square of mean velocity gradient $\dot{\gamma} = O(k_{ce}\langle \boldsymbol{u} \rangle)$. At high frequencies the dominant contribution to dissipation arises from the Stokes layers whose volume per unit suspension volume is $O(\delta a^2 n)$, n being the number density of particles, and the velocity gradient in these layers is $O(\dot{\gamma}a/\delta)$. The effective viscosity must therefore roughly scale as a/δ or $a(\omega\rho_l/\mu_l)^{1/2}$ for frequencies at which δ is small compared with a. The observation that the real part of effective viscosity should increase with frequency as $\omega^{1/2}$ is consistent with the results of figure 2. The ratio $(\mu_l/\rho_l\omega a^2)^{1/2}$ is about 0.01 for $f = 1$ MHz indicating that indeed the Stokes layers are thin at these frequencies (note that we have replaced μ_l by its value for water divided by 1000).

The imaginary part of the effective viscosity is also seen to increase with increasing

frequency in figure 2. This elastic nature of the suspension is expected at higher frequencies.

We now compare the effective-medium results for λ_v with the known results. Recall that λ_v represents the ratio of the velocity amplitude in the particle phase to that in the suspension. At lower frequencies for which $k_{ce}a$ is small and the scattering losses are small, the attenuation will be dominated by the imaginary part of λ_v as suggested by Sangani *et al.* (1991) who evaluated the real and imaginary parts of λ_v for a special case when the frequency is large enough for the Stokes layers to be small compared with the particle radius but small enough for $k_{ca}a$ to be small, i.e. for the suspension to be essentially incompressible. We shall compare the results of effective-medium approximation with their results next.

Sangani *et al.* gave their results in terms of added mass, Basset, and viscous drag coefficients. The force balance on a particle in the suspension was written as

$$\langle \boldsymbol{F}(t)\rangle = \rho_l \mathscr{V}\langle \dot{\boldsymbol{u}}\rangle + \tfrac{1}{2}\rho_l \mathscr{V} C_a\langle \dot{\boldsymbol{u}}-\dot{\boldsymbol{v}}\rangle + 6a^2\sqrt{\pi\rho_l\mu_l}C_b\int_{-\infty}^{t}\langle \dot{\boldsymbol{u}}-\dot{\boldsymbol{v}}\rangle(\tau)\frac{\mathrm{d}\tau}{\sqrt{t-\tau}} + 6\pi a\mu_l C_d\langle \boldsymbol{u}-\boldsymbol{v}\rangle \tag{75}$$

where $\boldsymbol{F}$ is the force on the particle, $\mathbf{v}$ is the velocity of the particle, C_a, C_b and C_d are the added mass, Basset and viscous drag coefficients and $\mathscr{V}$ the volume of a particle. Dots above variables denote time derivatives. Noting that $\boldsymbol{F}(t) = \rho_p \mathscr{V}\dot{\boldsymbol{v}}$ and $\langle \boldsymbol{v}\rangle = \lambda_v\langle \boldsymbol{u}\rangle$, and taking the time-dependence of variables to be $\mathrm{e}^{-\mathrm{i}\omega t}$, the force balance (75) gives

$$C_a + 9\Omega C_d + 9\Omega^2 C_d = \frac{2(\rho^*\lambda_v - 1)}{1-\lambda_v}, \tag{76}$$

with $\Omega \equiv (\mathrm{i}\mu_l/(\rho_l\omega a^2))^{1/2}$ and $\rho^* \equiv \rho_p/\rho_l$. Sangani *et al.*'s analysis is valid when the magnitude of Ω is small compared with unity, and the terms of $O(\Omega^3)$ or smaller are neglected in (76). For small Ω, λ_v can be expanded in a series $\lambda_v = \lambda_v^{(0)} + \Omega\lambda_v^{(1)} + \cdots$ to yield the relations

$$C_a = \frac{2(\rho^*\lambda_v^{(0)} - 1)}{1-\lambda_v^{(0)}}, \qquad C_b = \frac{2\lambda_v^{(1)}(\rho^* - 1)}{9\left(1-\lambda_v^{(0)}\right)^2}. \tag{77}$$

The coefficients $\lambda_v^{(0)}$ and $\lambda_v^{(1)}$ were evaluated from the effective-medium theory results for λ_v at small $k_{cl}a$ and small $|\Omega|$ by extrapolating to $\Omega = 0$ and numerically differentiating the results with respect to Ω, respectively. Figures 3 and 4 show a comparison with the rigorous multiparticle calculations of Sangani *et al.* who determined C_a, C_b, and C_d as a function of ϕ and ρ^* for periodic as well as random arrays of spheres. The results for C_a for the body-centred cubic and random arrays were very close to each other while that for the simple cubic arrays differed by about 12% at $\phi = 0.5$. It was also found that the dependence on ρ^* was rather weak, typically variations within 5% occurred as ρ^* was varied from zero to infinity. The results of Sangani *et al.* shown in figures 3 and 4 correspond to $\rho^* = 0$ while the effective-medium results correspond to glass particles in water with $\rho^* = 2.55$. We see an excellent agreement between the added mass coefficient obtained by the effective-medium approximation and for random or body-centred cubic arrays. The effective-medium approximation for C_b deviates systematically from the random arrays result with the maximum deviation of about 20% at $\phi = 0.5$. The theory in this case is much closer to the results for the simple cubic arrays.

Next we consider the case when Ω is very large, i.e. frequencies at which the

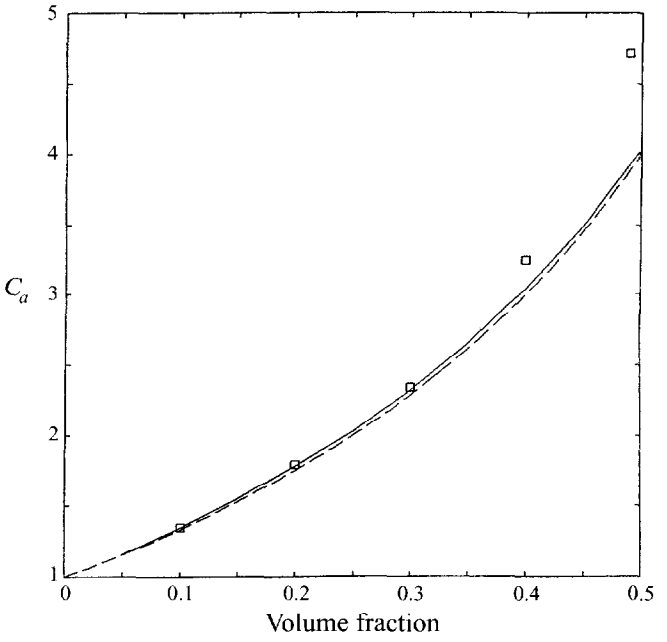

FIGURE 3. Added mass coefficient C_a as a function of volume fraction. Solid line is the theoretical result for wavelengths and viscous boundary layers much larger than particle size. Broken line and squares are the random array and simple cubic array results of Sangani *et al.* (1991). Particle to liquid density ratio is 2.55.

viscous drag coefficient makes the leading contribution to λ_v. The results in this case can be compared with the results of multiparticle Stokes flow calculations by Ladd (1990) and Mo & Sangani (1994). Two kinds of results are available in the Stokes flow literature. The first is the hindrance factor in sedimentation in which the average velocity of the particles is determined for the case when the forces acting on all the particles are the same. The second is the calculation of the permeability of a fixed bed of particles. There the average force on the particles is calculated for particles that all have the same (zero) velocity, different from the mean velocity of the suspension. Neither situation applies to oscillatory flows but one expects that the results for the fixed bed resistivity would be most applicable for large ρ^* and those of the hindrance factor for very small ρ^*. Figure 5 compares the results of Ladd and Mo & Sangani for these two quantities with the results obtained using the effective-medium approximation with $\rho^* = 10$. These results were obtained with $|\Omega| = 22$ and $k_{cl}a = 0.001$. The results for the sedimentation-hindrance factor were obtained only up to $\phi = 0.45$ in the present investigation while Mo & Sangani had obtained an additional value for the fixed bed resistivity at $\phi = 0.6$. Their result for $\phi = 0.6$ was in excellent agreement with the well-known Carman–Kozney correlation. We see that at least up to $\phi = 0.45$, the hindrance factor and the fixed-bed resistivity are not too different from each other, and that the effective-medium results are in excellent agreement for the entire range of ϕ.

Next, we compare the results for the effective conductivity. When $k_{cl}a$ is small the viscous and thermal effects contribute most to the total attenuation. When the density ratio is close to unity the translational oscillations and hence viscous attenuation are small and the thermal effects become the primary source of attenuation. The effective

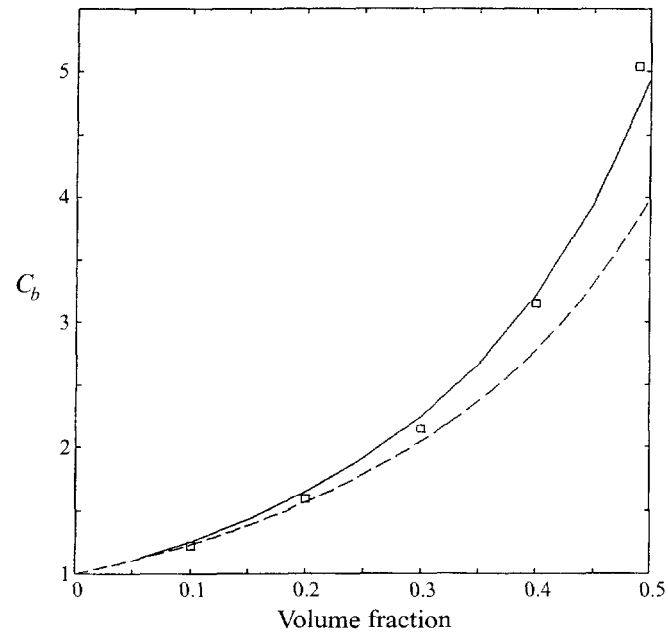

FIGURE 4. Basset coefficient C_b as a function of volume fraction. Solid line is the theoretical result for wavelengths and viscous boundary layers much larger than particle size. Broken line and squares are the random array and simple cubic array results of Sangani *et al.* (1991). Particle to liquid density ratio is 2.55.

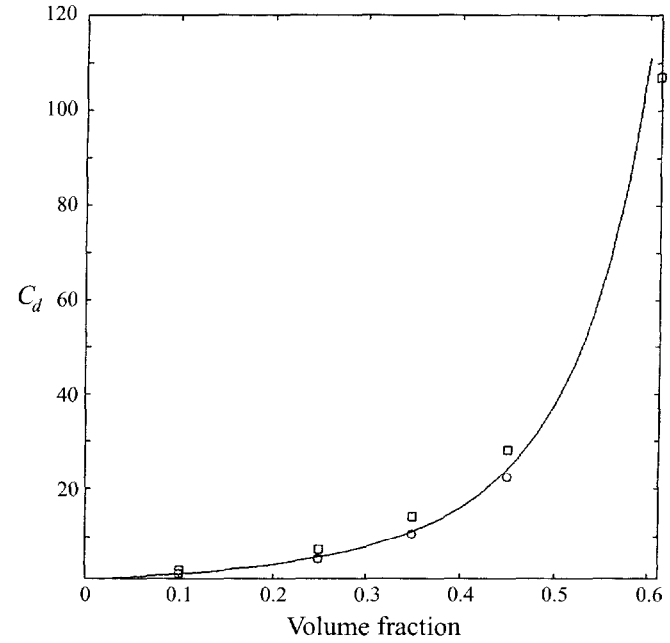

FIGURE 5. C_d as a function of volume fraction. Lines are theoretical results obtained for wavelengths much larger and viscous boundary layers much smaller than particle size. Squares are numerical simulation results for the fixed-bed resistivity by Mo & Sangani (1994), circles are numerical simulation results for the hindrance factor by Ladd (1990).

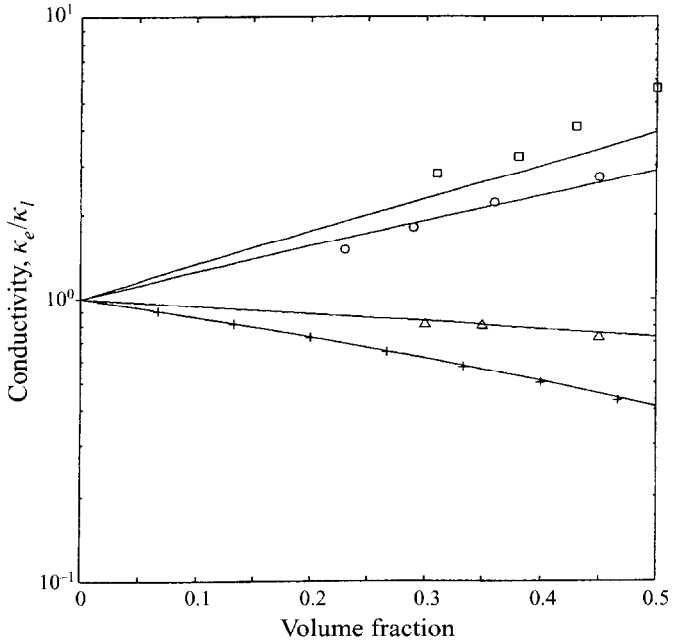

FIGURE 6. Ratio of effective conductivity to liquid conductivity as a function of volume fraction. Lines are theory for wavelengths large compared to particle size, symbols are experimental data from Turner (1976). Results are shown for $\kappa_p/\kappa_l = 0.01$ (+), 0.51 (△), 10.8 (○) and 160 (□).

conductivity as a function of ϕ and the conductivity ratio κ_p/κ_l was determined experimentally by Turner (1976) who used liquid fluidized beds of nearly monodisperse spheres. Sangani & Yao (1988) and Bonnecaze & Brady (1991) have carried out multiparticle calculations for the same cases and found generally good agreement between the simulations results and the experimental data of Turner. Figure 6 shows the comparison between the effective-medium approximation and the data of Turner. Calculations were made with the polystyrene–water system with $f = 1$ MHz for which $k_{cl}a$ equals 4.2×10^{-4} and the ratio of unsteady term to the steady conduction term $\rho_l C_{p,l}\omega a^2/k_l$ equals 0.05. The thermal conductivity of the particles was varied keeping other parameters fixed to determine the effect of conductivity ratio. Agreement is generally very good except for the highest particle-to-liquid conductivity ratio of 160 and $\phi = 0.5$ for which the effective-medium approximation underpredicts the effective conductivity by about 30%. At such high conductivity ratios the narrow gap regions between pairs of particles in dense suspensions contribute siginificantly to the overall heat flux and this is not captured accurately by the effective-medium approximation. The spatial distribution of the particles could also affect significantly the results at high ϕ. For low-conductivity particles we see an excellent agreement between the experiments and the effective-medium approximation. It may be noted that the well-known Maxwell relation

$$\frac{\kappa_e}{\kappa_l} = \frac{1+2\alpha\phi}{1-\alpha\phi} \tag{78}$$

with $\alpha = (\kappa_p - \kappa_l)/(\kappa_p + 2\kappa_l)$ also gives accurate estimates of the effective conductivity for $\kappa_p/\kappa_l = 0$.

Figure 7 shows the results for the real and imaginary parts of the effective con-

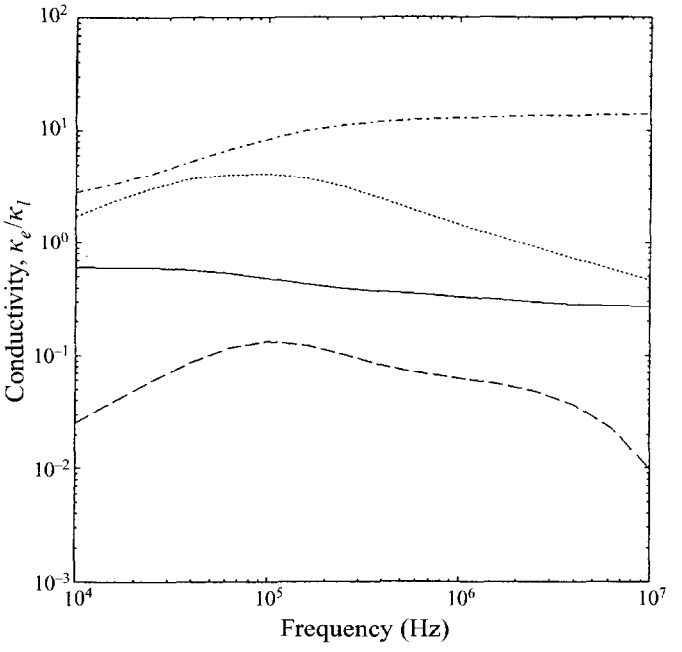

FIGURE 7. Real and imaginary part of the ratio of effective conductivity to liquid conductivity as functions of frequency. Particle volume fraction is 0.3; $k_{cl}a = 4 \times 10^{-2}$ at 10 MHz for all cases. Solid line (real part) and dashed line (imaginary part), $\kappa_p/\kappa_l = 2 \times 10^{-3}$; dashed-dotted line (real part) and dotted line (imaginary part), $\kappa_p/\kappa_l = 20$.

ductivity as a function of frequency for two particle-to-liquid conductivity ratios. For $\kappa_p/\kappa_l > 1$ the real part of the conductivity is seen to increase with the frequency. This result is similar to the one discussed for the effective viscosity (cf. figure 2). The opposite is true for the particles whose conductivity is smaller than the fluid conducitivity. The imaginary part of the conductivity is seen to reach a maximum at frequencies for which the thermal layer thickness is comparable to particle radius.

In summary, we have shown in this section that the effective-medium approximation yields very accurate estimates of the coefficients λ_d (effective viscosity), λ_v (added mass, Basset force, and viscous drag), and λ_κ (conductivity) for the monodisperse, random suspensions in the limits in which the results of exact multiparticle interactions are available.

The two coefficients for which no exact results are available are λ_ρ and λ_T but the computed results for these coefficients show expected trends. For example, figure 8 shows results for the real and imaginary parts of λ_T which represents the ratio of average temperature amplitude inside the particles to that in the suspension. The results are shown for polystyrene–water mixture with $a = 0.11\,\mu$m, a system which was studied by Allegra & Hawley (1972). When the thermal diffusion length, $(\kappa_p/\omega\rho_p C_{v,p})^{1/2}$, becomes much larger than the particle radius, the temperature inside the particle will be the same as the suspension temperature and λ_T will approach unity. This is the situation for frequencies less than 1 MHz. At frequencies that are large enough so that the thermal layer inside the particles is thin compared with the radius but small enough to keep the wavelength large compared with the radius, we expect the particle temperature amplitude to be governed by the temparature variations in the adiabatic case. A simple calculation shows that in this limit λ_T and

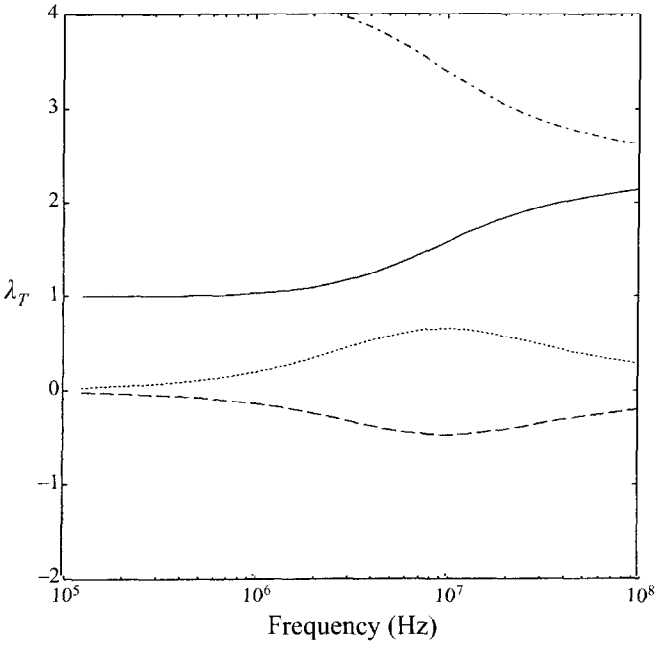

FIGURE 8. Real and imaginary parts of λ_T as a function of frequency for polystyrene particles (0.11 μm radius) in water at 0.3 volume fraction. Solid line (real part) and dashed line (imaginary part) are the full results; the dashed-dotted line (real part) and the dotted line (imaginary part) are the adiabatic result (79).

λ_ρ are related by

$$\lambda_T = \frac{(\gamma_p - 1)\lambda_\rho k_{ce}^2}{i\omega b_{ce}\beta_p}. \tag{79}$$

The dot-and-dashed curve in figure 8 is obtained by first computing λ_ρ using the effective-medium approximation and then using (79) to estimate λ_T. We see that at high frequencies the result for λ_T obtained in this manner approaches that obtained from the direct evaluation using the effective-medium approximation. The imaginary part of λ_T is seen to vanish in the limits of high and low frequencies as one approaches, respectively, the adiabatic and isothermal limits.

All the results discussed in this section correspond to the limit of small $k_{cl}a$ for which the scattering losses are insignificant. Since all indications suggest that the effective-medium approximation is very accurate, we expect the theory to predict the thermal and viscous attenuations for small $k_{ce}a$ very accurately. Rigorous calculations are not available for $k_{cl}a = O(1)$ and we shall mostly depend on the experimental data to assess the effective-medium theory in this regime.

4. Experimental set-up

The experimental set-up for measuring attenuation is shown in figure 9. The suspension is hand-stirred in a vessel with transmitting and receiving transducers mounted flush with the inner walls. The distance between the transducers in a typical vessel was 5 cm, the width and the height of the vessel being 8 and 13 cm, respectively. In dense suspensions for which greater attenuation is expected, the experiments were carried out with smaller vessels with the acoustic path lengths as small as 1.3 cm.

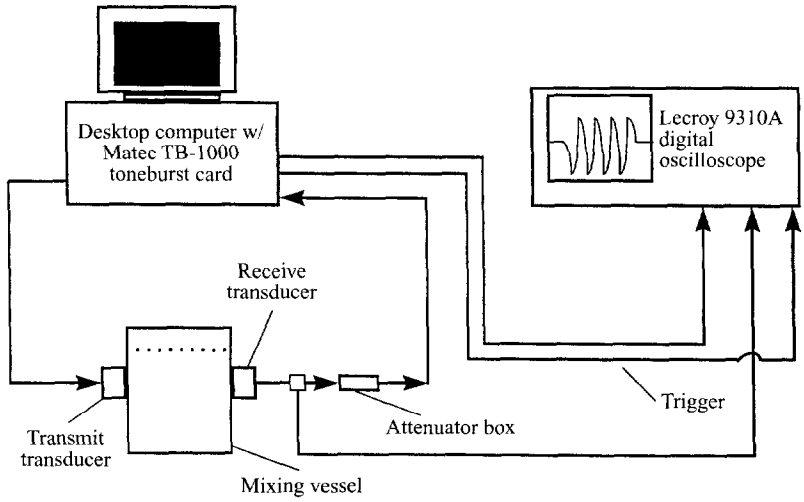

FIGURE 9. The schematic of the experimental set-up.

The transducers were of piezoelectric videoscan immersion type manufactured by Panametrics Inc. To cover a relatively broad range of frequencies, we used transducers with centre frequencies of 1.0, 2.25, 5.0, 7.5 and 10.0 MHz. The first two were 1.3 cm in radius while the other two were 1 cm in radius.

A Matec TB-1000 digital synthesizer card installed in a desk-top computer was used to generate monochromatic tonebursts that propagated through the suspension and were received by the receiving transducer. The signal was then sent to a LeCroy Model 9310A digital oscilloscope where its amplitude was measured. Attenuation data were obtained for six to eight frequencies for each transducer pair. Thus, the measurements were typically carried out at frequencies between 1 and 12 MHz. The suspension was hand-stirred before each measurement. To calculate the excess attenuation caused by the presence of particles, we also measured the amplitude of the signal received by the transducer for the pure liquid case. The excess attenuation for a given particle concentration is then determined using

$$\alpha = -\frac{1}{L}\log\left(\frac{V_{\mathrm{mix}}}{V_l}\right), \tag{80}$$

where V_{mix} and V_l are the voltage amplitudes of the received signals in the mixture and pure liquid, respectively, and L is the distance between the transducers.

Further details about the experimental set-up can be found in Norato (1999).

5. Comparison with experiments

Several experimental results have been presented for dense slurries in the literature. In this section we shall compare with these data as well as with results obtained in our laboratory. Allegra & Hawley (1972) measured attenuation for nearly monodisperse polystyrene particles of radius 0.11 μm in water. The acoustic frequency range used by these investigators was roughly 5–50 MHz. This corresponds to the non-dimensional wavenumbers $k_{cl}a$ in the range of 0.002–0.02. At such small wavenumbers the scattering losses are negligible, and since the density of polystyrene (1.07 g cm^{-3}) is close to that of water, the translational oscillations of the particles and hence the vis-

cous attenuation are negligible. Thus, the thermal effects dominate the attenuation in Allegra & Hawley's experiments. The difference in thermal expansion coefficients between the particles and the suspending liquid causes the temperature amplitude inside the particles to differ from that in the liquid. This causes a heat flux through the surface of the particles that is out of phase with the sound wave and leads to thermal attenuation.

Allegra & Hawley showed that when the thermal boundary layers as well as the wavelength are much greater than the particle radius and the suspension is dilute (i.e. when $\kappa_l/(\rho_l C_{p,l}\omega a^2) \gg 1$, $k_{cl}a \ll 1$, and $\phi \ll 1$), the attenuation is given by

$$\alpha = \tfrac{1}{6}\phi\omega^2 a^2 c_l T \rho_l \rho_p^2 C_{p,p}^2 \left(\frac{\beta_l}{\rho_l C_{p,l}} - \frac{\beta_p}{\rho_p C_{p,p}}\right)^2 \frac{1}{\kappa_p}\left[\frac{1}{5} + \frac{\kappa_p}{\kappa_l}\right]. \tag{81}$$

The attenuation increases as f^2 in this limit. On the other hand, when the boundary layers are much smaller than the particles while $k_{cl}a$ is still small, their analysis predicts that the attenuation will increase with frequency as $f^{1/2}$.

Allegra & Hawley (1972) compared their data with a theory for dilute suspensions and found good agreement between the two for dilute suspensions. Since the effective-medium theory reduces to their theory for dilute suspensions as $\phi \to 0$, we also expect a very good agreement at small volume fractions. Allegra & Hawley compared the two in several of their figures but did not specify the volume fraction of the particles used in obtaining the data except for one in which they show the attenuation as a function of ϕ at several frequencies. We show their data for the lowest volume fraction, $\phi = 0.058$, in figure 10. The asymptotic expression (81) is also shown in the figure; it is seen that the experiments were carried out at frequencies for which the thermal layers are comparable to particle radius.

As noted by Allegra & Hawley, the attenuation is sensitive to the thermal properties of polystyrene particles. If we take these properties to be the same as given by these investigators and reported in table 1, we find that the predicted attenuation is slightly greater than the experimental values as indicated by the solid line in figure 10. However, there is some uncertainty about the values of the physical properties as given by Allegra & Hawley. In their paper they show that their results depend quite strongly on the equilibrium temperature – because the physical properties do – and that there is a significant discrepancy between the theory and experiments in this temperature dependence. Especially, the attenuation at temperatures $\leqslant 20°$ C is overpredicted. Allegra & Hawley mentioned that the factor $\beta_p/(\rho_p C_{p,p})$ (cf. (81)) introduces the uncertainty. To be able to have a fair comparison between the dense slurry data and the effective-medium theory we have therefore changed the value of β for polystyrene somewhat (decreased by 11%) to get the best fit at low volume fractions, which is seen to be excellent.

Figure 11 compares the effective-medium approximations with the attenuation data as a function of volume fraction of the particles at different frequencies. We see an excellent agreement at all volume fractions. (Slight differences seen are within the error introduced in reading the data from Allegra & Hawley's figures or due to small temperature variations that could occur during the experiments.) Note that simply using the dilute theory of Allegra & Hawley (1972) would have overpredicted the attenuations at 0.5 volume fraction by as much as 50%.

The scattering attenuation was small in the experiments by Allegra & Hawley (1972) since $k_{cl}a$ for their experiments was much less than unity. To extend the range of $k_{cl}a$ over which the theory can be tested against experiments we have conducted

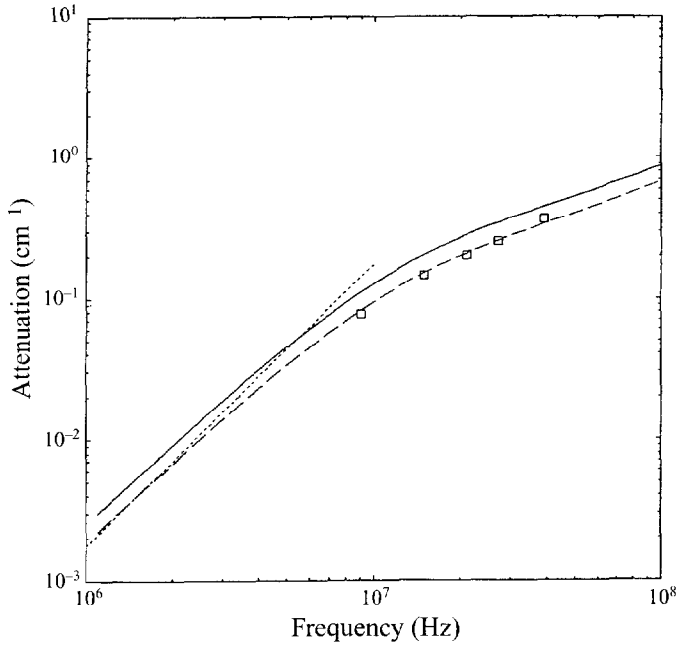

FIGURE 10. Comparison with experimental dilute-slurry results by Allegra & Hawley (1972) for the attenuation in a mixture of polystyrene particles of 0.11 μm radius in water at 0.05 volume fraction. Squares are experiments, solid line is the theoretical result. The broken line is the theoretical result when the thermal expansion coefficient is changed from 2.04×10^{-4} to 1.82×10^{-4} K^{-1}. The dotted line is the asymptotic result (81).

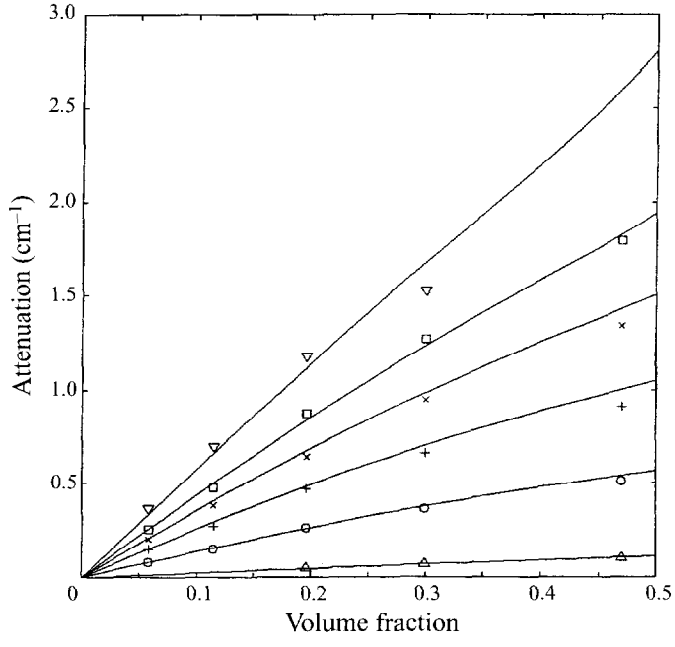

FIGURE 11. Comparison with experimental dense-slurry results by Allegra & Hawley (1972) for the attenuation for polystyrene particles of 0.11 μm at different frequencies. △, 3 MHz; ○, 9 MHz; +, 15 MHz; ×, 21 MHz; □, 27 MHz and ▽, 39 MHz.

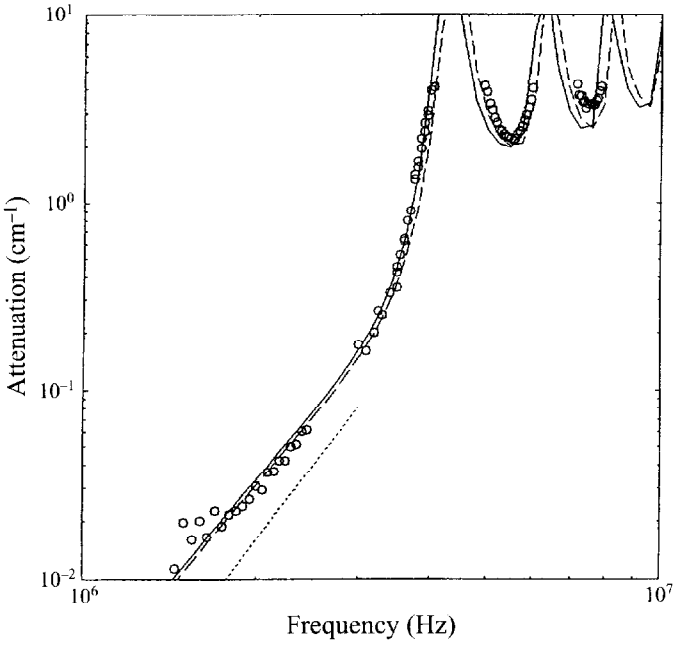

FIGURE 12. Experimental and theoretical results for the attenuation in a mixture of polystyrene particles (mean radius $79 \pm 3\,\mu$m and $1.8\,\mu$m standard deviation) in water at 0.05 volume fraction. Circles are experiments, solid and broken lines are the theory for monodisperse particles of $79\,\mu$m and $77\,\mu$m radius, respectively.

experiments for much larger polystyrene particles. The particles were specified by the manufacturer to have a mean radius of $79 \pm 3\,\mu$m with a standard deviation of $1.8\,\mu$m; $k_{cl}a$ in our experiments varied between 0.5 and 2.6. The comparison between the theory and experiments is shown in figure 12. At small frequencies (or small $k_{cl}a$) the attenuation due to scattering is expected to increase in proportion to f^4. This behaviour is observed roughly for $k_{cl}a < 1.3$. At higher frequencies the resonance effects due to various shape deformations of the particles become important as discussed in more detail by Spelt *et al.* (1999) who examined the problem of determining size distributions for dilute suspensions. The first three peaks seen in figure 12 correspond to the resonances in $n = 2,3$, and 4 modes (cf. (56)).

As we can see from figure 12, the agreement between the theory and the experiments is very good. A possible explanation for the slight differences observed near the resonance peaks is the uncertainty in the mean particle size as specified by the manufacturer. Changing the size of the particles from 79 to $77\,\mu$m radius (which is within the specifications) is seen in figure 12 to improve the comparison. Alternatively, an excellent agreement can also be observed by accounting for the size distribution of particles.

Most of the data shown in figure 12 were taken for a suspension with $\phi = 0.05$. High attenuation near the resonance peaks is not measurable and this explains the gaps seen in the data near those frequencies. We repeated some experiments with $\phi = 0.025$ and with smaller vessels which decreased the acoustic path length between the two transducers and obtained a few data points near the resonances but additional measurements with very low volume fractions appeared unnecessary.

Since the volume fraction used in this measurement is rather small ($\phi = 0.05$), an

excellent comparison between the theory and experiments should not be regarded as a true test of the effective-medium approximation. Rather, it shows that the data taken in our laboratory are reliable and that our analysis and the computer program for the effective-medium approximation gives correct results over a wide range of frequencies. To test the effective-medium theory higher volume fractions must be used but we encounter two problems. First, the monodisperse polystyrene particles in this size range are extremely expensive and secondly the range of frequencies for which the attenuation at higher volume fractions would be measurable will be rather narrow to provide a good test of the effective-medium approximation.

Experiments on dense slurries in the frequency range that is dominated by scattering effects before the resonance peaks were done by Atkinson (1991) and Atkinson & Kytömaa (1992). We have compared their data for the dilute suspensions with the present theory and found that, although the agreement at the lower half of their frequency range is reasonable, at higher frequencies the experimental results for the attenuation were consistently lower than the theoretical results (at 0.045 volume fraction and 0.7 MHz frequency the difference was a factor two). It was found that the differences could not be resolved by changing the physical properties, the size of the particles or by allowing for a size distribution of the particles. Since we do not see any reason for the theory to be inapplicable at such low volume fractions, we did not pursue further comparison at higher volume fractions. Instead, we shall compare the theory with the experiments we have conducted for the glass–water system.

Since the large glass particles are difficult to keep suspended in water, we added glycerol to increase the viscosity and density of the suspending medium. Soda-lime glass particles were used. The volume fraction size distribution was measured using a light scattering instrument and gave a mean radius of 63 μm and a standard deviation of 8.5 μm (the volume fraction distribution is related to the size distribution $P(a)$ by $\phi(a) = (4/3)\pi a^3 P(a)$). The distribution is shown in figure 13 together with a fit used in calculations discussed below (a lognormal size distribution for $P(a)$ was used). The instrument could measure the particle radius up to about 240 μm. It was estimated that about 1.5% of the particles by volume had radius that exceeded this value.

We first discuss results for a dilute suspension. Figure 14 shows the attenuation as a function of frequency at $\phi = 0.05$. At the frequency of 1 MHz, the non-dimensional wavenumber $k_{cl}a$ based on mean radius is about 0.25. Thus, throughout the frequency range we expect the scattering losses to be the most significant. At low frequencies, the attenuation is approximately proportional to f^4. Note that at very low frequencies the viscous attenuation will become more significant, and if the Stokes layers are small compared with the particle radius, then the attenuation will be proportional to $f^{1/2}$. At higher frequencies the attenuation appears to level off, unlike the case of polystyrene particles which exhibited distinct resonance peaks. This qualitative difference arises due to different shear moduli of glass and polystyrene (Spelt *et al* 1999).

The solid curve in figure 14 is obtained by using the size distribution shown in figure 13 which ignores the particles larger than 240 μm. We see that the agreement between the theory and the experiments is very good at frequencies above 2 MHz. Significant discrepancy exists, however, at lower frequencies. This may be due to the presence of larger particles. If we assume that, in addition to the size distribution shown in figure 14 we had 1.5% by volume of particles with a radius of 540 μm, then we obtain the dashed curve shown in figure 14. These larger particles contribute most to the attenuation for smaller frequencies. Alternatively, it is possible that some of the assumed physical properties of the water–glycerol system (cf. table 1) may

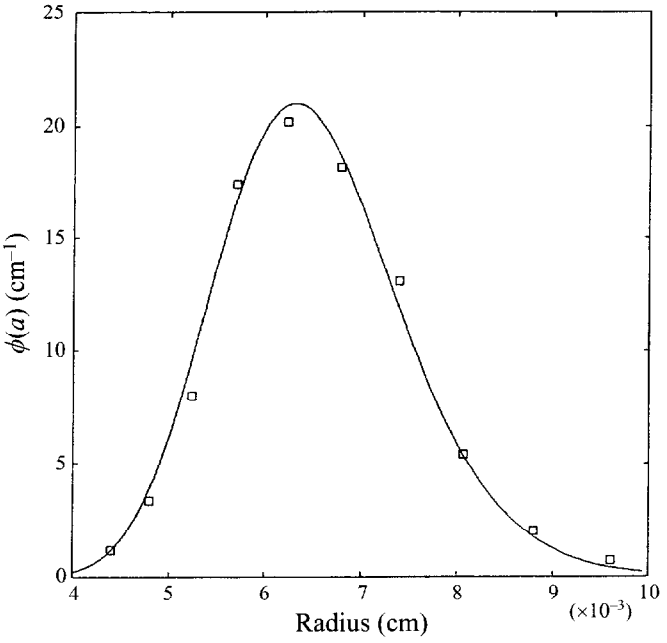

FIGURE 13. Volume-fraction distribution of the glass particles used in figure 14. Circles are measurements, the solid line is a fit using a log-normal size distribution.

be inaccurate and this may lead to the observed discrepancy at lower frequencies. The density and viscosity were measured in our laboratory but the other properties (sound speed and attenuation) were estimated using a volume-average mixture rule. In view of these uncertainties we shall only compare the experimental data for dense suspensions for frequencies greater than 2 MHz where the agreement for dilute suspensions is good.

Since the size distribution is somewhat broad, we must modify the effective-medium theory to account for polydispersity. The coefficients λ_ρ, etc. to be used in determining the effective properties of the suspension are now replaced by $\sum_{n=0}^{M} \phi(a_i)\lambda_\rho(a_i)$, etc. where M is the number of particle size bins. Here, $\lambda_\rho(a_i)$ represents the ratio of average dilatation amplitude inside the particle of radius a_i to that in the suspension. To estimate such coefficients we assume that the particle of radius a_i is surrounded by the liquid up to $r = R_i$ and the effective medium for $r > R_i$. We take R_i/a_i to be the same for all particle sizes and given by the same expression as in the case of a monodisperse suspension (cf. (52)). This is probably not a good estimate of R_i/a_i since one would expect R_i/a_i for larger particles to be smaller than for monodisperse suspensions as the volume exclusion for larger particles is smaller when smaller particles are present in the suspension. However, since there are no known analytical, rigorous solutions for polydisperse suspensions, a more complicated scheme for estimating R_i/a_i would be difficult to justify.

The dense-slurry data for the glass–water/glycerol suspensions are shown in figure 15. The frequency range is 2.5–5 MHz for which the comparison at $\phi = 0.05$ shown in figure 14 was good. The agreement is seen to be very good up to $\phi = 0.3$. At higher volume fractions, however, we observe significant discrepancy. The theory predicts the attenuation to be a monotonically increasing function of ϕ while the experiments exhibit maxima near $\phi = 0.3$. The measurements were made two or

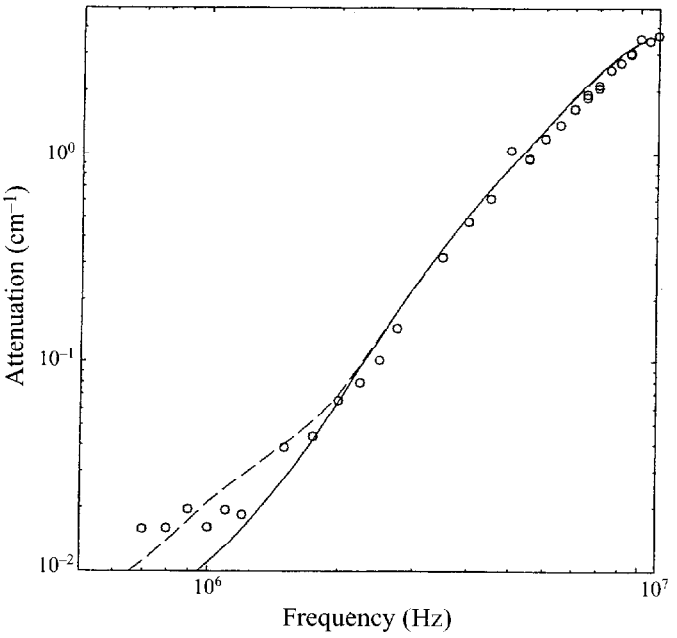

FIGURE 14. Experimental and theoretical results for the attenuation in a mixture of glass particles (mean radius 63 μm and 8.5 μm standard deviation) in glycerol at 0.05 volume fraction. Circles are experiments, solid and broken lines are the theoretical predictions.

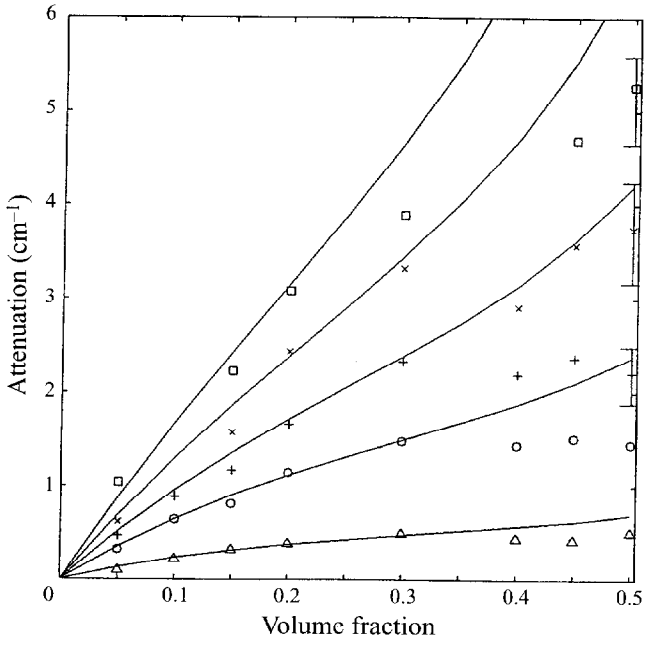

FIGURE 15. Experimental and theoretical results for the attenuation as a function of volume fraction for different frequencies, using the same glass particles and glycerol as in figure 11. Symbols are experiments, solid lines theory for monodisperse particles and broken lines theory for polysdisperse particles. △, 2.5 MHz; ○, 3.5 MHz; +, 4 MHz; ×, 4.5 MHz; □, 5 MHz.

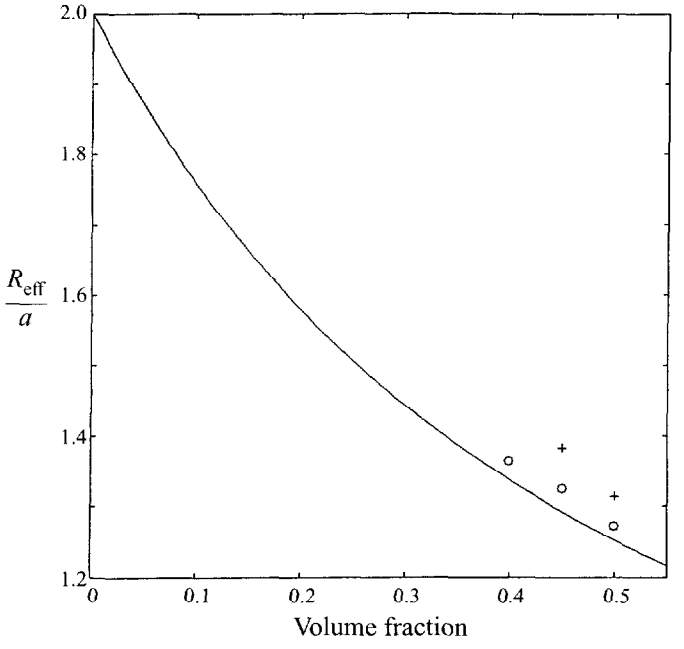

FIGURE 16. Liquid-shell to particle radius ratio as a function of volume fraction. Solid line is (52). Symbols are the values that would have to be used to get very good agreement with the experimental data shown in figure 15 at high volume fractions. ○, 2.5 MHz data; +, 5 MHz.

three times for each f at $\phi = 0.3$ and 0.5. At smaller volume fractions the data were quite reproducible and the error bars were typically smaller than the size of the symbols shown in figure 15. However, larger variations were observed at higher volume fractions as exemplified by the vertical bars around the data points. Although these error bars are quite significant, we see that the theory consistently overpredicts the attenuation for $\phi > 0.3$.

As mentioned earlier, there is some concern about the proper choice of R_i/a_i to be used in the effective-medium approximations for polydisperse suspensions. To see how the choice of R_i/a_i affects the results, we calculated the values of R_i/a_i (assumed to be independent of the particle radius) at which the theory and experiments would coincide for $\phi \geqslant 0.3$ at 2.5 and 5 MHz. The results are shown in figure 16. The solid line in that figure corresponds to the value used in the results presented in figure 15. We see that only slight changes in R/a are needed to make the theory predictions coincide with the experimental data. In other words, the results for the attenuation are very sensitive to the choice of R/a in very dense suspensions. Finally, the fact that the scatter in the attenuation data is significant at higher volume fractions suggests that the attenuation might be quite sensitive to the manner in which the suspension is stirred. As noted earlier we used hand-stirring just before taking the attenuation measurement. Perhaps using a fluidized bed would have produced different attenuation data at high volume fractions.

The comparisons shown so far were dominated by the thermal and scattering effects. Experiments in which the viscous losses are significant were carried out by Hampton (1967), but those were for clay particles which are highly non-spherical. To assess the theory for the viscous regime, we have measured attenuation for a suspension of small glass particles in water. The size distribution for these particles is shown in figure

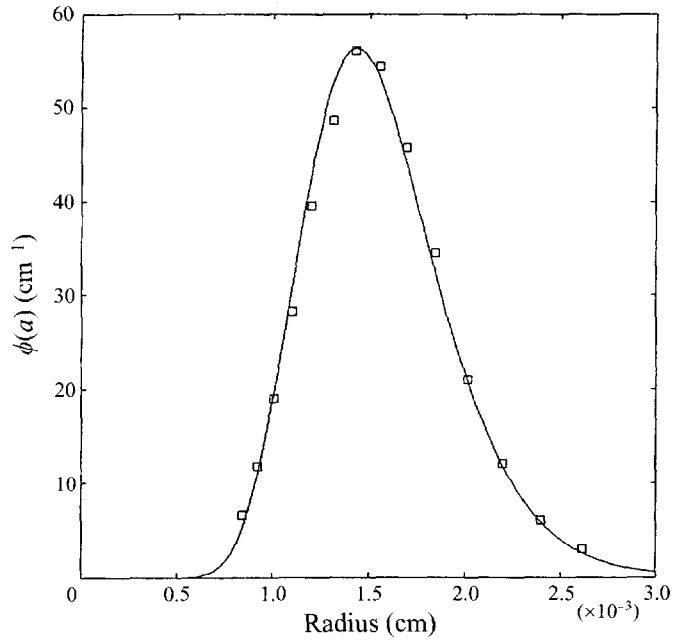

FIGURE 17. Volume-fraction distribution of the glass particles used in figure 18. Circles are measurements, the solid line is a fit using a log-normal size distribution.

17 together with the fit used in the calculations. The mean radius is 15 μm and the standard deviation is 3.5 μm. These particles have a very small terminal velocity and it is not necessary to add glycerol to keep them suspended. For the frequency range over which we could measure attenuation, i.e. for 0.7–10 MHz, the non-dimensional wavenumber $k_{cl}a$ varies from 0.03 to 0.5. The particle-to-liquid (pure water) density ratio in this case is 2.55, and the viscous attenuation dominates the lower part of the frequency range, while the scattering attenuation becomes important at higher frequencies.

The results for volume fractions 0.05, 0.2, 0.3, and 0.4 are shown in figure 18. We see that the measured attenuation is proportional to $f^{1/2}$ in the viscous range, which is to be expected for the case when the Stokes layers are thin compared with the particle radius (see, e.g., Allegra & Hawley 1972). We see an excellent agreement between the theory and experiments. It may be noted that the attenuation does not vary linearly with the volume fraction, indicating that the effective-medium approximation represents a significant improvement over the dilute theory. We also note that, unlike the case of larger particles, the attenuation increases monotonically with the volume fraction for the entire range of frequencies over which the measurements are made.

6. Phase speed

While the physics of acoustics is very interesting, it appears that the determination of the particle volume fraction from acoustic measurements will be, in general, difficult because of the sensitive dependence of the acoustics on physical properties of the particles and liquid and the particle size distribution. Since the phase speed is relatively less sensitive to the particle size, it might be more advantageous to measure the phase speed. The scattering regime can lead to large attenuation and resonance

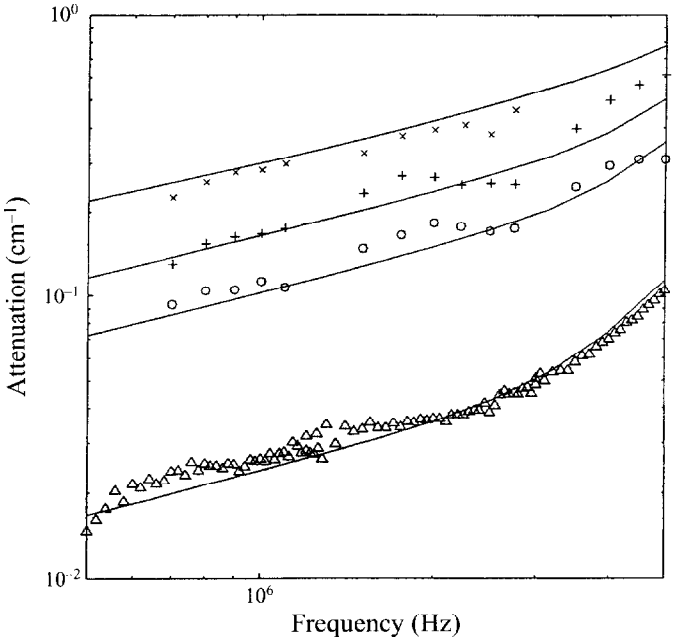

FIGURE 18. Experimental and theoretical results for the attenuation as a function of frequency at different volume fractions, using glass particles in water. Symbols are experiments, solid lines are theory. Volume fractions are △, 0.05; ○, 0.2; +, 0.3 and ×, 0.4.

behaviour sensitive to the mechanical properties of particles. The phase speed near the resonance frequencies can vary significantly. Thus, it is desirable to carry out measurements at low frequencies where the scattering effects will be insignificant.

When $k_{cl}a$ is small the phase speed can be measured for cases for which the Stokes layers are much smaller than the particle radius. In this limit the speed is nearly independent of the particle radius. Figure 19 shows the phase speed as a function of volume fraction in this limit for a glass–water system with two different sizes. Note that the speed is essentially the same for both particle sizes. The attenuation under these conditions would be proportional to a^{-1} (Allegra & Hawley 1972). Figure 19 also shows results for the case when the Stokes layers are much thicker than the particle radius. Once again, in this limit the phase speed is nearly independent of the particle radius while the attenuation would vary significantly with the particle radius as a^2. Note that the phase speed as a function of volume fraction goes through a minimum in the low-frequency limit. The monotonic increase at high frequency might be more suitable for determining the volume fraction. Thus, the ideal frequency for measuring the phase speed corresponds to the one for which the Stokes layers are thin compared with the particle radius and $k_{cl}a$ is small.

7. Summary

We have derived equations for describing small-amplitude acoustic wave propagation through a suspension. The equations are similar to those for a single-phase medium but require closures for estimating the effective properties of the suspension. We used an effective-medium model to solve for the conditionally averaged temperature, density, and velocity fields inside a test particle, and estimated thereby the

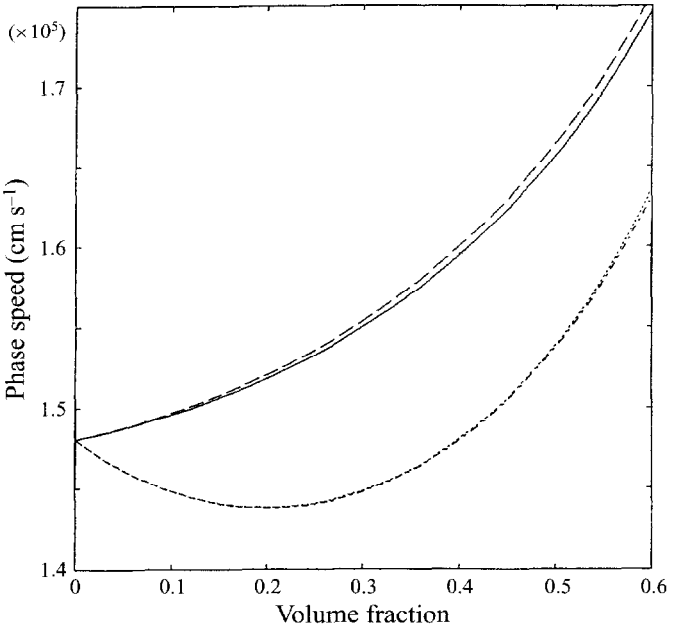

FIGURE 19. Wave speed as a function of volume fraction for two limiting cases. Solid line, $a^2\omega\rho_l/\mu_l = 3 \times 10^3$ and $k_{cl}a = 8 \times 10^{-4}$; long-dashed line the same, but with the particle radius increased by a factor of 5; dashed-dotted line, $a^2\omega\rho_l/\mu_l = 3 \times 10^{-4}$ and $k_{cl}a = 8 \times 10^{-4}$; short-dashed line the same but with the particle radius increased by a factor of 5.

effective properties such as the density, heat capacity, conductivity, viscoelasticity, and compressibility in a self-consistent manner. When the wavelength is large compared with the particle radius the multiparticle interactions in the suspension can be approximated by Stokes or Laplace equations for which a number of effective properties have been determined in recent years through rigorous multiparticle calculations. We show that the estimates obtained using the effective-medium approximation for various properties are in excellent agreement with these rigorous calculations. The theory is also shown to be excellent agreement with the experimental data for the polystyrene–water system by Allegra & Hawley (1972). The ratio of particle radius to wavelength was small in these experiments. To test the theory for larger particles we have conducted experiments both for polystyrene particles and glass particles in water. The agreement with the data for the polystyrene–water system which exhibits several resonances due to shape oscillations is excellent. However, the comparison was limited to dilute suspensions because of the unavailability of concentrated monodisperse suspensions in the particle size range of interest. The glass–water system had significant polydispersity but covered a broad range of volume fractions. The agreement between the theory and experiments for small particles in which the viscous attenuation dominates is excellent while for large particles for which the scattering losses dominate the agreement is good only up to $\phi = 0.3$. At higher volume fractions the attenuation measured in our laboratory decreased, in contrast with the theory prediction.

In view of the remarkable success of the effective-medium approximation in predicting the attenuation in solid–liquid systems, it seems that the procedure used here may also find applications in other acoustic problems, e.g. in the electroacoustics of

colloidal suspensions (O'Brien 1990) and in acoustics of fluid-saturated porous media (Burridge & Keller 1981).

This work was supported by the Department of Energy, Environmental Science Management Program, under Grant DE-FG07-96ER14729. The computations were performed using the resources of NCSA at University of Illinois. AS also acknowledges the support provided by the National Science Foundation under Grant CTS-9632227.

REFERENCES

ALLEGRA, J. R. & HAWLEY, S. A. 1972 Attenuation of sound in suspensions and emulsions: theory and experiments. *J. Acoust. Soc. Am.* **51**, 1545–1563.

ATKINSON, C. M. 1991 Acoustic wave propagation and non-intrusive velocity measurements in highly concentrated suspensions. PhD Thesis, MIT.

ATKINSON, C. M. & KYTÖMAA, H. K. 1992 Acoustic wave speed and attenuation in suspensions. *Intl J. Multiphase Flow* **18**, 577–592.

BONNECAZE, R. T. & BRADY, J. F. 1991 The effective conductivity of random suspension of spherical particles. *Proc. R. Soc. Lond.* A **432**, 455–465.

BURRIDGE, R. & KELLER, J. B. 1981 Poroelasticity equations derived from microstructure. *J. Acoust. Soc. Am.* **70**, 1140–1146.

CARSTENSEN, E. L. & FOLDY, L. L. 1947 Propagation of sound through a liquid containing bubbles. *J. Acoust. Soc. Am.* **19**, 481–501.

DODD, T. L., HAMMER, D. A., SANGANI, A. S. & KOCH, D. L. 1995 Numerical simulations of the effect of hydrodynamic interactions on diffusivities of integral membrane proteins. *J. Fluid Mech.* **293**, 147–180.

DURAISWAMI, R., PRABHUKUMAR, S. & CHAHINE, G. L. 1998 Bubble counting using an inverse acoustic scattering method. *J. Acoust. Soc. Am.* **104**, 2699–2717.

EPSTEIN, P. S. & CARHART, R. R. 1953 The absorption of sound in suspensions and emulsions. I. Water fog in air. *J. Acoust. Soc. Am.* **25**, 553–565.

GRADSHTEYN, I. S. & RYZHIK, I. M. 1994 *Table of Integrals, Series, and Products*, 5th Edn. Academic.

HAMPTON, L. D. 1967 Acoustic properties of sediments. *J. Acoust. Soc. Am.* **42**, 882–890.

JEFFREY, D. J. 1973 Conduction through a random suspension of spheres. *Proc. R. Soc. Lond.* A **335**, 355–367.

JU, J. W. & CHEN, T. M. 1994 Effective elastic moduli of two-phase composites containing randomly dispersed spherical inhomogeneities. *Acta Mech.* **103**, 123–144.

KIM, S. & RUSSEL, W. B. 1985 Modelling of porous media by renormalization of the Stokes equations. *J. Fluid Mech.* **154**, 269–286.

LADD, A. J. C. 1990 Hydrodynamic transport coefficients of random dispersions of hard spheres. *J. Chem. Phys.* **93**, 3484–3494.

LANDAU, L. D. & LIFSHITZ, E. M. 1986 *Theory of Elasticity*, 3rd Edn. Pergamon.

MO, G. & SANGANI, A. S. 1994 A method for computing Stokes flow interactions among spherical objects and its application to suspension of drops and porous particles. *Phys. Fluids* **6**, 1637–1652.

NORATO, M. A. 1999 Acoustic probe for the characterization of solid-gas-liquid slurries. PhD Thesis, Syracuse University.

O'BRIEN, R. W. 1990 The electroacoustic equations for a colloidal suspension. *J. Fluid Mech.* **212**, 81–93.

PROSPERETTI, A. 1984 Bubble phenomena in sound fields: part one. *Ultrasonics* **22**, 69–77.

SANGANI, A. S. & MO, G. 1997 Elastic interactions in particulate composites with perfect as well as imperfect interfaces. *J. Mech. Phys. Solids* **45**, 2001–2031.

SANGANI, A. S. & YAO, C. 1988 Bulk thermal conductivity of composites with spherical inclusions. *J. Appl. Phys.* **63**, 1334–1341.

SANGANI, A. S., ZHANG, D. Z. & PROSPERETTI, A. 1991 The added mass, Basset, and viscous drag coefficients in nondilute bubbly liquids undergoing small-amplitude oscillatory motion. *Phys. Fluids* A **3**, 2955–2970.

SPELT, P. D. M., NORATO, M. A., SANGANI, A. S. & TAVLARIDES, L. L. 1999 Determination of particle size distributions from acoustic wave propagation measurements. *Phys. Fluids* **11**, 1065–1080.

TURNER, J. C. R. 1976 Two-phase conductivity, the electrical conductance of liquid-fluidized beds of spheres. *Chem. Engng Sci.* **31**, 487–492.

Determination of particle size distributions from acoustic wave propagation measurements

Peter D. M. Spelt, Michael A. Norato, Ashok S. Sangani, and Lawrence L. Tavlarides
Department of Chemical Engineering and Materials Science, Syracuse University, Syracuse, New York 13244

(Received 4 August 1998; accepted 20 January 1999)

The wave equations for the interior and exterior of the particles are ensemble averaged and combined with an analysis by Allegra and Hawley [J. Acoust. Soc. Am. **51**, 1545 (1972)] for the interaction of a single particle with the incident wave to determine the phase speed and attenuation of sound waves propagating through dilute slurries. The theory is shown to compare very well with the measured attenuation. The inverse problem, i.e., the problem of determining the particle size distribution given the attenuation as a function of frequency, is examined using regularization techniques that have been successful for bubbly liquids. It is shown that, unlike the bubbly liquids, the success of solving the inverse problem is limited since it depends strongly on the nature of particles and the frequency range used in inverse calculations. © *1999 American Institute of Physics.* [S1070-6631(99)01405-1]

I. INTRODUCTION

Determining the particle size distribution of a solid–liquid mixture is of great practical interest. It has been suggested in the literature that this distribution may be determined by measuring the attenuation of a sound wave propagating through the mixture as a function of the frequency of the wave. The main premise is that the attenuation caused by a particle as a function of frequency depends on its size and therefore the attenuation measurements can be inverted to determine the particle size distribution—at least when the total volume fraction of the solids is small enough so that the particle interactions and detailed microstructure of the slurry play an insignificant role in determining the acoustic response of the slurry. Indeed, this general principle has been exploited successfully to determine the size distribution of bubbles in bubbly liquids.[1–3] Commercial "particle sizers" based on acoustic response are in the process of being developed/marketed for characterizing solid–liquid mixtures.[4] The main objective of this paper is to investigate under what circumstances such a problem can be solved for solid–liquid systems. It will be shown that the success of the acoustic method for determining detailed particle size distributions is limited, depending on the nature of the particles and the frequency range over which input data (attenuation) are available.

The problem of determining the acoustic response of a slurry given its particle size distribution is referred to as the forward problem. When the total volume fraction of the particles is small, the problem is relatively simple since then one only needs to understand the interaction between a single particle and the incident sound wave. This has been examined by a number of investigators in the past with notable contributions from Allegra and Hawley[5] and Epstein and Carhart[6] who considered suspensions of particles as well as drops. The former investigators also reported experimental results verifying the theory for relatively small particles for which the acoustic wavelength is large compared with the particle radius. The theory developed by these investigators is quite general and accounts for attenuation by thermal, viscous, and scattering effects as described in more detail in Secs. II and III. The case of monodisperse nondilute suspensions has been examined by Varadan *et al.*[7] who used an effective medium approximation to account for particle interactions, but their analysis was concerned only with the attenuation due to scattering. In Sec. II we present the theory for the forward problem with the main aim of reviewing the important physical effects causing the attenuation. The derivation for the attenuation proceeds along different lines than that followed by Epstein and Carhart or Allegra and Hawley in the way the one particle analysis is used to predict the attenuation of the suspension. These investigators calculated the energy dissipation per one wavelength to estimate the attenuation while we use the method of ensemble averages to determine both the phase speed and attenuation of waves. The method of ensemble averages will be more convenient for developing a suitable expression for attenuation in nondilute suspensions, if desired, using either an appropriate effective-medium approximation or direct numerical simulations.

In Sec. III we present new experimental data for nearly monodisperse polystyrene particles whose radii are comparable to the wavelength and validate the theory described in Sec. II over a nondimensional frequency range much broader than examined by previous investigators. We also summarize in that section the different physical mechanisms that cause attenuation in suspensions. The attenuation as a function of frequency is shown to undergo several peaks owing to the resonances in shape oscillations in agreement with the theory prediction. It also gives some indication of the range of frequency and attenuation measurable with our acoustic device.

In Sec. IV we consider the inverse problem, i.e., the

 © 1999 American Institute of Physics

problem of determining the particle size distribution given the total attenuation as a function of frequency and the physical properties of the particles and the suspending liquid. At small particle volume fractions, this amounts to solving a linear integral equation for the unknown size distribution. This is an ill-posed problem: small changes/errors in the attenuation data can cause large changes in the size distribution. Thus, for example, several very different particle distributions could give rise to essentially the same attenuation-frequency curve. This, of course, is a rather well-known difficulty in most inverse problems which involve solving a Fredholm integral equation of the first kind with a smooth kernel. Techniques have been developed to "regularize" the problem. We use the well-known Tikhonov regularization techniques,[8] which replaces the ill-posed original problem with another well-posed problem involving an integro-differential equation whose solution minimizes the fluctuations in the particle size distribution. Minimizing of the fluctuations is rationalized on the grounds that in most practical situations the particle size distribution is smooth. This regularization technique has been shown to work very well for the inverse problem in bubbly liquids.[2]

We apply the above technique to suspensions of polystyrene and glass particles. We find that the technique works well for the polystyrene particles but not for all glass particles. We also find that for polystyrene particles the technique works only when the attenuation is given over an appropriate frequency range—a frequency range that is too narrow or too broad may give erroneous estimates of the distribution. An alternative inverse technique based on linear programing also failed to produce the correct particle size distribution for the cases for which the Tikhonov scheme failed. This suggests that the prospects for determining the detailed particle size distribution from acoustic measurements are somewhat limited. (In situations where more might be known about the nature of particle size distribution, e.g., unimodal with a Gaussian or log-normal distribution, one might be able to determine the size distribution through appropriate curve fitting as has been done, for example, by McClements and Coupland,[9] but this is not addressed here.)

The reasons why the size distributions for some particle suspensions are not recovered by the inverse techniques while the same techniques were found to be quite successful for bubble suspensions can be given in terms of differing resonance nature of these suspensions. In the case of bubbles in most typical applications, the resonance occurs at frequencies for which the wavelength is relatively large compared with the bubble radius. This resonance is due to volume oscillations; the shape-dependent resonances are unimportant and, as a consequence, there is effectively one resonance frequency for each bubble size. Thus, the peaks in the attenuation-frequency curve give a reasonable indication of the bubble sizes. The situation with the particles is different as their resonance behavior is governed by shape oscillations. For polystyrene particles, several resonance peaks corresponding to different shape oscillations arise even for monodisperse particles, and, as a result, it is difficult to determine whether a given resonance peak arises from a different shape oscillation mode of the same particle or from a particle of different size. For glass particles, on the other hand, there are no significant resonance peaks even for monodisperse particles, and the attenuation behavior for different sizes is not significantly different to allow accurate results for the size distribution.

II. THE FORWARD PROBLEM

The wave equations for both the interior and exterior of particles have been derived by Epstein and Carhart.[6] They were interested in the attenuation of sound waves in fog and therefore their analysis was concerned with drops instead of particles. The stress tensor for a viscous fluid used by them for the interior of the drops was subsequently replaced by Allegra and Hawley[5] by that of an elastic solid to determine the attenuation of sound waves in a solid–liquid suspension. In this section we shall ensemble average a resulting wave equation to obtain the effective wave number of the suspension at arbitrary volume fraction, the real and imaginary parts of which give the wave speed and attenuation. Thus, the attenuation is not calculated by means of an energy dissipation argument,[5,6] but directly from averaging the relevant wave equation. The result contains certain coefficients that remain to be evaluated for a given microstructure. In the present study, since we are primarily concerned with determining the size distribution, we shall evaluate the coefficients in the limit of small volume fractions. In a separate study, where we shall present experimental results for nondilute suspensions, we shall extend the theory to treat nondilute suspensions.

A. Theory

Epstein and Carhart[6] first linearized the conservation equations for mass, momentum, and energy. The pressure and internal energy were then eliminated by introducing the linearized equations of state to yield equations in terms of density, velocity, and temperature. Next, the time dependence of all quantities were expressed by the factor $\exp(-\iota\omega t)$—which is henceforth suppressed—and the velocity was expressed as

$$\mathbf{v} = -\nabla\Phi + \nabla\times\mathbf{A},$$

with $\nabla\cdot\mathbf{A}=0$. With this form of $\mathbf{v}$ it is possible to eliminate the temperature and density from the governing equations to yield a fourth-order partial differential equation for Φ and a second-order equation in $\mathbf{A}$. The former, in turn, can be split into two second-order wave equations upon a substitution $\Phi=\phi_c+\phi_T$ to finally yield three wave equations:

$$(\nabla^2+k_c^2)\,\phi_c=0, \tag{1}$$

$$(\nabla^2+k_T^2)\,\phi_T=0, \tag{2}$$

$$(\nabla^2+k_s^2)\,\mathbf{A}=\mathbf{0}. \tag{3}$$

The wave numbers in the above equations are given by

$$\frac{1}{k_c^2}=\frac{c^2}{2\omega^2}[1-\iota(e+\gamma f)+((1-\iota(e+\gamma f))^2 +4f(\iota+\gamma e))^{1/2}], \tag{4}$$

$$\frac{1}{k_T^2}=\frac{c^2}{2\omega^2}[1-\iota(e+\gamma f)-((1-\iota(e+\gamma f))^2 +4f(\iota+\gamma e))^{1/2}], \tag{5}$$

$$k_s=(1+\iota)(\omega\rho/2\mu)^{1/2}, \tag{6}$$

with

$$e\equiv(4\mu/3+\kappa)\omega/(\rho c^2); \quad f\equiv\sigma\omega/c^2. \tag{7}$$

Here, c is the phase speed in pure liquid, ρ is the density, κ and μ are, respectively, the compressional and dynamic viscosity, $\gamma=C_p/C_v$ is the ratio of specific heats at constant pressure and volume, τ is the thermal conductivity, and $\sigma=\tau/\rho C_p$ is the thermal diffusivity.

Inside the particles similar equations hold with the dynamic viscosity replaced by $\tilde{\mu}/(-\iota\omega)$ and the wave speed by $((\tilde{\lambda}+2\tilde{\mu}/3)/\tilde{\rho})^{1/2}$, where $\tilde{\mu}$ and $\tilde{\lambda}$ are the Lamé constants, while the compressional viscosity is left out. Henceforth a tilde refers to the interior of particles.

At small values of e and f (such as in water), the above expressions for k_c and k_T simplify to

$$k_c=\omega/c+\frac{\iota}{2}[(4\mu/3+\kappa)/\rho+(\gamma-1)\sigma]\omega^2/c^3,$$
$$k_T=(1+\iota)(\omega/2\sigma)^{1/2}. \tag{8}$$

Equation (1) and its counterpart inside the particles describe the sound wave propagation through the suspension. Note that the wave number has an imaginary part; sound waves in pure fluid are attenuated by viscous and thermal energy dissipation;[10] the term inside the square brackets in (8) is commonly referred to as the "diffusivity of sound." The total attenuation coefficient in both liquid and in the solid particle will henceforth be treated as additional physical properties. The other two wave equations describe waves that arise from thermal conduction and finite viscosity: we note that the modulus of k_T in Eq. (8) is inversely proportional to the thermal penetration depth $\sqrt{\sigma/\omega}$ and that of k_s to the viscous penetration depth $\sqrt{\mu/\rho\omega}$. The thermal (ϕ_T) and shear (**A**) waves have generally very high attenuation and are unimportant in acoustic applications.

We now proceed to ensemble average the wave equation (1) to find an expression for the effective wave number of a wave propagating through a solid–liquid suspension. Introducing an indicator function g, defined to be unity inside the particles and 0 outside, the ensemble-averaged value of ϕ_c is

$$\langle\phi_c\rangle=\langle g\tilde{\phi}_c+(1-g)\phi_c\rangle.$$

To obtain a wave equation for $\langle\phi_c\rangle$ we first take the gradient of the above equation to yield

$$\nabla\langle\phi_c\rangle=\langle g\nabla\tilde{\phi}_c+(1-g)\nabla\phi_c\rangle+\langle(\nabla g)(\tilde{\phi}_c-\phi_c)\rangle. \tag{9}$$

As argued by Sangani,[11] upon assuming that the particles' spatial distribution is homogeneous on a macroscale, the last term in (9), being a vector, can only depend on quantities such as $\nabla\langle\phi_c\rangle$ and $\nabla\nabla^2\langle\phi_c\rangle$. Anticipating that $\langle\phi_c\rangle$ will satisfy a wave equation we express the last term on the right-hand side of the above equation in terms of $\nabla\langle\phi_c\rangle$, i.e., we write

$$\langle(\nabla g)(\tilde{\phi}_c-\phi_c)\rangle=\lambda_1\nabla\langle\phi_c\rangle,$$

where λ_1 depends on the parameters such as the volume fraction, k_c, and $\tilde{k}_c$. The divergence of (9) is given by

$$\begin{aligned}\nabla^2\langle\phi_c\rangle&=\langle g\nabla^2\tilde{\phi}_c+(1-g)\nabla^2\phi_c\rangle+\langle(\nabla g)\\&\quad\cdot(\nabla\tilde{\phi}_c-\nabla\phi_c)\rangle+\lambda_1\nabla^2\langle\phi_c\rangle\\&=-k_c^2\langle\phi_c\rangle-(\tilde{k}_c^2-k_c^2)\langle g\tilde{\phi}_c\rangle+\langle(\nabla g)\\&\quad\cdot(\nabla\tilde{\phi}_c-\nabla\phi_c)\rangle+\lambda_1\nabla^2\langle\phi_c\rangle.\end{aligned} \tag{10}$$

Writing

$$\langle(\nabla g)\cdot(\nabla\tilde{\phi}_c-\nabla\phi_c)\rangle=\lambda_2\tilde{k}_c^2\langle\phi_c\rangle, \quad \langle g\tilde{\phi}_c\rangle=\lambda_3\langle\phi_c\rangle,$$

we find that $\langle\phi_c\rangle$ satisfies a wave equation

$$(\nabla^2+k_{\text{eff}}^2)\langle\phi_c\rangle=0 \tag{11}$$

with the effective wave number given by

$$k_{\text{eff}}^2=\frac{k_c^2+\lambda_3(\tilde{k}_c^2-k_c^2)-\lambda_2\tilde{k}_c^2}{1-\lambda_1}. \tag{12}$$

The real part of the effective wave number is the frequency divided by the phase speed in the mixture and the imaginary part the attenuation.

Up to this point the analysis is rigorous and without any assumption. Applying the boundary conditions of continuity of temperature, flux, velocity, and traction at the surface of the particles, and solving the resulting boundary value problem numerically, it is possible, in principle, to determine the phase speed and attenuation at arbitrary volume fraction using the above formulation. Special simplifications can be made when the wavelength is large compared with the particles and when the viscous and thermal depths are small compared with the particle radius for which numerical computations using the multipole expansions developed in recent years (see, e.g., Ref. 12) can be readily used for determining the attenuation at arbitrary volume fractions. Alternatively, one may use a suitable effective-medium approximation to account for the particle interactions in nondilute suspensions using the above framework. We shall pursue this further in a separate study[13] devoted to nondilute suspensions where we shall also present experimental data. Since our interest in the present study is in determining size distributions, it is necessary to consider only the simplest case of dilute suspensions.

In dilute suspensions the particle interactions can be neglected, and the coefficients λ_{1-3} can be evaluated from the solution for ϕ_c for a single particle given by Allegra and Hawley.[5] Accordingly, the conditionally averaged $\langle\phi_c\rangle(\mathbf{x}|\mathbf{x}_1)$ given a particle centered at $\mathbf{x}_1$ is given by

$$\langle\phi_c\rangle(\mathbf{x}|\mathbf{x}_1)=\exp(\iota\mathbf{k}_c\cdot\mathbf{x})+\exp(\iota\mathbf{k}_c\cdot\mathbf{x}_1)\times\sum_{n=0}^{\infty}\iota^n(2n+1)A_n h_n(k_c r)P_n(\mu), \tag{13}$$

where $r=|\mathbf{x}-\mathbf{x}_1|$, $\mu=\cos\theta$, θ being the angle between $\mathbf{x}-\mathbf{x}_1$ and $\mathbf{k}_c$, h_n is the spherical Bessel function of the third kind (corresponding to an outgoing scattered wave), and P_n is the Legendre polynomial of degree n. The first term on the right-hand side of the above expression is the unconditionally averaged $\langle\phi_c\rangle(\mathbf{x})$ whose amplitude is taken to be unity with no loss of generality.

Inside the particle centered at $\mathbf{x}_1$ we have

$$\langle\tilde{\phi}_c\rangle=(\mathbf{x}|\mathbf{x}_1)=\exp(\imath\mathbf{k}_c\cdot\mathbf{x}_1)\sum_{n=0}^{\infty}\imath^n(2n+1)\times\tilde{A}_n j_n(\tilde{k}_c r)P_n(\mu), \tag{14}$$

where j_n is the spherical Bessel function of the first kind. Similar expressions are written for the conditionally averaged ϕ_T and $\mathbf{A}$. This results in expressions with a set of six unknowns for each mode n. Application of the aforementioned boundary conditions of continuity of velocity, traction, temperature, and heat flux yield six equations in these six unknowns for each n. There were some typographical errors in the equations given by Epstein and Carhart[6] and Allegra and Hawley;[5] the correct equations are given in the Appendix. Although it is possible to solve for the unknowns analytically in certain limiting cases, it is best to solve them numerically since we are interested in covering a wide frequency range for inverse calculations.

We now return to the calculations of the coefficients λ_{1-3}. Upon using the identity

$$\nabla g=-\mathbf{n}\delta(\mathbf{x}-\mathbf{x}_i),$$

with $\mathbf{x}_i$ being a point on solid–liquid interface and $\mathbf{n}$ the unit normal vector at the point, λ_1 is given by

$$\lambda_1\nabla\langle\phi_c\rangle(\mathbf{x})=-\int_{|\mathbf{x}-\mathbf{x}_1|=a}\mathbf{n}[\langle\tilde{\phi}_c\rangle(\mathbf{x}|\mathbf{x}_1)-\langle\phi_c\rangle(\mathbf{x}|\mathbf{x}_1)]\times P(\mathbf{x}_1)dA_1. \tag{15}$$

Here, $P(\mathbf{x}_1)$ is the probability density for finding a particle in the vicinity of $\mathbf{x}_1$. Similarly, we have for λ_2 and λ_3

$$\lambda_2\tilde{k}_c^2\langle\phi_c\rangle(\mathbf{x})=-\int_{|\mathbf{x}-\mathbf{x}_1|=a}\mathbf{n}\cdot\nabla[\langle\tilde{\phi}_c\rangle(\mathbf{x}|\mathbf{x}_1)-\langle\phi_c\rangle(\mathbf{x}|\mathbf{x}_1)]P(\mathbf{x}_1)dA_1, \tag{16}$$

and

$$\lambda_3\langle\phi_c\rangle(\mathbf{x})=\int g(\mathbf{x})\langle\tilde{\phi}_c\rangle(\mathbf{x}|\mathbf{x}_1)P(\mathbf{x}_1)dV_1. \tag{17}$$

The above integrals must be evaluated while keeping in mind that the integration variable is $\mathbf{x}_1$. Thus, for example, in (15) and (16) we must consider all particles whose surfaces pass through the point $\mathbf{x}$. To carry out these integrals we use the identity

$$e^{\imath\mathbf{k}_c\cdot\mathbf{x}_1}=e^{\imath\mathbf{k}_c\cdot\mathbf{x}}e^{-\imath r k_c\mu}=e^{\imath\mathbf{k}_c\cdot\mathbf{x}}\sum_{m=0}^{\infty}\imath^m(-1)^m(2m+1)j_m(k_c r)P_m(\mu) \tag{18}$$

and the orthogonality of the Legendre polynomials over spherical surfaces. The resulting expressions are

$$\lambda_1=\frac{3\phi}{z}\sum_{n=0}^{\infty}[(n+1)j_{n+1}(z)-nj_{n-1}(z)]\times[\tilde{A}_n j_n(\tilde{z})-j_n(z)-A_n h_n(z)], \tag{19}$$

$$\lambda_2=-\frac{3\phi}{\tilde{z}}\sum_{n=0}^{\infty}(2n+1)j_n(z)\times\left[\tilde{A}_n j_n'(\tilde{z})-\frac{z}{\tilde{z}}j_n'(z)-A_n\frac{z}{\tilde{z}}h_n'(z)\right], \tag{20}$$

$$\lambda_3=\frac{3\phi}{2z\tilde{z}}\tilde{A}_0\left(\frac{\sin(\tilde{z}-z)}{\tilde{z}-z}-\frac{\sin(\tilde{z}+z)}{\tilde{z}+z}\right)+\frac{3\phi}{z^2-\tilde{z}^2}\sum_{n=1}^{\infty}(2n+1)\times\tilde{A}_n[\tilde{z}j_{n-1}(\tilde{z})j_n(z)-zj_n(\tilde{z})j_{n-1}(\tilde{z})], \tag{21}$$

where in the expression for λ_1 the j_{n-1}-term in the $n=0$ contribution is to be left out. Here, ϕ is the volume fraction of the solids, $z\equiv k_c a$ and $\tilde{z}\equiv\tilde{k}_c a$ are the nondimensional wavenumbers, and primes denote derivatives. Expressions (19)–(21), together with the expression for the effective wave number (12), complete the description of a solid–liquid mixture at low volume fractions.

In the above we have derived expressions for the attenuation and wave speed by calculating the effective wave number directly. An alternative derivation of the attenuation coefficient is to calculate the energy dissipation per wavelength in the mixture and divide the result by the energy per wavelength. The result for the attenuation per unit length is then[5,6]

$$\alpha=-\frac{3\phi}{2z^2a}\sum_{n=0}^{\infty}(2n+1)\mathrm{Re}\,A_n. \tag{22}$$

It can be shown that the two methods give essentially the same result for the attenuation in the limit $\phi\to 0$ with $z^{-2}\mathrm{Re}\,A_n$ in the above replaced by $\mathrm{Re}(A_n/z)/\mathrm{Re}(z)$ in the ensemble-averaging method presented here.

The above analysis may be extended to account for the effect of finite volume fraction through a suitable effective-medium approximation. Sangani[11] showed that the first correction of $O(\phi^{3/2})$ to the dilute $O(\phi)$ approximation for bubbly liquids can be simply derived through an effective-medium approximation. This correction is most significant near the resonance frequency of bubbles, and to correctly capture the behavior near resonance it is important to replace the pure liquid wave number (k_c in the above analysis) by the effective wave number. Thus, in the present context, $z\equiv k_c a$ in (19)–(21) for λ_{1-3}, is replaced by $z_{\mathrm{eff}}\equiv k_{\mathrm{eff}}a$, while the wave number in pure liquid in the expression for k_{eff}, (12), has to be retained. The latter expression is then iterated to obtain a converged solution for k_{eff}. The effective-medium approximations have been found to be quite useful in the related study of light scattering by suspensions (see, e.g., Ref. 14). For very high volume fractions the other physical properties of the so-called effective medium must also be modified. In a separate study,[13] where we shall

report experimental data for dense slurries, we shall examine several different versions of effective-medium approximations in more detail.

Finally, the above analysis can be extended in a straightforward manner to account for the particle size distribution when the total volume fraction of the particles is small. Let us write the attenuation by particles of radius between a and $a+da$ as an attenuation density $\hat{\alpha}(f,a)$ [where f is the frequency of the wave, $f=\omega/(2\pi)$] times the volume fraction of those particles $\phi(a)da$; we shall refer to $\phi(a)$ as the volume fraction distribution. At low volume fractions these contributions can be "summed" over all particle sizes to give for the total attenuation $\alpha_{\text{tot}}(f)$:

$$\alpha_{\text{tot}}(f)=\int_{a=0}^{\infty}\hat{\alpha}(f,a)\phi(a)da. \tag{23}$$

It is customary to express the particle size distribution in terms of its number density distribution $P(a)$. The volume fraction distribution is related to $P(a)$ by $\phi(a)=(4\pi a^3/3)P(a)$.

The effective-medium approach described earlier can also be readily extended to account for the particle size distribution. The coefficients λ_{1-3} are first determined as functions of a for an assumed value of the effective wave number and these are integrated after multiplying by $\phi(a)da$ to yield estimates for the average values of λ_{1-3} for the suspension. These are substituted in (12) to determine k_{eff}. If this estimate of k_{eff} is different from the the assumed value, then λ_{1-3} are estimated for the new value of k_{eff}, and the process is repeated until the assumed and estimated values of the effective wave numbers agree with each other.

III. DISCUSSION AND COMPARISON WITH EXPERIMENTAL DATA

Figures 1 and 2 show the predictions for the attenuation and wave speed as a function of frequency f for 79 μm radius polystyrene particles at a volume fraction of 0.05. The frequency f in Hz is related to ω by $\omega=2\pi f$. The physical properties used in the computations are given in Table I.[15] We note that the wave speed only changes if the frequency becomes very large and that these changes coincide with strong changes in the attenuation as well. Hence we expect that the measurement of the phase speed will not provide significantly new information over that obtained from the attenuation measurements alone as far as the problem of determining the size distribution is concerned. On the other hand, since the phase speed at low frequencies is nearly independent of the frequency or $k_c a$, it might be possible to use the low frequency speed data to determine the total volume fraction of the particles regardless of its size distribution. We shall focus in the present study on the results for attenuation as they are the most sensitive to the particle size distribution.

The attenuation of sound waves in a suspension is different from that in pure liquid because of four effects. First, the attenuation of sound in pure solid is different from that in pure liquid, and hence simply the presence of the particles changes the attenuation from that of pure liquid. Second, changes in temperature are different in a solid than in a liquid, and this causes a heat flux through the surface of the particles. This heat flux is out of phase with the sound wave passage and this leads to attenuation referred to as the thermal attenuation. Third is the viscous energy dissipation caused due to the motion of the boundary of the suspended particles. Finally, the fourth effect is the attenuation due to scattering.

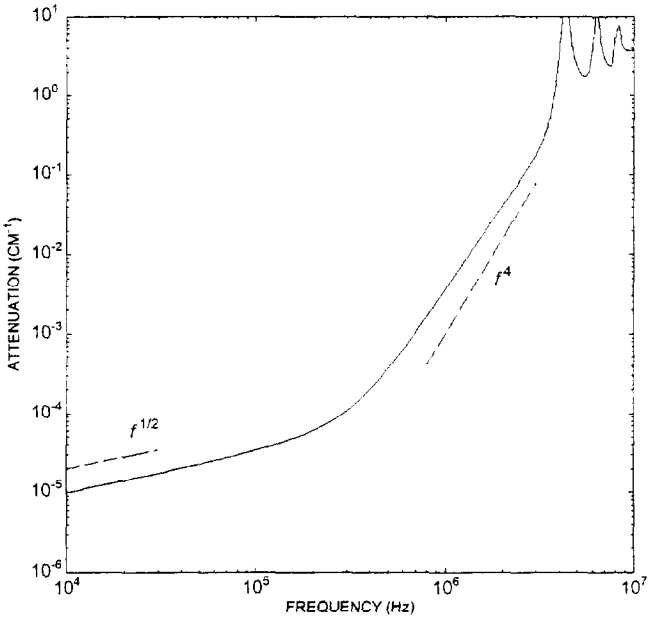

FIG. 1. Example of the dependence of attenuation on frequency f for a mixture of monodispersed polystyrene particles in water. Dashed lines are asymptotic slopes of the attenuation for small and large frequencies.

Allegra and Hawley[5] showed that when the particle size is much smaller than the wavelength and much greater than the thermal and viscous penetration depths $(\sigma/\omega)^{1/2}$ and

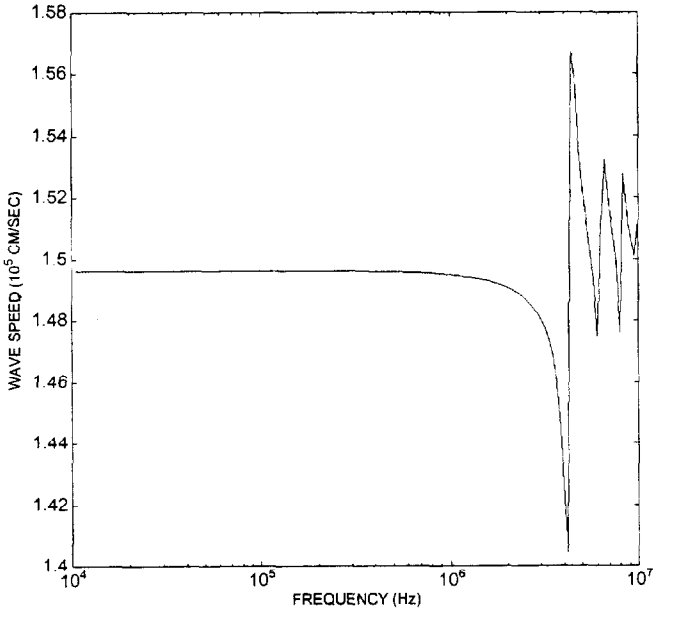

FIG. 2. Example of the dependence of wave speed on frequency f for a mixture of monodispersed polystyrene particles in water.

TABLE I. The values of the physical properties that are used in this paper. The properties of water and polystyrene were taken from Ref. 6; the properties of glass from various sources, most notably Ref. 15.

	Polystyrene	Glass	Water
density (g/cm^3)	1.055	2.3	1.0
thermal conductivity (J/K·cm·sec)	1.15×10^{-3}	9.6×10^{-3}	5.87×10^{-3}
specific heat (J/g·K)	1.19	0.836	4.19
thermal expansion coefficient (1/K)	2.04×10^{-4}	3.2×10^{-6}	2.04×10^{-4}
attenuation coefficient per freq^2 (sec^2/cm)	10^{-15}	10^{-15}	2.5×10^{-16}
sound speed (cm/sec)	2.3×10^{5}	5.2×10^{5}	1.48×10^{5}
shear viscosity (g/cm·sec^2)	...	...	1.01×10^{-2}
shear rigidity (g/cm·sec^2)	1.27×10^{10}	2.8×10^{11}	...

$(\nu/\omega)^{1/2}$, the resulting viscous and thermal attenuations increase as $f^{1/2}$. On the other hand, when the penetration depths are much greater than the particles, both attenuation contributions increase as f^2. This transition occurs at very low frequencies—about 2 Hz for 100 μ radius particles in water—and will not be considered here. Attenuation due to scattering becomes important when the nondimensional wave number $z=k_c a$ becomes comparable to unity. For small but finite z the scattering losses increase as f^4. Thus, one expects that the change in the attenuation behavior from $f^{1/2}$ at low frequencies to f^4 at high frequencies will provide an important indication of the particle size. These asymptotic ranges are indicated in Fig. 1. We see that the transition to the f^4 behavior does not fully occur for the particles considered here. As the frequency is increased particles undergo several resonances as described in more detail below, and this is responsible for the several peaks seen in Fig. 1.

Figure 3 shows the contributions to the total attenuation from each P_n mode. The $n=0$ mode corresponds to radial (volume) oscillations of the particles, $n=1$ to the translational oscillations, $n=2$ to the ellipsoidal P_2-shape deformation oscillations, and so on. The density of polystyrene particles is essentially the same as that of water, hence the particles' translational oscillations are very small. As a consequence, the viscous attenuation is small and the small frequency behavior is governed by the thermal attenuation of the $n=0$ mode. At higher frequencies the $n=0$ mode begins to increase first as f^4 due to scattering losses but the contribution from the $n=2$ mode soon becomes important as it undergoes a resonance at about 3 MHz frequency. The $n=3$ and $n=1$ modes undergo resonances next, and so on. We see that the $n=0$ mode undergoes a broad maximum around 9 MHz. Although not shown here, it too undergoes a resonance with a sharp downward peak at about 21 MHz. Thus, we see that the attenuation varies with frequency in a rather complicated manner at high frequencies owing to various resonances. We should note here that the behavior of this kind for polystyrene particles has also been reported by other investigators in the past. For example, Anson and Chivers[16] and Ma, Varadan, and Varadan,[14] who restricted their analysis to scattering losses only, found essentially the same behavior, and in earlier investigations[17,18] mainly focusing on the determination of waves reflected by immersed objects, high-amplitude reflected waves were found at certain resonance frequencies.

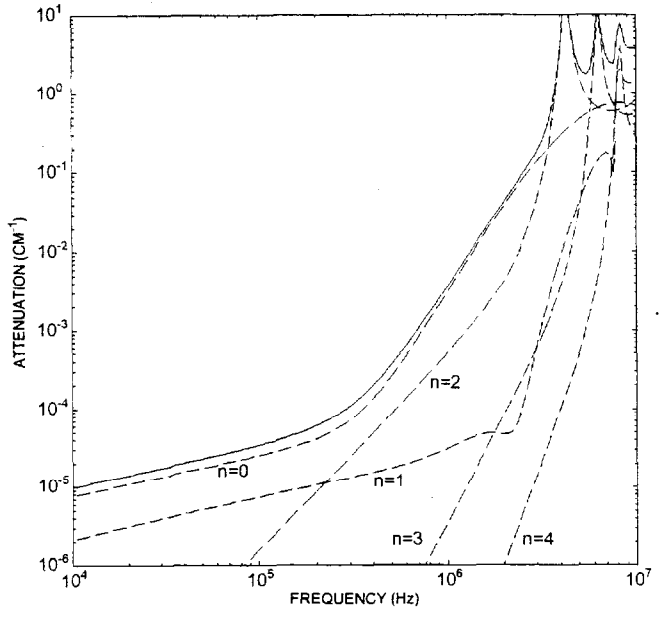

FIG. 3. Contributions from the first five modes n in (19)–(21) to the total attenuation [the imaginary part of k_{eff}, which is given by (12)]. Polystyrene particles in water.

Figure 4 shows attenuation as a function of nondimensional wave number $k_c a$ for particles of radii 50 and 79 microns. We see that the curves for these two radii are essentially the same, indicating that, at least for polystyrene particles, the thermal or viscous effects have negligible influence on the resonance frequency. The first resonance corresponding to $n=2$ appears at $k_c a \simeq 1.4$.

Allegra and Hawley[5] tested (22) extensively against their experiments and found very good agreement. However, their particles were always smaller than 1 μm radius, so that the wavelength was always much greater than the particle size. No resonance behavior was observed in their experiments. Although the above-mentioned paper by Ma, Varadan, and Varadan[14] presents experimental data on light scattering in the small-wavelength regime, no data on attenuation of sound waves by particles were presented. To test how well the theory works for larger particle sizes, we carried out an experiment that will be described in detail (along with more experiments on concentrated slurries) elsewhere.[13] In this experiment the attenuation of sound waves was measured in a frequency range of 1–10 MHz in a solid–liquid mixture of

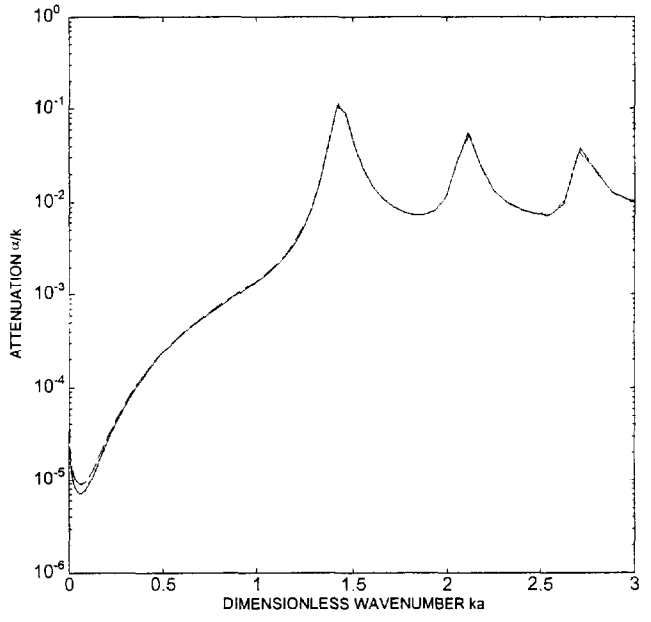

FIG. 4. Attenuation divided by wave number as a function of the wave number times the particle radius in the scattering regime for monodispersed polystyrene particles (—, $a=79$ μm; ---, $a=50$ μm). The volume fractions of the particles in both cases are the same and equal to 0.05.

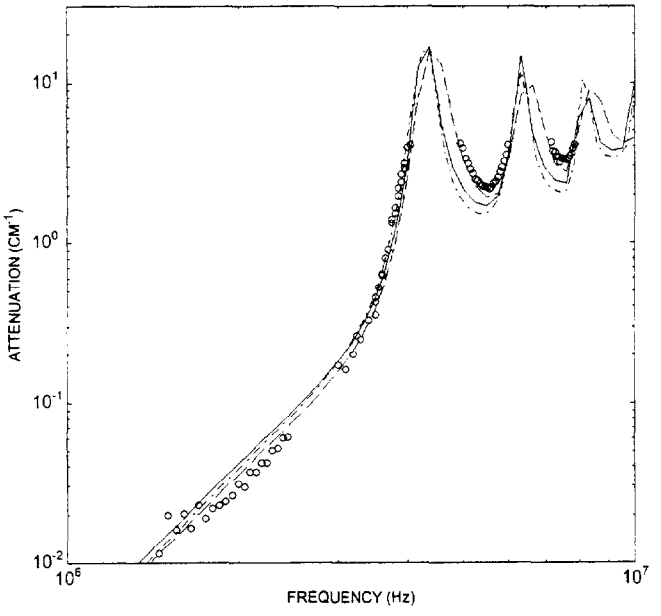

FIG. 5. Comparison with experimental data for the attenuation as a function of frequency. Polystyrene particles of radius $a=79$ μm and 0.05 volume fraction. O, experiments; ———, theory for monodispersed particles; -.-.-., theory for monodispersed particles with effective medium correction for finite volume fraction effects; ---, theoretical result with a particle size distribution with a mean particle radius of 77 μm and standard deviation of 2.5 μm (this is within the range specified by the manufacturer).

polystyrene particles with $79\pm3\mu$ mean radius and 1.8 μ standard deviation at 0.05 volume fraction. Monochromatic tonebursts, at incremental frequencies, were transmitted by a transducer on one side of a small vessel in which the mixture was being stirred; a second transducer received the signal and sent it to a LeCroy 9310A digital oscilloscope. The amplitude of the signal for pure water was measured, as was that for the solid–liquid mixture. The excess attenuation was determined by

$$\alpha=-\frac{1}{d}\log\left(\frac{V_{\mathrm{mix}}}{V_{\mathrm{H_2O}}}\right),$$

where d is the distance between the transducers and V_{mix} and $V_{\mathrm{H_2O}}$ are the voltage amplitudes of the received signals in the mixture and pure water, respectively. The distance between the transducers was 2 in. at low frequencies and 1 in. at higher frequencies; this was necessary because the attenuation at higher frequencies was too large to produce significant signal-to-noise ratio in the larger vessel.

Figure 5 shows the comparison between theory and experiment. At the two gaps in the frequency domain (where the theory predicts very high peaks) the attenuation became again so large that the signal-to-noise ratio vanished even in the smallest vessel. Good agreement is found between experiments and the theory except near resonance frequencies where small differences are seen. There are two possible reasons for these small differences. The first is concerned with the finite volume-fraction effect. To investigate this we have also plotted in Fig. 5 a result from an effective-medium approach described in the previous section. The resulting attenuation changes, but in the wrong direction. The second reason is that the particles were not exactly monodispersed. Using the method described in the previous section, a log-normal particle size distribution was introduced with a mean radius of 77 and 2.5 μm standard deviation, which lies within the manufacturers' specifications. The result for the attenuation, the dashed curve in Fig. 5, shows close agreement with the data. Thus, we conclude that the agreement between the theory and experiment is excellent, and that the small observed differences are due to small polydispersity of the suspension.

The attenuation behavior displayed by polystyrene particles is not generic, as can be seen from Fig. 6 which shows the attenuation behavior for glass particles. Since the density of the glass particles is significantly different from that of water, the glass particles execute significant translational oscillations. As a consequence, the low-frequency behavior is completely governed by the viscous effects and the $n=1$ mode. Note that the small frequency attenuation is about two orders of magnitude greater for glass particles than for the polystyrene particles. Also we see a considerably different behavior at higher frequencies. The attenuation does not seem to peak at several frequencies. Rather, for each n we see broad "hills" separated by narrow "valleys." The total attenuation does not appear to go through several resonances. The difference in the behavior for the glass and polystyrene particles at these high frequencies seems to arise mainly from the different elastic properties of the two materials.

IV. THE INVERSE PROBLEM

We now consider the inverse problem: given the total attenuation α_{tot} as a function of f we wish to determine $\phi(a)$ using (23). The straightforward method of solving the inte-

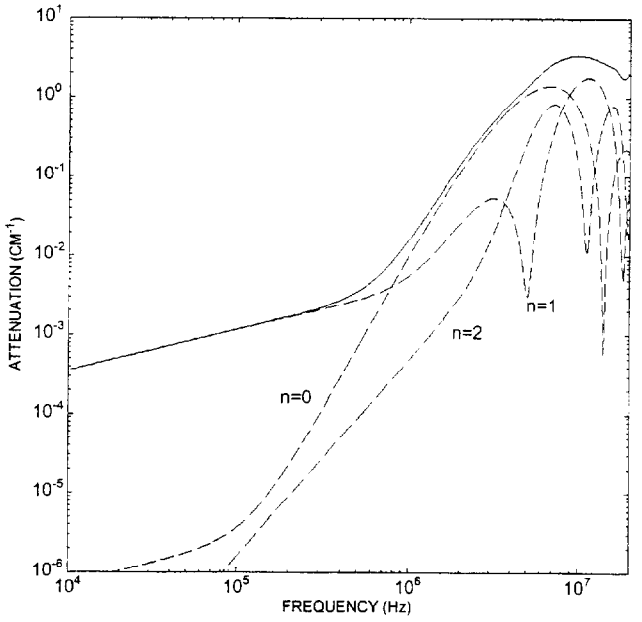

FIG. 6. Attenuation by monodispersed glass particles (of 79 μm radius) in water as a function of frequency and the contributions from the first three modes n in (19)–(21) to the total attenuation [the imaginary part of k_{eff}, which is given by (12)].

gral equations, i.e., discretizing the integral domain into a number of elements and converting the integral equation into a system of linear equations in unknowns $\phi(a_k)$ at a selected number of points a_k in the domain, cannot be used since the resulting equations will be ill conditioned. Figure 7 illustrates the ill-posed nature of the problem. Figure 7(a) shows two very different particle distributions whose attenuation versus frequency curves are seen in Fig. 7(b) to be essentially the same. These curves were obtained by starting with a smooth, log-normal particle size distribution [the dashed curve in Fig. 7(a)] and generating the attenuation versus frequency data using the forward theory [the circles in Fig. 7(b)]. A 1% random noise was then added to the data and (25) with $\epsilon=0$, which is equivalent to the integral equation (23), was subsequently solved to yield the particle size distribution indicated by the solid line in Fig. 7(a). The pluses in Fig. 7(b) correspond to the attenuation determined from the forward theory using the new particle distribution. Note that the attenuation is evaluated with a smaller frequency increment than the one used for the original distribution. We see that the attenuation from the two distributions agree with each other to within 1% for the frequencies marked by circles. The highly oscillatory particle distribution does show an oscillatory behavior in between the frequency increments, particularly at 10 MHz, but these oscillations occur only for a very narrow frequency range and would have been missed altogether had the attenuation been determined only at the input frequencies.

A. Method

Since the true particle distribution is expected to be smooth, we must only allow solutions that are reasonably smooth. There are several ways of accomplishing this. In the

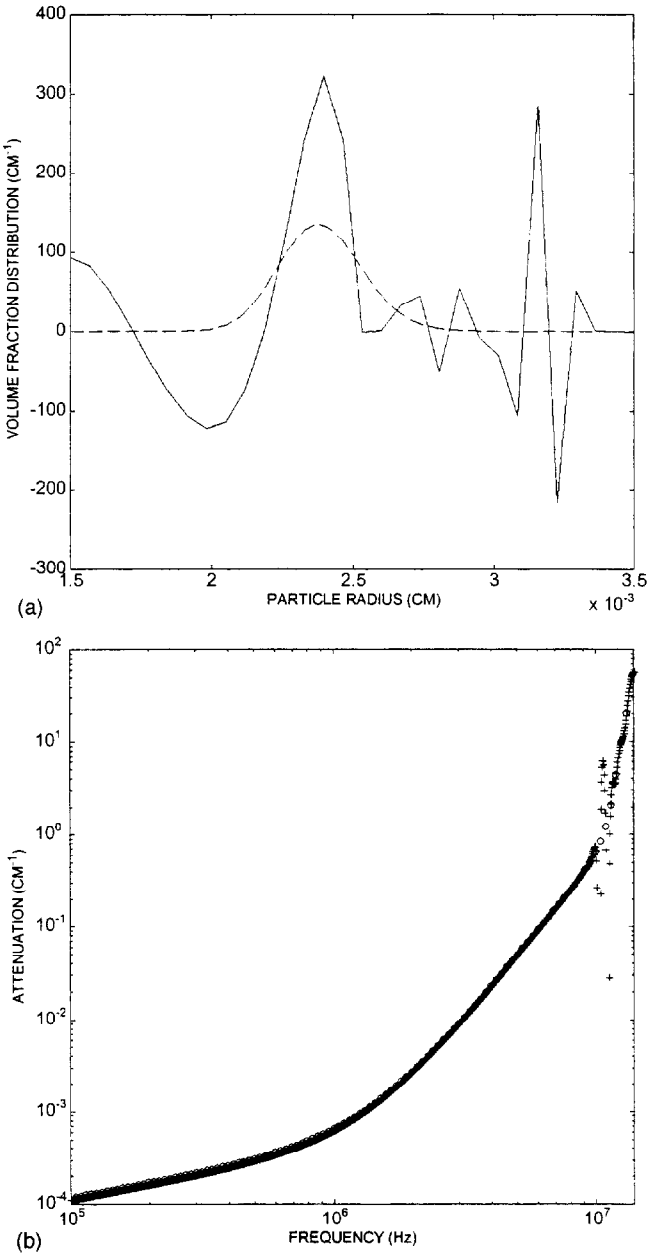

FIG. 7. Influence of fluctuations superimposed on the volume fraction distributions (a) on attenuation data (b). In (b) the circles correspond to the result when using the dashed distribution of (a) and the pluses when using the solid line in (a).

present study, we shall use primarily a regularization technique due to Tikhonov[8] which was successfully used for bubbly liquids by Duraiswami.[2] An alternative method is presented at the end of this section. Accordingly, we multiply (23) with $\hat{\alpha}(f,a)df$ and integrate over the frequency range to obtain a simpler integral equation in which the right-hand side is only a function of a:

$$\int_{f_{\min}}^{f_{\max}} \int_{a_{\min}}^{a_{\max}} \hat{\alpha}(f,a)\hat{\alpha}(f,a')\phi(a')da'df$$

$$= b(a) \equiv \int_{f_{\min}}^{f_{\max}} \alpha_{\text{tot}}(f)\hat{\alpha}(f,a)df, \tag{24}$$

where $(a_{\min}, a_{\max})$ and $(f_{\min}, f_{\max})$ are the radius and frequency ranges. The above integral equation is now regular-

ized as explained below by adding a small term $\epsilon(\phi - l^2\phi'')$ (where primes denote derivatives) to its left-hand side. Thus, we obtain

$$\epsilon[\phi(a) - l^2\phi''(a)] + \int_{a_{\min}}^{a_{\max}} K(a,a')\phi(a')da' = b(a), \quad (25)$$

where l is a suitably chosen lengthscale and $K(a,a')$ is a kernel defined by

$$K(a,a') = \int_{f_{\min}}^{f_{\max}} \hat{\alpha}(f,a)\hat{\alpha}(f,a')df. \quad (26)$$

Equation (25) is an integro-differential equation and needs two boundary conditions. Usual practice is to take the derivative of $\phi(a)$ to be zero at the two end points:

$$\phi'(a_{\min}) = \phi'(a_{\max}) = 0. \quad (27)$$

Note that $a_{\min}$ and $a_{\max}$ are not known *a priori* in general. One expects ϕ to be zero also at the two end points. Thus, the range $(a_{\min} - a_{\max})$ must be determined by trial and error so that both ϕ and its derivatives are approximately zero at the extreme values of a.

Now it can be shown that the solution of (25) subject to the boundary conditions given by (27) minimizes

$$E + \epsilon \int_{a_{\min}}^{a_{\max}} [\{\phi(a)\}^2 + l^2\{\phi'(a)\}^2]da, \quad (28)$$

where E is the measure of error between the actual attenuation and the computed attenuation:

$$E = \int_{f_{\min}}^{f_{\max}} \left| \int_{a_{\min}}^{a_{\max}} \hat{\alpha}(f,a)\phi(a)da - \alpha_{\text{tot}}(f) \right|^2 df. \quad (29)$$

Since both E and the second term in (28), i.e., the integral, are non-negative, minimization of (28) ensures that the solution of (25) will be free from large oscillations in ϕ. In other words, highly oscillatory distributions such as the one shown in Fig. 7(a) are rendered inadmissible when (25) is solved with finite, positive ϵ in place of the original integral equation (24). Thus, we have regularized the problem of determining ϕ.

If we choose a large ϵ, then we decrease the oscillations in ϕ but increase the error in $\phi(a)$ since then the equation solved is significantly different from the original integral equation. Small ϵ, on the other hand, yields unrealistic $\phi(a)$ having large oscillations when the data $\alpha_{\text{tot}}(f)$ are not exact. An optimum choice of ϵ then depends on the magnitude of uncertainty/error in the attenuation-frequency data. In the calculations we shall present here the exact $\alpha_{\text{tot}}(f)$ is first determined using the forward theory for a given $\phi(a)$ and a small random noise of about 1% magnitude is added to it before the inverse calculations are made (the effect of noise magnitude is discussed below). Thus, we have an estimate of the error in the data, but in general this estimate may not be known reasonably accurately. To determine the optimum ϵ, we solve (25) for several different ϵ's and plot E versus ϵ to find a minimum in E. This, however, may lead to distributions in which $\phi(a)$ may have unphysical negative values for some a. The constraint $\phi(a) \geq 0$ for all a is satisfied *a posteriori* by setting $\phi(a) = 0$ for all a's for which the solution of (25) gave negative values of ϕ. The computed value of E for a given ϵ is then based on $\phi(a) \geq 0$.

The integro-differential equation (25) was solved as follows. After discretizing the domain $(a_{\min} - a_{\max})$ into $N-1$ equal segments and the frequency domain into $M-1$ logarithmically equal segments we first evaluate the kernel $K(a_i,a_j)$ for $i,j = 1,2,...,N$ [cf. (26)] using a trapezoidal rule for the integration over the frequency range. As pointed out by Duraiswami,[2] it is essential to calculate the integral over particle radius very accurately. We assume that $\phi(a)$ varied in a piecewise linear manner in each segment and use a 12-point Gauss–Legendre quadrature to evaluate the integral in (25). A second-order central difference formula was used to evaluate $\phi''(a)$ at all points except the end points $a_{\min}$ and $a_{\max}$. The boundary conditions $\phi'(a_{\min}) = 0$ and $\phi'(a_{\max}) = 0$ were approximated using, respectively, second-order forward and backward difference formulas. Application of (25) at all the discretization points together with the boundary conditions can be expressed with the above scheme as a system of linear equations:

$$\sum_{j=1}^{N} A_{ij}\phi_j = b_i, \quad i = 1,2,...,N, \quad (30)$$

where $\phi_j = \phi(a_j)$ and $b_i = b(a_i)$. The above set of equations was normalized by dividing all the equations with the greatest element of the kernel $K(a_i,a_j)$, K_m for all i,j, times the segment length $\Delta a = (a_{\max} - a_{\min})/(N-1)$. This set of equations was subsequently solved using a standard IMSL subroutine for linear equations.

Once ϕ_j are determined for a selected value of ϵ, we satisfy the constraint $\phi_j \geq 0$ by setting, as mentioned earlier, $\phi_j = 0$ for all negative ϕ_j. The error E as given by (29) was subsequently evaluated using a trapezoidal rule for integration over the frequency range. The optimum value of ϵ was determined by stepping logarithmically through several values of ϵ and plotting E versus ϵ.

A typical result ($N = 30$, $M = 112$, $f_{\min} = 0.1$ MHz, $f_{\max} = 17$ MHz, $a_{\min} = 15$ μm and $a_{\max} = 35$ μm) for the error E in the resulting attenuation as a function of ϵ is shown in Fig. 8. Note that ϵ here is the actual ϵ divided by $K_m\Delta a$. We see a clearly defined optimum value of ϵ. Computations were also made with larger M to confirm that the resulting volume fraction distribution was not affected by the further refinement in the integration over the frequency range. A remark should also be made of the choice for the length l in (25). We may regard both ϵ and l as parameters to be chosen so as to minimize the error E. Taking $l = (a_{\max} - a_{\min})/n$ we computed E by varying both ϵ and n with n varied from 1 to N. The three-dimensional plot of E versus n and ϵ showed that E was much more sensitive to the choice of ϵ than it was to n. In general, the results with n close to N were slightly better than with those near $n = 1$. Based on this observation we chose $n = 30$. For larger values of $N(N > 40)$ we found that choosing $n = N$ led to more oscillatory behavior for ϕ_j. This is to be expected since choosing larger n, and, hence, smaller l, permits larger values of $\phi'(a)$.

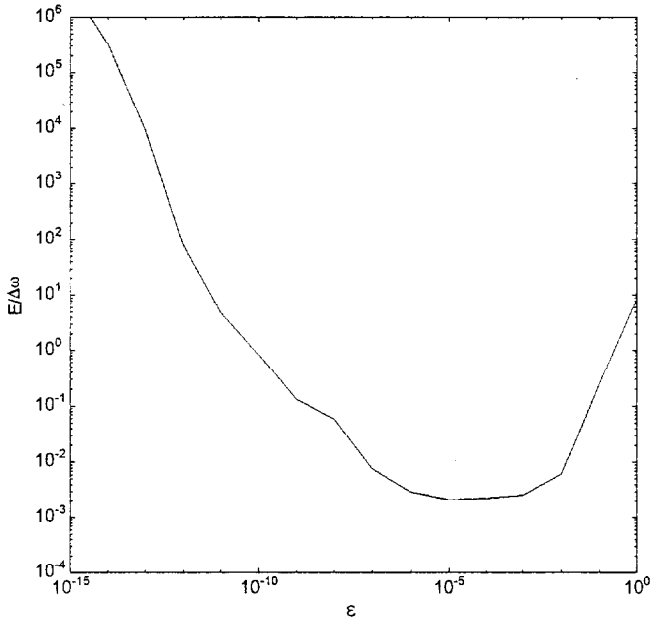

FIG. 8. Typical dependence of the error in the attenuation for the solved volume fraction distribution as a function of the regularization parameter ϵ. The (small) parameter ϵ should be chosen such that this error is minimized. The minimum was always found to be well-defined.

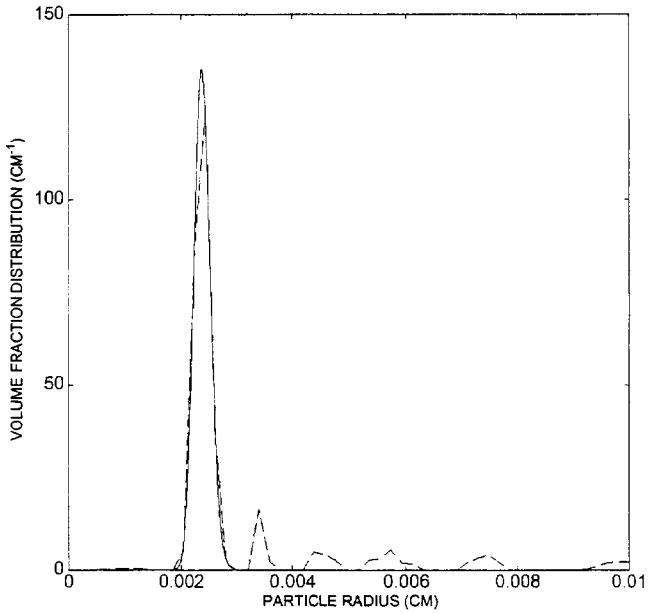

FIG. 9. Solving the inverse problem for polystyrene particles. The solid line is the volume fraction distribution used to generate attenuation data [shown in Fig. 12(a), with f_{max} as indicated by a square]; the dashed line is the solution of the inverse problem when taking the particle radius range to be 1–100 μm and using 50 "bins" of particle sizes.

B. Results and discussion

We now present results for the volume fraction distribution obtained using the above technique. As mentioned earlier, we used the forward theory to generate attenuation data for an assumed volume fraction distribution. Small random noise can be added to the data thus generated to mimic possible errors arising in the attenuation measurement. This is satisfactory since we are primarily interested in assessing the procedure for solving the inverse problem. If the procedure gives erroneous results even for this case, it will certainly break down in practice using the experimentally generated data.

The frequency range over which the attenuation measurements are carried out in our laboratory is 0.1–15 MHz. We shall choose here the same range to investigate the success and limitations of the above technique to solve the inverse problem although we shall also consider cases with a larger frequency range to inquire if better estimates of $\phi(a)$ could be achieved if the attenuation data at higher frequencies were to be made available. This is important since the acoustic instruments operating up to 150 MHz are available.

We consider first particle sizes that are of the same order of magnitude as the wavelength somewhere in this frequency range, which is the case for particles of about 10–100 μ radius (for larger particles observed behavior of the attenuation is shifted to lower frequencies). A particle size distribution that is often used is a log-normal distribution, which results in volume fraction distributions such as the smooth one shown in Fig. 7(a). We attempt therefore to recover that distribution from the corresponding attenuation data. As in the forward problem, we shall investigate polystyrene particles and glass particles in water, as the first are almost neutrally buoyant and deformable while the latter are very rigid and much heavier than water; the physical properties used in the present calculations are listed in Table I.

We begin with the results for polystyrene particles with a narrow size distribution in the range of 20–30 μm. The particle size range for the inverse calculations is first taken to be much greater—5–100 μm; the frequency range was 0.1–17 MHz. Figure 9 shows that the volume fraction distribution as evaluated from the inverse technique is in very good agreement with the input distribution. The result for the size distribution can be improved further by making the particle size range smaller (a close-up of the improved result is shown in Fig. 11).

In Fig. 10 we consider a more complicated, bimodal size distribution in the range of 20–45 μm with peaks at about 25 and 38 μm. The attenuation as a function of frequency for this distribution is shown in Fig. 10a. The maximum frequency used for inverse calculations is indicated by a square; it is seen that the frequency range includes the first two resonance peaks of the attenuation curve. From Fig. 10(b) we see once again that the inverse procedure recovers this distribution very well.

One of the difficulties in solving an ill-posed problem is that small errors in the input (attenuation) data can cause large changes in the solution. Of course, errors are always present in the experimentally obtained attenuation data. The calculations presented so far were made with no added noise. To mimic the practical situation, we added random noise of 5% standard deviation to the input data; this is about the same as the order of magnitude of the errors present in the experimental results shown in Fig. 5. The resulting volume fraction distribution, shown in Fig. 11, does confirm that small fluctuations in the input data only cause small deviations in the output. When the calculations were repeated with

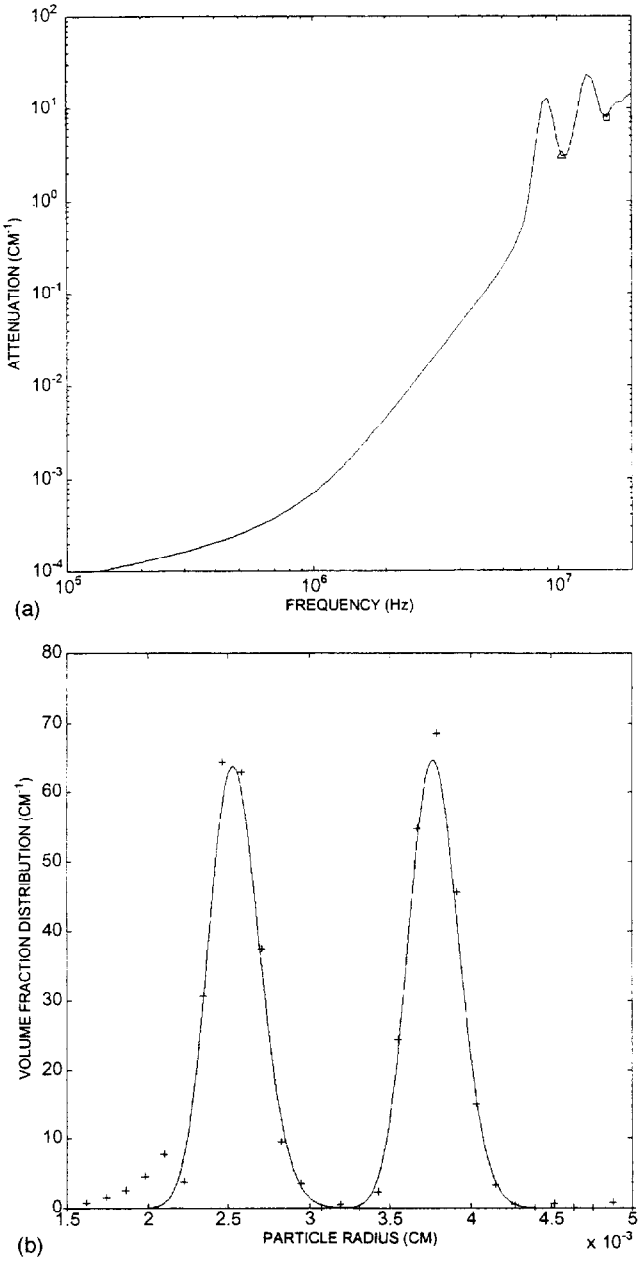

FIG. 10. Attenuation (a) and the solution of the inverse problem (b) for a bimodal distribution of polystyrene particles, using 30 particle size bins. In (b), the solid line is the exact result, markers represent the inverse problem solution when using for f_{max} the value indicated by a square in (a). Results when cutting of the frequency range at the point marked by a triangle are discussed along with Fig. 14.

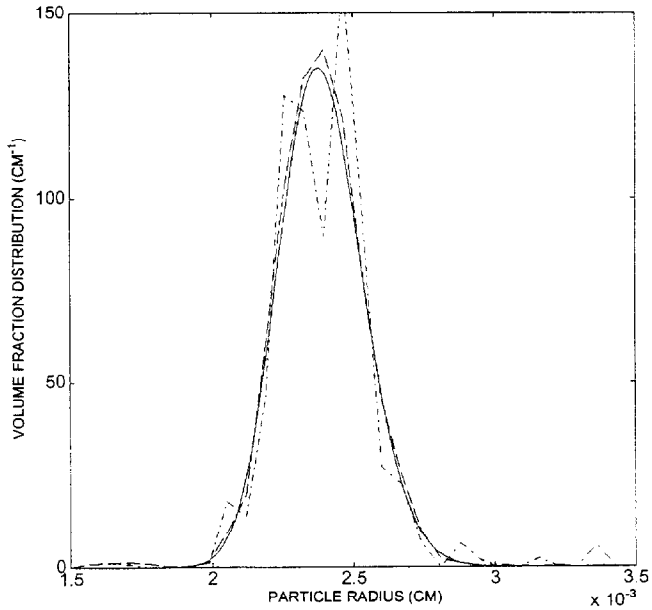

FIG. 11. Solution of the inverse problem when random noise of 5% standard deviation is introduced in the attenuation (input) data. Solid line is the exact result; the broken line is the result when no noise is introduced (already shown in Fig. 8); and the dash–dotted curve is the result after introduction of the noise. Polystyrene particles in water.

a noise of 10% standard deviation, the computed particle size distribution was found to be considerably different from the input distribution, although the main features of the size distribution were preserved by the inverse computations.

The results discussed so far suggest that the inverse problem can be solved with reasonable success. We now illustrate some limitations. The inverse method gave erroneous particle size distributions for smaller particles when the same frequency range as the above was used. Of course, in order that the size of the particles be determined there must be at least one transition—from the thermal attenuation dominated regime to the scattering dominated regime which occurs roughly speaking at $k_c a = O(1)$. If the particles are very small, then this transition may not occur over a fixed frequency range. However, as we shall presently see, the results are very sensitive to the frequency range chosen for computations even when this transition is included in the range.

Figure 12 shows the effect of varying f_{max} on the computed distribution. As seen in the figure the resonance in the shape oscillations of the (polystyrene) particles leads to a change in the slope of the curve just before the first resonance. This transition occurs just beyond the point marked by a circle in Fig. 12(a). We see a marked improvement in the results in Fig. 12(b) when f_{max} is chosen corresponding to a point marked plus in Fig. 12(a) over those obtained with a point corresponding to the circle which does not include the second change in slope. The point marked plus corresponds to a frequency greater than the frequency at which the second change in slope occurs for larger particles but smaller than that for smaller particles. This seems to give rise to an inverse solution which is reasonably accurate for larger particles but not for smaller particles. Also shown in Fig. 12(b) are the results when f_{max} is chosen to coincide with the end of first peak, the point marked square in Fig. 12(a). This is seen to yield very accurate results for the size distribution.

One might suppose that covering a broad enough frequency range will alleviate the difficulties seen above. This, unfortunately, is not the case. Figure 13 shows the results for three different f_{max}. The dashed curve corresponds to cutting off the frequency range at the end of first peak as in Fig. 12, the dashed–dotted line to the end of three peaks, and the dotted line to 10^9 Hz, a frequency about 50 times greater than the first resonance frequency. We see that the results of

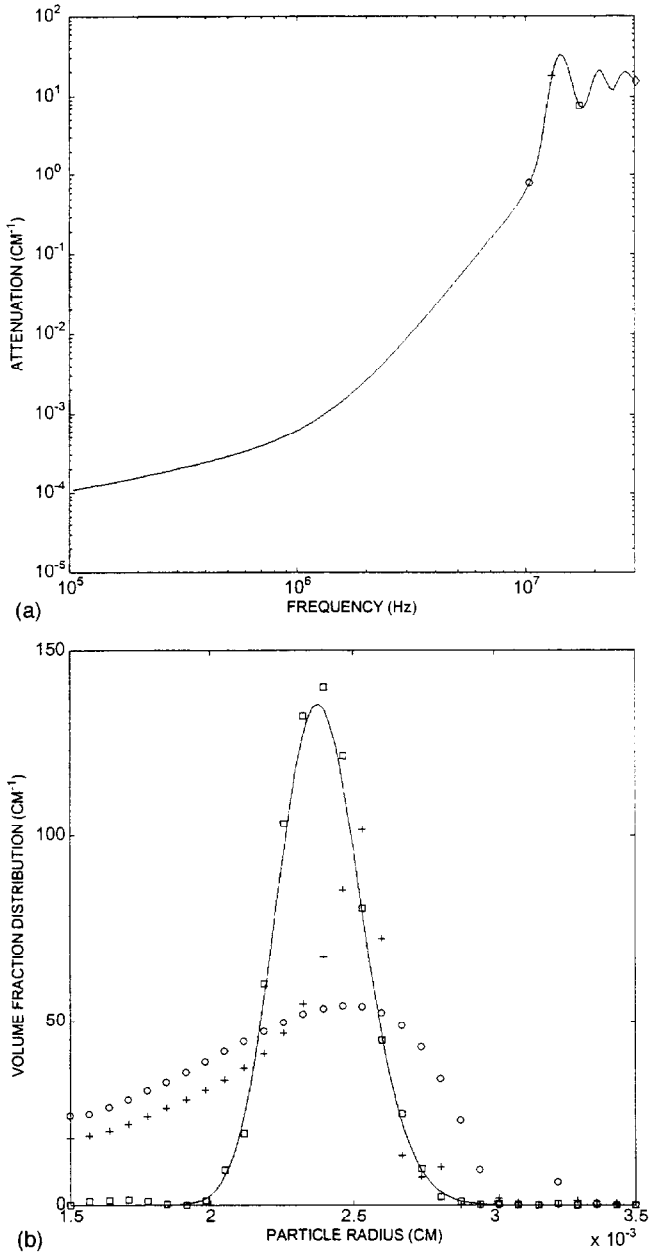

FIG. 12. Influence of the size of the frequency range over which attenuation is specified on the solution of the inverse problem. Polystyrene particles. (a) Input-attenuation data and four different upper bounds on the frequency. (b) Results from the inverse problem from these different ranges, using the same marker type. The solid line is the exact result; □, result when cutting off the frequency range just at the end of the first peak in the attenuation; +, result when cutting of the frequency range after the second change in slope of the attenuation; and ○, result when cutting off before the second change in slope. Cutting off the frequency range at the point marked "◇" is discussed along with Fig. 13.

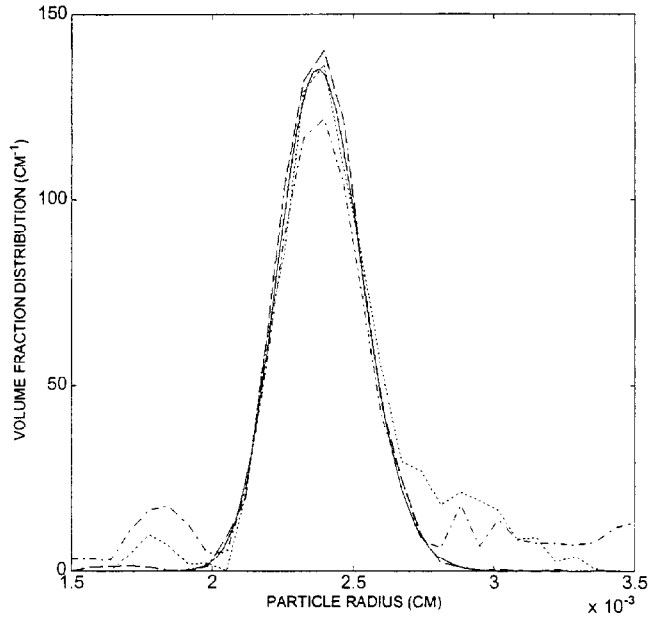

FIG. 13. Too big a frequency range over which the attenuation is available for polystyrene particles also deteriorates the result: the solid line is the exact result; the dashed line is the inverse problem result when using attenuation data of Fig. 12(a) below the point marked by "□," the dashed-dotted line represents the result when this end point is shifted to the point marked by "◇" and the dotted line is the result when this end point is shifted to 1000 MHz.

inverse calculations actually deteriorate if a much larger range of frequency is employed, notwithstanding the fact that measurements over such a broad frequency range could itself be a very challenging task. One may rationalize this result as follows. As seen in Fig. 1 a monodisperse suspension will exhibit several resonance frequencies corresponding to various shape oscillation P_n ($n=2,3,...$) modes. Thus, a second peak in the attenuation-frequency curve for polystyrene particles may correspond either to say, a P_3 mode of a larger particle, or may correspond to a P_2 mode of a smaller particle. In our calculations we used only up to the first six modes ($n \leqslant 5$), but in practice the acoustic response may be further complicated by the higher-order modes for frequencies of order 10^9 Hz considered here.

Since including a wide frequency range with several resonance peaks seems to adversely affect the inverse calculation, one may consider cutting off the attenuation data beyond first peak. This, however, may not work if the distribution is truly bimodal as was the case considered earlier in Fig. 10. If we omit the second resonance peak from the attenuation data by considering a maximum frequency that is less than the point marked square in Fig. 10(a), say, that marked by the circle, we get a poor inversion as shown in Fig. 14. The inverse technique computes accurately the volume fraction distribution of larger particles whose resonance was included in the data but fails to predict that for smaller particles.

Figure 15 shows results for a broad, unimodal distribution. The resonance peaks of different particles overlap in this case resulting in the absence of peaks in the attenuation-frequency curve [Fig. 15(a)]. Figure 15(b) shows the results of inversion for three different cut-off frequencies. The largest frequency, marked by a square in Fig. 15(a), is larger than the second transition frequency of small as well as large particles, and this seems to produce excellent inverse results.

In most of the inverse calculations shown so far which yielded poor results, we note that the failure is particularly severe for smaller particles. One may rationalize this by observing that the total error E will be dominated by the errors at large frequencies since the attenuation there is very large.

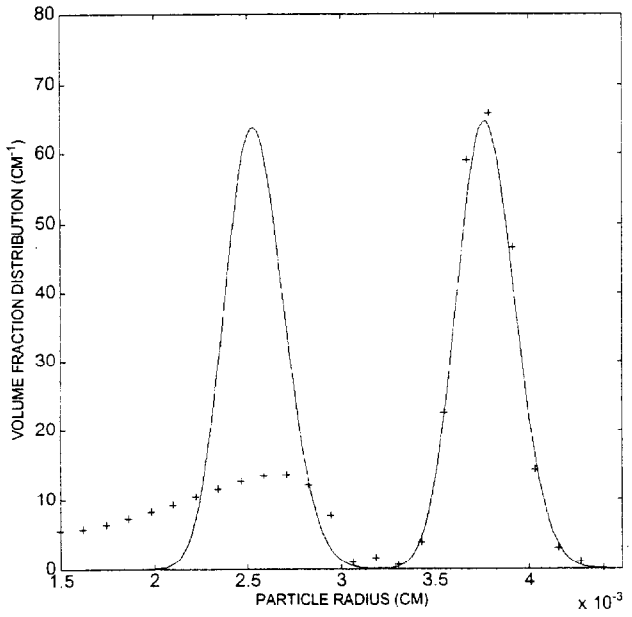

FIG. 14. As in Fig. 10(b), but after cutting off the frequency range over which the attenuation was given between the first and second (attenuation) peak, indicated by a triangle in Fig. 10(a).

When $k_c a_{\min} < 1$ in the frequency domain that is considered, the small particles' volume fraction is seen from Figs. 12(b) and 14 to be underestimated, while the large particles' volume fraction is overestimated. To decrease the relative importance of the attenuation at high frequencies, we solved a slightly different inverse problem in which both the attenuation and $\hat{\alpha}$ were divided by f^2. However, only small improvements were found by modifying the attenuation data this way. The inverse-problem result shown in Fig. 14 was in fact obtained in this way.

Some insight into why the choice of $f_{\max}$ drastically affects the results may be gained from Fig. 16, which shows the three-dimensional plots for the kernel $K(a_i, a_j)$ for the same values of $f_{\max}$ as considered in Fig. 12. We see that when $f_{\max} = 10.4$ MHz, corresponding to the circle in Fig. 12(a), the kernel has a maximum for $a_i = a_j = a_{\max}$. The kernel for smaller particles is very small and, as a consequence, the inverse technique could determine the larger particle size volume fraction correctly but failed for smaller particles. In contrast to this the kernel for $f_{\max} = 17.1$ MHz, corresponding to the end of first peak, shows significant variations for a wide range of values of a_i and a_j, and this apparently leads to a much better inverse solution. Finally, the kernel for $f_{\max} = 30.4$ MHz, corresponding to the end of the third resonance peak, shows a less pronounced structure.

It is also instructive to examine the kernel and the results of inverse calculations for the problem of determining bubble-size distribution in bubbly liquids examined by Duraiswami.[2] The inverse procedure works very well for bubbly liquids as can be seen from Fig. 17(a) which shows the input and computed bubble size distributions to be in excellent agreement. The kernel for this case has smooth variations over a wide range of bubble radii as seen in Figure 17(b). The attenuation as a function of frequency is shown in

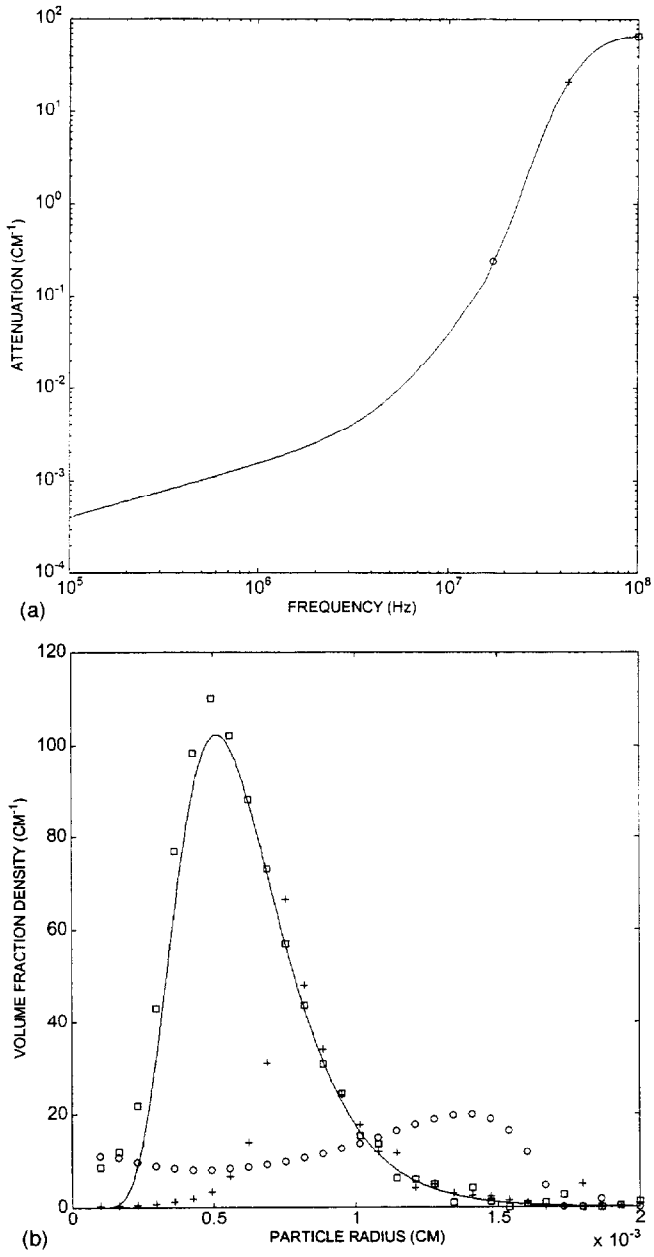

FIG. 15. As Fig. 12, but with a broader size distribution.

Fig. 17(c). The main reason for the success of the inverse technique for bubbly liquids seems to be that there is one resonance frequency for bubbles of each size. As long as the frequency range is broad enough to cover the resonance frequency of all the bubbles, it is possible to determine the size distribution.

The results presented so far were for polystyrene particles. We have also carried out inverse calculations for glass particles. As indicated earlier (cf. Fig. 6) there is no clear, sharp resonance frequency peak for glass particles. As a consequence, the inverse calculations for the glass particles did not show, in general, good agreement with the input size distribution.

The results presented so far show that the success of Tikhonov regularization to solve the inverse problem is limited. Although we have given plausible reasons for why the

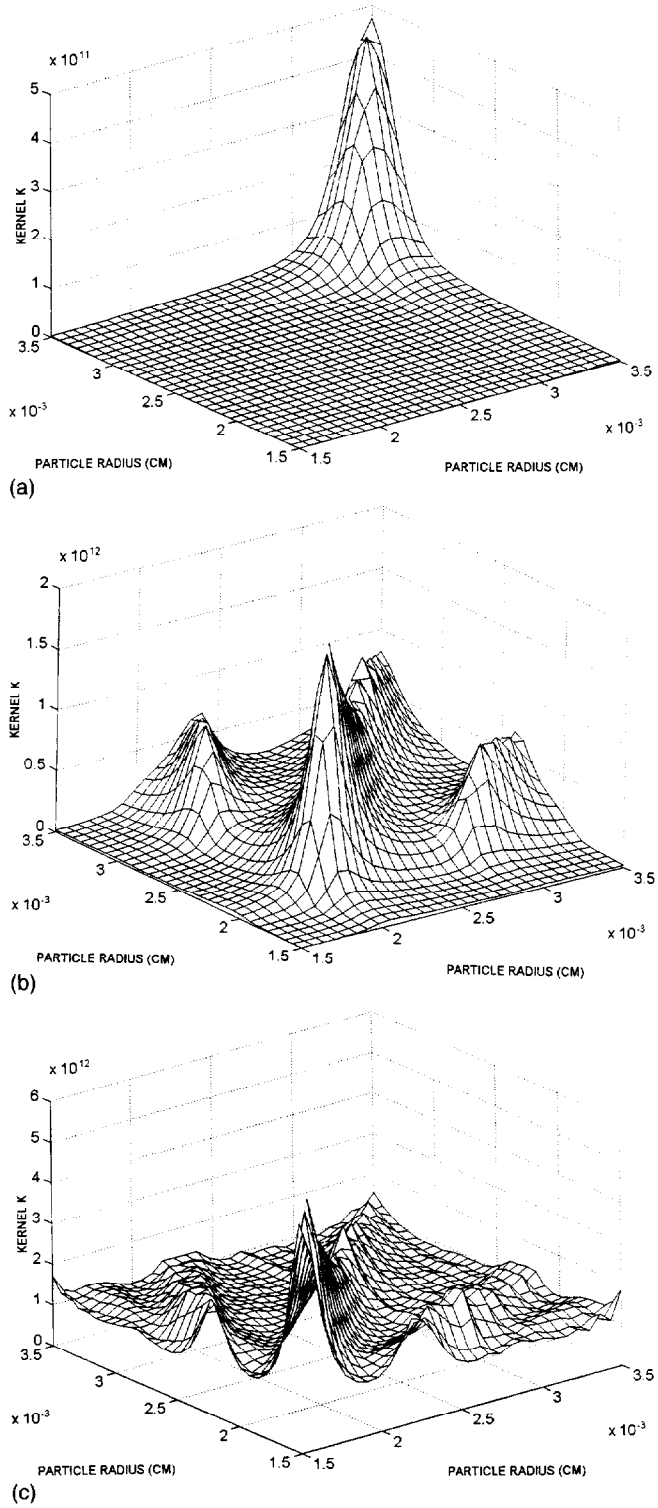

FIG. 16. The kernel $K(a_i,a_j)$ for polystyrene particles when using for $f_{\max}$ the value indicated in Fig. 12(a) by a ○ (a), + (b), and □ (c).

method works well for bubbles but not for all particles, it is possible that other techniques for solving the inverse problem may be more successful. For that reason we have attempted an alternative method[2,3,19] based on linear programming that we shall briefly describe here.

The constraint $\phi(a)\geqslant 0$ for all a was satisfied only *a posteriori* in the Tikhonov scheme. To ensure that the error is minimized while satisfying this constraint, we reformulate the original inverse problem as an optimization problem. The simplest scheme is to minimize the error

$$\int_{f_{\min}}^{f_{\max}} \left| \int_{a_{\min}}^{a_{\max}} \hat{\alpha}(f,a)\phi(a)da - \alpha_{\text{tot}}(f) \right| df. \tag{31}$$

instead of the integral of the square of the quantity enclosed by two vertical bars at each frequency. Constraints on the solution are used *a priori* in optimization via linear programming; here we use that $\phi(a)\geqslant 0$. Imposing an upper bound on the total volume fraction (maximum packing) can also be incorporated but is not essential. After discretizing the frequency range by M and $\phi(a)$ in N discrete values we write

$$\sum_{j=1}^{N} B_{ij}\phi(a_j) - \alpha_{\text{tot}}(f_i) = u_i - v_i, \quad u_i, v_i \geqslant 0, \quad i=1,2,\ldots,M. \tag{32}$$

Here, B_{ij} is the discretized form of the integral operator in (31) and u_i and v_i are, as yet, unknown, non-negative variables. Now, it can be shown[19] that minimizing the absolute value of (32) is equivalent to minimizing

$$\sum_{i=1}^{M} (u_i + v_i) \tag{33}$$

with (32) as a constraint together with the constrains u_i, $v_i \geqslant 0$ $(i=1,\ldots,M)$ and $\phi(a_i)\geqslant 0$ $(i=1,\ldots,N)$. Essential here is the notion that at the optimum $u_i v_i = 0$ for each i, which makes the solutions of the two minimization problems (31) and (33) identical.

The above scheme was applied to a number of cases that were also examined using the Tikhonov method. It was found that, in general, the linear programing scheme produced inferior results. A typical example is shown in Fig. 18 where the Tikhonov method is seen to yield far better results for the size distributions. This technique also did not yield good inverse results for the case of glass particles.

V. CONCLUSION

A theory for the attenuation and wave speed of solid–liquid suspensions at low particle volume fractions is described. The theory is shown to be in excellent agreement with the experimental data measured in our laboratory. Tikhonov regularization and linear programing techniques are employed to solve the inverse problem of determining the particle size distribution from the attenuation-frequency data. Although these techniques are successful in solving the inverse problem in several cases, we have also shown that the results are very sensitive to the choice of frequency range, the physical properties of the particles, and the nature of particle size distribution (unimodal, bimodal, etc.). Since the same techniques worked very well for bubbly liquids, we attribute the failure in solving the inverse problem satisfactorily to the complex resonance behavior of slurries. We conclude therefore that the prospects of using acoustic probes for on-line monitoring of particle size distribution of slurries are somewhat limited unless some additional information on the particle size distribution (e.g., unimodal) is available.

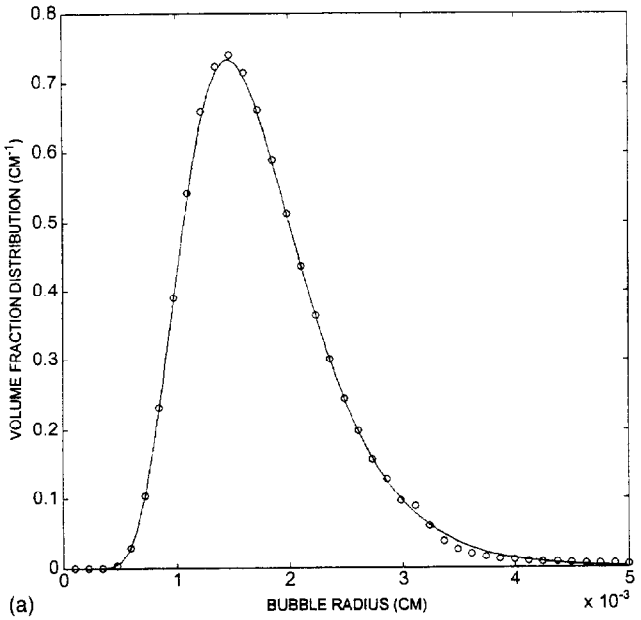

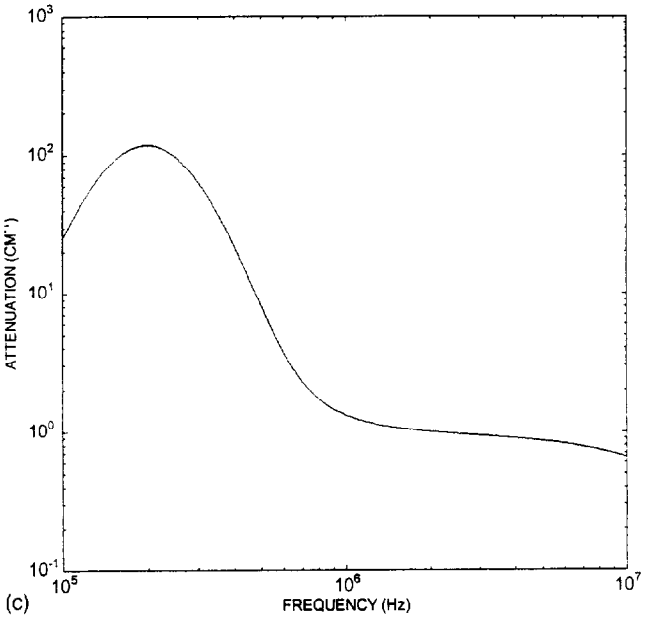

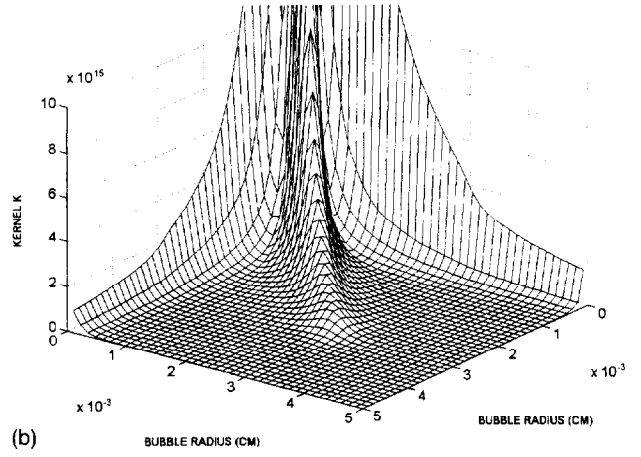

FIG. 17. Results for air bubbles in water. (a) Inverse problem result with a total volume fraction equal to 0.004, together with the the kernel $K(a_i, a_j)$ (b) and the attenuation as a function of frequency (c).

ACKNOWLEDGMENTS

Financial support for this work was provided by U.S. Department of Energy, Environmental Management Science Program, under Grant No. DE-FG07-96ER14729. Computations were made using the facilities of the Cornell Theory Center and the National Center of Supercomputing Applications at the University of Illinois at Urbana–Champaign.

APPENDIX: EQUATIONS FOR A_n

In this appendix we give the set of linear equations for unknowns that include the coefficients A_n required to calculate the attenuation from (12) and (19)–(21) or (22). These equations are derived from the boundary conditions on the surface of a test particle. In addition to the coefficients A_n, $\tilde{A}_n$ of the solution of (1) outside and inside the particle, respectively, similar coefficients arise due to the solution of (2) and (3), denoted by B_n and C_n. Note that (3) is an equation for the vector **A** rather than a scalar velocity potential, but only the azimuthal component of **A** is nonzero, hence only a scalar coefficient C_n. In the following, we use the notation $z_c = k_c a$, $z_T = k_T a$, and $z_s = k_s a$:

$$z_c j_n'(z_c) + A_n z_c h_n'(z_c) + B_n z_T h_n'(z_T) - C_n n(n+1) h_n(z_s) = \tilde{A}_n \tilde{z}_c j_n'(\tilde{z}_c) + \tilde{B}_n \tilde{z}_T j_n'(\tilde{z}_T) - \tilde{C}_n n(n+1) j_n(\tilde{z}_s), \quad \text{(A1)}$$

$$j_n(z_c) + A_n h_n(z_c) + B_n h_n(z_T) - C_n(h_n(z_s) + z_s h_n'(z_s)) = \tilde{A}_n j_n(\tilde{z}_c) + \tilde{B}_n j_n(\tilde{z}_T) - \tilde{C}_n(j_n(\tilde{z}_s) + \tilde{z}_s j_n'(\tilde{z}_s)), \quad \text{(A2)}$$

$$b_c[j_n(z_c) + A_n h_n(z_c)] + B_n b_T h_n(z_T) = \tilde{A}_n \tilde{b}_c j_n(\tilde{z}_c) + \tilde{B}_n \tilde{b}_T j_n(\tilde{z}_T), \quad \text{(A3)}$$

$$\tau(z_c b_c[j_n'(z_c) + A_n h_n'(z_c)] + B_n b_T z_T h_n'(z_T)) = \tilde{\tau}(\tilde{A}_n \tilde{b}_c \tilde{z}_c j_n'(\tilde{z}_c) + \tilde{B}_n \tilde{b}_T \tilde{z}_T j_n'(\tilde{z}_T)), \quad \text{(A4)}$$

$$\begin{aligned}(-\iota\omega\mu)([(z_s^2 - 2z_c^2) j_n(z_c) - 2z_c^2 j_n''(z_c)] + A_n[(z_s^2 - 2z_c^2) h_n(z_c) - 2z_c^2 h_n''(z_c)] + B_n[(z_s^2 - 2z_T^2) h_n(z_T) \\ - 2z_T^2 h_n''(z_T)] + C_n 2n(n+1)[z_s h_n'(z_s) - h_n(z_s)]) \\ = \tilde{A}_n[(\omega^2 \tilde{\rho} a^2 - 2\tilde{\mu}\tilde{z}_c^2) j_n(\tilde{z}_c) - 2\tilde{\mu}\tilde{z}_c^2 j_n''(\tilde{z}_c)] \\ + \tilde{B}_n[(\omega^2 \tilde{\rho} a^2 - 2\tilde{\mu}\tilde{z}_T^2) j_n(\tilde{z}_T) - 2\tilde{\mu}\tilde{z}_T^2 j_n''(\tilde{z}_T)] \\ + \tilde{C}_n 2\tilde{\mu} n(n+1)[\tilde{z}_s j_n'(\tilde{z}_s) - j_n(\tilde{z}_s)],\end{aligned} \quad \text{(A5)}$$

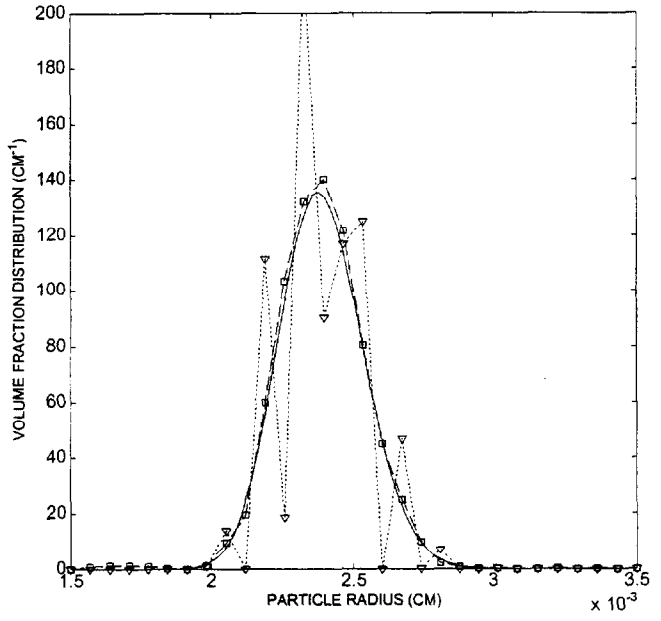

FIG. 18. Comparison of the results for the inverse problem of polystyrene particles (exact solution is the solid line) using the linear programming method (..▽..) and the Tikhonov method (--□--). In both cases the attenuation was cut off at the same frequency, indicated by the square in Fig. 12(a).

$$
\begin{aligned}
&(-\iota\omega\mu)(z_c j_n'(z_c)-j_n(z_c)+A_n[z_c h_n'(z_c)-h_n(z_c)]\\
&\quad+B_n[z_T h_n'(z_T)-h_n(z_T)]-(C_n/2)[z_s^2 h_n''(z_s)\\
&\quad+(n^2+n-2)h_n(z_s)])\\
&\quad=\tilde{\mu}(\tilde{A}_n[\tilde{z}_c j_n'(\tilde{z}_c)-j_n(\tilde{z}_c)]+\tilde{B}_n[\tilde{z}_T j_n'(\tilde{z}_T)-j_n(\tilde{z}_T)]\\
&\quad-(\tilde{C}_n/2)[\tilde{z}_s^2 j_n''(\tilde{z}_s)+(n^2+n-2)j_n(\tilde{z}_s)]). \qquad \text{(A6)}
\end{aligned}
$$

Here, b_c and b_T are given by

$$
b_c=\frac{(1-\gamma)\omega^2}{\beta c^2}, \quad b_T=-\frac{\gamma}{c_1^2\beta}\left[\omega^2-\left(\frac{c_1^2}{\gamma}-\frac{4\iota\omega\mu}{3\rho}\right)k_T^2\right], \qquad \text{(A7)}
$$

with β the thermal expension coefficient and c_1 the liquid-equivalent of the speed of sound for spherical compressional waves in an elastic isotropic solid $\tilde{c}_1=\sqrt{(\tilde{\lambda}+2\tilde{\mu}/3)/\tilde{\rho}}$. The Lamé constant $\tilde{\lambda}$ is not really needed when the speed of sound (c) of longitudinal compressional waves is specified, as we can also write $c_1^2=c^2(1-4\tilde{\mu}/(3\rho c^2))$. The above equations have also been given by Epstein and Carhart[5] and Allegra and Hawley.[6] However, in both there are typographical errors: in Ref. 5, the last $j_n'(\tilde{z}_s)$ in (A2) is erroneously replaced by $h_n'(\tilde{z}_s)$; in Ref. 6 the signs of both (n^2+n-2)-terms are wrong, while the last $h_n(z_s)$ on the left-hand side of (A6) has the argument $\tilde{z}$ instead and the first z_s after C_n is replaced by $\tilde{z}_s$. Not correcting the typographical errors in Ref. 6 would have altered the results significantly.

[1] K. W. Commander and R. J. McDonald, "Finite-element solution of the inverse problem in bubble swarm acoustics," J. Acoust. Soc. Am. **89**, 592 (1991).

[2] R. Duraiswami, "Bubble density measurement using an inverse acoustic scattering technique," in ASME Cavitation and Multiphase Forum, Washington DC, edited by O. Furuya (ASME, New York, 1993), Vol. 153, p. 67.

[3] R. Duraiswami, S. Prabhukumar, and G. L. Chahine, "Bubble counting using an inverse acoustic scattering method," J. Acoust. Soc. Am. **104**, 2699 (1998).

[4] T. Oja and F. Alba, "Acoustic attenuation spectroscopy for particle sizing of high concentration dispersions," presentation at the NIST International Workshop on Ultrasonic and Dielectric Characterization Techniques for Suspended Particulates Gaithersburg, MD (1997).

[5] J. R. Allegra and S. A. Hawley, "Attenuation of sound in suspensions and emulsions: Theory and experiments," J. Acoust. Soc. Am. **51**, 1545 (1972).

[6] P. S. Epstein and R. R. Carhart, "The absorption of sound in suspensions and emulsions. I. Water fog in air," J. Acoust. Soc. Am. **25**, 553 (1953).

[7] V. K. Varadan, V. N. Bringi, V. V. Varadan, and Y. Ma, "Coherent attenuation of acoustic waves by pair-correlated random distribution of scatterers with uniform and Gaussian size distributions," J. Acoust. Soc. Am. **73**, 1941 (1983).

[8] R. Kress, *Linear Integral Equations* (Springer, Berlin, 1989).

[9] D. J. McClements and J. N. Coupland, "Theory of droplet size distribution measurements in emulsions using ultrasonic spectroscopy," Colloids Surf., A **117**, 161 (1996).

[10] M. J. Lighthill, "Viscosity effects in sound waves of finite amplitude," in *Surveys in Mechanics*, edited by G. K. Batchelor and R. M. Davies (Cambridge U.P., Cambridge, England, 1956).

[11] A. S. Sangani, "A pairwise interaction theory for determining the linear acoustic properties of dilute bubbly liquids," J. Fluid Mech. **232**, 221 (1991).

[12] A. S. Sangani, D. Z. Zhang, and A. Prosperetti, "The added mass, Basset, and viscous drag coefficients in nondilute bubbly liquids undergoing small-amplitude oscillatory motion," Phys. Fluids A **3**, 2955 (1991).

[13] P. D. M. Spelt, M. A. Norato, A. S. Sangani, M. S. Greenwood, and L. L. Tavlarides, "Attenuation of sound in concentrated suspensions: Theory and experiments," submitted to J. Fluid Mech.

[14] Y. Ma, V. K. Varadan, and V. V. Varadan, "Comments on 'Ultrasonic propagation in suspensions,'" J. Acoust. Soc. Am. **87**, 2779 (1990).

[15] R. E. Bolz, *CRC Handbook of Tables for Applied Engineering Science* (CRC, Boca Raton, FL, USA, 1973).

[16] L. W. Anson and R. C. Chivers, "Ultrasonic propagation in suspensions—A comparison of a multiple scattering and an effective medium approach," J. Acoust. Soc. Am. **85**, 535 (1989).

[17] J. J. Faran, "Sound scattering by solid cylinders and spheres," J. Acoust. Soc. Am. **23**, 405 (1951).

[18] R. C. Chivers and L. W. Anson, "Calculations of the backscattering and radiation force functions of spherical targets for use in ultrasonic beam assessment," Ultrasonics **20**, 25 (1982).

[19] L. M. Delves and J. L. Mohamed, *Computational Methods for Integral Equations* (Cambridge U.P., Cambridge, England, 1985).

Ultrasonic Characterization of Low Volume Fraction Solid-Liquid Slurries

by

Mark Jefferson Hedges

Abstract of Thesis

January 2001

The United States is encumbered with a huge amount of liquid radioactive waste as a result of the nuclear weapons program. The waste is stored in underground tanks, all of which need to be emptied and many of which are leaking. In order to process the waste it must be transported by pipeline to the treatment centers. The waste contains suspended solids so plugging of the pipeline is a major concern. There is a need to characterize the waste during transfer in order to reduce the risk of plugging.

Ultrasound is an attractive choice for this application. It has the ability to penetrate optically dense liquids and its non-intrusive nature protects operators from the harmful effects of radiation.

Previous work on using ultrasound to characterize slurries examined relatively ideal systems of monodispersed particles in water. No work was done on systems with volume fractions less than 0.05. Theory is available which accurately predicted attenuation at low volume fractions but it was not known if reliable experimental data could be collected under these conditions.

Attenuation measurements are performed on systems of soda-lime glass beads (radius = 16 μm) in water, clay in water, and a nuclear waste simulant consisting of precipitated salts in saturated supernate. Solids volume fraction studied range from 0.004 to 0.05. Both a Pulse/FFT and a Toneburst method are used to measure attenuation. The Pulse/FFT method is found to be more accurate. As expected the relationship between attenuation and volume fraction is found to be linear, and it is found that reliable attenuation measurements can be made in all three systems even at solids volume fraction of under 0.01.

Sound speed is measured in systems of soda-lime glass beads (radius 16 μm) and Potter's beads (radius 60 μm). Volume fraction ranged from 0 to 0.4. Experiments indicate that particle size has little effect on sound speed. Experimental data of sound speed in soda-lime glass slurries agrees well with theory. Experiments performed at low volume fraction showed that with very precise monitoring of temperature it is possible to use speed to characterize slurries, however, practical considerations weigh against this.

Future work involves automating the procedure to measure attenuation and creating an on-line monitor on a spoolpiece that can be installed in a flow loop. The system will monitor slurry and the suspending liquid simultaneously and give data in real time.

Ultrasonic Characterization of Low Volume Fraction Solid-Liquid Slurries

by

Mark Jefferson Hedges
B.S. Ch.E., Syracuse University, 1998

Thesis

Submitted in partial fulfillment of the requirements for the degree of Master of Science in Chemical Engineering in the Graduate School of Syracuse University

January 2001

Approved _____
Professor Lawrence L. Tavlarides

Date _____

Table of Contents

List of Tables

List of Figures

Acknowledgments

I would like to thank the following persons for their invaluable assistance toward the completion of this work:

Professor Lawrence L. Tavlarides, my research advisor, for his leadership and ability. His suggestions, ideas, and criticisms were the driving force behind this study and were essential to my graduate education.

Professor Ashok S. Sangani, for his help in the theoretical aspects of this study.

Dr. Peter Spelt, for his indispensable assistance in performing the theoretical calculations included in this study.

Professor D. Julian McClements, University of Massachusetts, Amherst, for his very generous assistance in helping me use his technique to measure phase speed.

My parents, **Daniel C. and Elizabeth Hedges**, for their support during my education.

Heather Marie Wilson, for her love and patience. I know it was not easy for her to wait for me but her support helped me complete this work.

Sandie Friske, for making me feel at home even when I was not.

The assistance of the following people is greatly appreciated:

Technicians: Mr. Dick Chave and Mr. John Banas

Students: Mr. Jun Sig Lee and Mr. Sang Kyun

Administrative Staff: Mrs. Ruth Dewey, Mrs. Linda Lowe, and Ms. Linda Vanderhoof.

The following organizations are recognized for their financial support:

Department of Chemical Engineering and Materials Science, Syracuse University.

The Graduate School of Syracuse University.

US Department of Energy, Environmental Management Science Program

Grant number DE-FG07-96ER14729.

1. Introduction

The cold war era nuclear arms race has left the United States encumbered with a large amount of radioactive waste. Currently hundreds of millions of gallons of radioactive waste are stored at several sites across the country. The waste, contained in underground tanks, is a non-uniform mixture of sludge, supernate, and salt cake. Generally, the major components are sodium nitrate and sodium nitrite. Additional ions present include aluminate, hydroxide, and carbonate. The supernates are basic, with pH ranging from 10 to greater than 14. Radioactive components in the supernate and dissolved salt cake are materials such as ^{99}Tc, ^{137}Cs, ^{235}Pu, ^{237}Np, and ^{90}Sr (Golcar 2000).

Production of new weapons grade radioactive material in the United Stated has stopped and the cleanup phase has been in progress for a number of years. The fact that many of the storage tanks are leaking only increases the urgency to deal with the problem.

In order to treat the waste it must first be removed from the storage tanks and transported to treatment centers located on site. The tanks are located some distance from the treatment centers, some as far as six miles away (Hylton, 2000). For safety reasons, it is often desirable to transfer the materials by pipeline, rather than tanker truck. Plugging is a major concern when transferring slurries by pipeline. If a pipeline becomes plugged there are major costs in money and time, as a new pipeline has to be laid, and the old pipeline remediated. As of 1996 five of the six cross-site pipelines at the Hanford Site were unusable due to plugging (Hudson 1996). The risk of plugging can be reduced by

careful monitoring of the slurry properties (suspended solids levels, density, and viscosity).

The treatment of nuclear waste is a complicated process, consisting of many different operations run in series and in parallel. Many of these operations involve handling of liquid/solid systems. For example, one of the methods for treating radioactive tank supernate involves using an adsorbent such as crystalline silica titanate to remove the radioactive cesium ions and then imprisoning the now radioactive absorbent in a glass frit. This disposal method largely involves the handling of solid/liquid systems and some method of characterizing the flowing stream is needed.

Ultrasound has several properties which make it an attractive choice for characterizing radioactive slurry. It has the ability to penetrate optically dense slurries. When used properly it can give accurate information even in the presence of small amounts of gas bubbles. It is nonintrusive, protecting the operator from the effects of radiation. It also is a very sensitive technique and can give accurate readings at very low solid concentrations.

Two different kinds of information that can be obtained from ultrasound are attenuation and speed. Attenuation is the absorbency of sound by the material. It is almost always highly dependent on the frequency of the ultrasonic signal and the size and physical properties of the particles. Attenuation is highly sensitive to the presence of solids particles and gas bubbles, and is somewhat tolerant of changes in temperature. In theoretical terms, attenuation is the imaginary part of the wave number.

The three modes of attenuation are viscous, thermal, and scattering. The nondimensional number $k_{cl}a$, which is the product of particle radius and wavenumber, can

be used to determine which modes are significant. The viscous energy dissipation results from translational, volume, and shape oscillations of particles. Thermal attenuation arises as a result of non-adiabatic changes in temperature of the particles, as the particles expand and contract due to the passage of a sound wave. Viscous and thermal attenuation are most significant at small values of $k_{cl}a$. Thermal attenuation is particularly significant at low $k_{cl}a$ when the densities of the particles and liquid are similar. Attenuation due to scattering is the major source of attenuation at higher frequencies, i.e. when $k_{cl}a = O(1)$.

Other kind of information that can be obtained using ultrasound is sound speed. In many materials (such as water) speed is nearly independent of frequency. However, in some systems such as suspensions, speed is dependent on the frequency of the ultrasonic signal. Such systems are termed highly dispersive. Speed is not very dependent on particle size and is not as sensitive to the presence of solid particles as is attenuation, particularly when the speed of sound in the solid phase is close to the speed of sound in the liquid phase. Speed is strongly dependent on temperature.

There are several methods currently being evaluated for the characterization of radioactive slurries. A study was conducted which evaluated 12 in-line or in-tank monitoring systems. Based on this study, two systems were selected for testing with radioactive slurries (Hylton and Bayne, 1999). One method, studied by Hylton (2000) uses Coriolis meters, which measure density of a material. Two meters are used, one measuring the density of the slurry and another the density of the supernate. Solids loading is calculated assuming a constant solids density. The other method given consideration is an ultrasonic probe developed by Argonne National Laboratory (Hylton